

A Chemical Percolation Model for Devolatilization: Temperature and Heating Rate Effects*

Thomas H. Fletcher and Alan R. Kerstein
Combustion Research Facility
Sandia National Laboratories
Livermore, California 94551-0969

Ronald J. Pugmire and David M. Grant
Department of Chemistry
University of Utah
Salt Lake City, Utah 84112

INTRODUCTION

It is well known that the yield of volatile matter obtained from a pulverized coal is dependent upon the temperature history of the particle. However, the effect of heating rate on volatiles yield is difficult to study independently of final temperature. For example, the volatile yields obtained in an entrained flow reactor study by Kobayashi, et al. [1] increase with both temperature and heating rate, but the independent contribution of heating rate could not be assessed. Heated screen experiments were developed to study devolatilization behavior at different heating rates independently from the final particle temperature. The data of Anthony and Howard [2] show little increase in volatiles yield when particles are heated to the same final temperature on a heated screen at different heating rates. In a more recent study, Gibbins-Matham and Kandiyoti [3] show evidence for small increases in the volatiles yield from a Pittsburgh #8 coal as the heating rate is increased from 1 K/s to 1000 K/s on a heated screen. Coal samples were heated at 5 different heating rates to a final temperature of 700°C and held for 30 s. Experiments were repeated several times in order to ensure accuracy of the data. The total volatiles yield increases from 41.5% at 1 K/s to 46.8% at 1000 K/s, a relative increase in yield of 13%. This increase in yield with increase in heating rate is small, but is larger than associated experimental errors.

The chemical percolation devolatilization (CPD) model [4] was developed as a means to describe coal devolatilization behavior based upon the chemical structure of the parent coal. Some of the input parameters for this model are obtained from NMR characterizations of the parent coal. Percolation statistics are used to describe the probability of generating finite tar fragments from the infinite coal matrix. Pyrolysis yields of tar, gas, and char for three different types of coal are described using a single set of kinetic parameters; only chemical structure parameters are changed for the different coals. The initial description of the CPD model [4] allowed for a temperature dependence of the competition between side chain formation and char formation. However, this option was not exercised in the initial study in order to demonstrate general utility of the model for one set of devolatilization data on three coals collected over a narrow range of temperatures and heating rates. In the present work, the Gibbins-Matham and Kandiyoti data are used to determine additional coefficients for the CPD model that accurately predict the changes in char and tar yield as a function of heating rate.

* Work supported by the U. S. Department of Energy's Pittsburgh Energy Technology Center's Direct Utilization AR&TD Program and by the National Science Foundation through the Advanced Combustion Engineering Research Center (ACERC) at Brigham Young University and the University of Utah.

THEORY

The Chemical Percolation Devolatilization Model

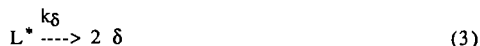
Coal is treated in the CPD model as a macromolecular array of clusters representing the interconnections of aromatic ring structures of various sizes and types. These clusters are connected by a variety of chemical bridges of different bond strengths. Percolation statistics applicable to a Bethe lattice (a loopless tree structure) allow a mathematical description of the bridge-breaking process in closed form, providing an efficient alternative to Monte-Carlo techniques. Tar is formed as finite aromatic clusters separate from the infinite coal lattice. Labile bridges L decompose into a reactive intermediate L^* , as follows:



The reactive intermediate is unstable, and reacts quickly in a competitive reaction sequence. In one reaction pathway, the reactive intermediate may recombine to form a stable char bridge c with the associated release of light gas g_2 :



In a competing reaction pathway, the reactive intermediate is stabilized and forms side chains δ (rather than recombining to form char):



The cleavage of the reactive intermediate in this step constitutes the bridge-breaking step, and is tied to the generation of tar fragments through percolation statistics. The side chains eventually react to form light gas g_1 :



The competition for L^* is governed by the ratio of the rate of side chain formation to the rate of char formation, and it is convenient to define a composite rate constant ρ :

$$\rho = \frac{k_\delta}{k_c} = \frac{A_\delta}{A_c} \exp\left[\frac{-(E_\delta - E_c)}{RT}\right] = A_\rho \exp\left[\frac{-E_\rho}{RT}\right] \quad (5)$$

The dynamic variables of the theory are the bridge population parameters, L and c , and the chain fragment parameter δ . A steady-state approximation is invoked for the reactive intermediate L^* (i.e., $dL^*/dt = 0$), yielding differential expressions for the reaction rates of L , c , and δ [4].

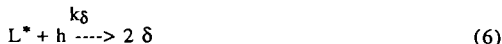
Modifications to the CPD Model

In the initial formulation of the CPD model [4], the temperature dependence of ρ was neglected by setting E_ρ to zero and adjusting A_ρ to match the experimental data. This approach was sufficient to allow determination of an effective rate coefficient ρ that explained the pyrolysis behavior of a limited set of data with a well-characterized temperature history obtained for three different coals

at one heating rate [5]. Measurements of the devolatilization rate performed recently at Sandia [6] include single particle temperature measurements, and show general agreement with the rates obtained by Serio, et al. [5]. In a subsequent study, the sensitivity of the CPD model to nonzero values of E_p was explored, and it was shown that the total yield predicted by the model changes as a function of heating rate, as expected. However, sensitivity studies show that regardless of the value of E_p , the model cannot accurately predict tar yields over a wide range of heating rates. Physical mechanisms that limit the production of tar were therefore considered that would allow more realistic predictions using the CPD model.

The ratio of the tar yield to the char yield is affected by the amount of hydrogen in the coal. For example, in the limiting case, anthracites contain little hydrogen, and hence release little volatile matter. All of the hydrogen in the coal, however, is not available to support the release of tar during devolatilization. In some coals, a considerable amount of hydrogen is contained in aliphatic groups, such as methyl (-CH₃) groups, which are released in the form of light gases rather than combining with larger reactive molecules to produce volatile tars. The amount of available hydrogen for tar stabilization is therefore not directly related to the total amount of hydrogen present in the coal. The amount of available hydrogen for tar formation has been used in several recent coal devolatilization models [7,8]. At present, quantitative experimental methods for measuring the amount of hydrogen available for stabilization of reactive intermediates that lead to tar are not available.

In the CPD model, production of tar can be limited by introduction of a variable to represent the amount of hydrogen available for stabilization of the reactive intermediate L^* . To include the available hydrogen h explicitly in the reaction sequence, Eq. 3 is modified as follows:



Here h is normalized by the total possible number of bridges in the lattice (the same basis as L). As h is depleted, the reactive intermediate is no longer able to form side chains, causing preferential formation of char. This equation becomes a bimolecular reaction, rather than a unimolecular decomposition reaction (Eq. 3), with an overall reaction order of two rather than one. The reaction rate for L is unchanged, but the reaction rates for c and δ include the term ρh instead of ρ . In addition, the reaction rate of h is formulated as follows:

$$\frac{dh}{dt} = -k_\delta L^* h = -\frac{k_\delta k_p L h}{k_c + k_\delta h} = -\frac{k_b \rho h L}{1 + \rho h} \quad (7)$$

where ρ is defined in Eq. 5. The variable h is highly coupled to the composite rate constant ρ , evidenced by the fact that ρ and h appear together in all of the equations except in the derivative term dh/dt in Eq. 7. As discussed later, this high degree of coupling restricts independent evaluation of ρ and the initial amount of available hydrogen h_0 using experimentally measured release rates of tar and total volatiles. The method of relating the production of finite clusters to the number of intact bridges remains unchanged by the introduction of the variable h ; the mass fractions of tar, gas, and char are therefore calculated as a function of the dynamic variables L , c , and δ [4].

DISCUSSION

Coal specific parameters for the CPD model are ideally obtained from independent chemical analyses, such as NMR characterizations [9]. In practice, the NMR data can only guide the

selection of coal specific parameters such as the coordination number ($\sigma+1$), the initial fraction of intact bridges p_0 , the initial fraction of char bridges c_0 , and the ultimate gas yield f_∞ . Refinements of these structural parameters are obtained from least squares fits of experimentally measured rates and yields of tar and total volatiles. The kinetic parameters used by the model are assumed to be coal independent, and these parameters were previously obtained [4] by comparison with data [5].

Determination of Structural Parameters for Pittsburgh #8 Coal

The coal investigated by Gibbins-Matham and Kandiyoti [3] was a Pittsburgh #8 hva bituminous coal. The results of Serio, et al. [5] for three different coals (Illinois #6 hvb bituminous, Montana Rosebud, and North Dakota Beulah Zap lignite) were previously used to set parameters for the original development of the CPD model [4], but data were unavailable for Pittsburgh #8 coal. A Pittsburgh #8 coal (PSOC-1451D) was investigated by Fletcher [6] and by Freihaut [10]. Based on the devolatilization rates obtained by Fletcher [6] which include single particle temperature measurements, the heated screen experiments performed by Gibbins-Matham and Kandiyoti and by Freihaut appear to have reasonable estimates of particle temperature during devolatilization. The tar and total volatiles yield data of Freihaut are therefore used to determine chemical structure parameters for the CPD model for the Pittsburgh #8 coal using the kinetic parameters from the previous study [4]. The parameters required by the CPD model that represent the chemical structure of the parent coal are the coordination number ($\sigma+1$), the initial concentration of labile bridges L_0 , the initial concentration of char (or refractory) bridges c_0 , and the ultimate gas yield f_∞ . The coordination number ($\sigma+1$) used in this study is 5.8, as determined for Pittsburgh #8 hva bituminous coal by ^{13}C NMR spectroscopy and carbon-counting techniques [9].

Values for L_0 , c_0 , and f_∞ are obtained from least squares fits to Freihaut's heated screen data (tar and char yields) at 1000 K/s with zero hold time at the maximum temperature. In these simulations, E_p was set to zero, and the coal was assumed to cool at 1000 K/s after the desired temperature was achieved. Results of this least squares fit are $L_0 = 0.311$, $c_0 = 0.138$, $f_\infty = 0.305$. The comparison with Freihaut's data is shown in Figure 1. The model predicts both the yield and temperature dependence of the char formation and tar release data. The fact that the predicted initial tar yield is non-zero is indicative of finite lattice clusters existing in the parent coal. A study of vaporization mechanisms of this tar precursor material is in progress.

Determination of A_p and E_p

The values of A_p and E_p in this model control the temperature dependence of the competition between char formation and gas formation, which is assumed to be relatively independent of coal type. It is anticipated that h_0 will be determined in the future from some type of chemical analysis of the parent coal structure, but for the present, existing methods are insufficient to determine this parameter. The experimental data on Pittsburgh #8 coal can be modeled equally well with different values of h_0 , as long as h_0 is large enough to permit adequate tar yields. Predicted tar yields decrease when values of h_0 of 0.2 or lower are used for the Pittsburgh #8 and Illinois #6 coals, since the available hydrogen is completely consumed and side chain formation is no longer possible. For values of h_0 greater than 0.25, finite concentrations of h exist after depletion of the labile bridges L, and the tar yield is not decreased. Successful CPD model predictions of the devolatilization behavior of both the Illinois #6 and Pittsburgh #8 coals can be made using values of h_0 ranging from 0.25 to 0.4. Studies to determine the appropriate value of h_0 as a function of coal type will be conducted in the future. For each value of h_0 used, a different set of values for A_p and E_p is required to fit the Serio, et al. [5] Illinois #6 data. Since these data were obtained at

only one heating rate, there is insufficient resolution to determine both A_p and E_p . A correlation for A_p was therefore determined for different input values of E_p that best fit the Serio, et al. data. Figure 2 shows the least squares fits to the data with $h_0 = 0.3$ and $E_p = 3.0$ kcal/mole. The reaction histories of the dynamic variables used in this calculation are shown in Figure 3. The available hydrogen, h , is consumed rapidly as the tar is released, but a modest residual value remains when the population of labile bridges goes to zero. The reaction histories of the dynamic variables other than h (L , c , g_1 , g_2 , and δ) are similar to those predicted by the original CPD model [4], and are seemingly unaffected by h except when the value selected for h_0 is low enough to restrict side chain formation (and hence affect tar and gas yields).

A fitting routine was used to determine a suitable value for E_p from the data of Gibbins-Matham and Kandiyoti. The total volatiles yield measured by Gibbins-Matham and Kandiyoti differs from the yield measured by Freihaut, which is not surprising, since all Pittsburgh #8 hva bituminous coals are not identical. Therefore, only the difference in measured yields as a function of heating rate were used in the determination of E_p , thereby avoiding problems in fitting the absolute yields at each heating rate. In this numerical simulation of the experiment, particles are heated to 700°C at the specified heating rate and held at that temperature for 30 s. The fitting procedure determines the changes in total yield using the chemical structure coefficients obtained from NMR analysis [9] and least squares fit to Freihaut's data [10] ($\sigma+1 = 5.8$, $L_0 = 0.311$, $c_0 = 0.138$, and $f_{\infty} = 0.305$). The only fitting parameter used to correlate the change in yield versus heating rate is E_p ; A_p is calculated from the correlation based on E_p developed from the Serio, et al. data. Results of this least squares fit are shown in Table 1 for $h_0 = 0.3$, $E_p = 3.0$ kcal/mole, and $A_p = 26.8$ s⁻¹. The ΔV columns represent the difference in total volatile yield from the 1 K/s condition. The modest value determined for E_p of 3 kcal/mole is not surprising since E_p is a difference of two activation energies ($E_{\delta} - E_c$). In contrast, the activation energy associated with labile bridge scission E_b is 55 kcal/mole [4]. Thus, the temperature dependence of side chain formation with rate k_{δ} is only slightly more favorable than the temperature dependence of the rate of char formation k_c under these conditions.

Table 1
Predicted and Measured Changes in Total Volatiles Yield
as a Function of Heating Rate for Pittsburgh #8 Hva Bituminous Coal

Heating Rate (K/s)	Measured by [3] ΔV (%)	CPD Model $h_0 = 0.30$ ΔV (%)
1	0.0	0.0
3	- 0.7	0.6
10	2.2	1.4
100	3.0	3.3
1000	5.3	5.3

Extension to Other Heating Rates and Temperatures

The CPD model can be used to predict the effects of heating rate over a broader range of temperatures and heating rates using the coefficients obtained from the least squares fits to the above-mentioned data sets. Figures 4-5 show the heating rate dependence of the model for the devolatilization of Illinois #6 coal. In these calculations, the coal is heated to 1500 K at rates from 1 K/s to 10⁵ K/s. The effect is two-fold: (a) the temperature at which the reactions occur

increases as the heating rate increases, and (b) the total volatiles yield (gas + tar) increases as the heating rate increases. The predicted change in yield with heating rate is only a function of E_p . When $E_p = 0$, there is no predicted difference in volatiles yield as a function of heating rate. The shift in reaction temperature with heating rate is a result of competition between the devolatilization rate and the heating rate. The competition between chemical reactions and heat transfer governs changes in reaction temperatures with heating rate. The decrease in overall tar yield at higher temperatures is due to gas phase thermal cracking, resulting in the production of light gas.

The temperature dependence of the model can be explored further by comparison with devolatilization data obtained at high heating rates and long hold times at different temperatures. Freihaut [10] performed devolatilization experiments on Pittsburgh #8 hva bituminous coal at 1000 K/s, and varied the hold time from 0 to 100 s at different temperatures. The tar yield measured at the 100 s hold time condition is much greater than the zero hold condition at any given temperature between 700 and 900 K. He postulates that additional low-temperature coking reactions are needed to model this phenomena. Using the chemical structure coefficients described above, and the values of E_p and A_p corresponding to the best fits to the Gibbins-Matham and Kandiyoti data with $h_0 = 0.3$, predictions of the Freihaut 100 s and 50 s hold-time data were performed using the modified CPD model (see Figure 6). The model successfully predicts both the temperature dependence of tar evolution and the increase in yield at the 100 s hold time condition. The comparison with the limited 50 s hold condition is not quite as good. It is interesting that the CPD model is able to explain these experimental data without additional low temperature reactions. In addition, the CPD model allows the tar to continue to crack and release light gas as if it were at the same temperature as the coal particle. This results in the predicted decrease in tar yield at 800 K for the 100 s hold time condition and at 1000 K for the immediate quench (zero hold time) condition.

SUMMARY

The chemical percolation devolatilization (CPD) model was modified to account for differences in total volatiles yield attained at different heating rates. Modifications include the addition of a new dynamic variable to account for the hydrogen available to stabilize side chains formed from reactive intermediates of labile bridge scission. The temperature dependence of the competition between side chain formation and char formation was explored in some detail and found to give rise to changing tar yields with variations in heating rate. Coefficients were developed for the resulting model based on (a) NMR data for Pittsburgh #8 hva bituminous coal [9], (b) tar and char yield data for Pittsburgh #8 coal [10], (c) kinetic rate data from an Illinois #6 hvb bituminous coal [5], and (d) volatiles yield data as a function of heating rate for a Pittsburgh #8 coal [3]. Simulations were performed to show the predicted effects of heating rate and final temperature. Successful predictions of the devolatilization behavior of the Pittsburgh #8 coal and the Illinois #6 coal were performed using values for the initial amount of available hydrogen h_0 ranging from 0.25 to 0.4. Future studies will explore methods to determine a suitable value for this parameter by comparison with additional experimental data on other coals at various heating rates.

ACKNOWLEDGEMENTS

The authors would like to thank Dr. James Freihaut, Dr. Jon Gibbins-Matham, and Dr. Peter Solomon for discussions regarding experimental data and regarding meaningful tests of model assumptions and capabilities.

REFERENCES

- [1] Kobayashi, H., Howard, J. B., and Sarofim, A. F., *Sixteenth Symp. (Int.) on Comb.*, The Comb. Inst., 411 (1976).
- [2] Anthony, D. B., Howard, J. B., Hottel, H. C., and Meissner, M. P., *Fifteenth Symp. (Int.) on Comb.*, The Comb. Inst., 1303 (1974).
- [3] Gibbins-Matham, J. and Kandiyoti, R., "The Effect of Heating Rate and Hold Time on Primary Coal Pyrolysis Product Distribution," ACS Div. of Fuel Chem. Prepr., **32:4**, 318 (Sept., 1987).
- [4] Grant, D. M., Pugmire, R. J., Fletcher, T. H., and Kerstein, A. R., *Energy and Fuels*, **3**, 175, (1989).
- [5] Serio, M. A., Hamblen, D. G., Markham, J. R., and Solomon, P. R., *Energy and Fuels*, **1**, 138 (1987).
- [6] Fletcher, T. H., "Time-Resolved Particle Temperature and Mass Loss Measurements of a Bituminous Coal During Devolatilization," accepted for publication *Comb. and Flame* (1989).
- [7] Ko, G. H., Sanchez, D. M., Peters, W. A., and Howard, J. A., "Correlations for Effects of Coal Type and Pressure on Tar Yields from Rapid Devolatilization," presented at the *Twenty-Second Symp. (Int.) on Comb.*, Seattle, Washington (August, 1988).
- [8] Solomon, P. R., Hamblen, D. G., Carangelo, R. M., Serio, M. A., and Deshpande, G. V., *Energy and Fuels*, **2**, 405 (1988).
- [9] Solum, M., Pugmire, R. J., and Grant, D. M., "¹³C NMR Structural Determination of the Coals in the Premium Coal Sample Bank," accepted for publication in *Energy and Fuels*, see also ACS Division of Fuel Chem. Prepr., **32:4**, 273 (Sept., 1987).
- [10] Freihaut, J. D., "Kinetics of Coal Pyrolysis and Devolatilization," Technical Progress Report for DOE Contract DE-AC22-84PC70768 by United Technologies Research Center, East Hartford, Connecticut (for the period Nov. 1, 1987 - Jan. 31, 1988).

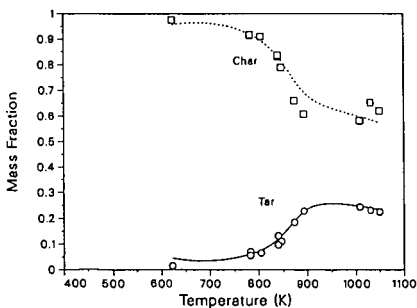


Figure 1. Results of least squares fit to Freihaut PSOC-1451D hva bituminous coal pyrolysis data [10] (points) using the CPD model (continuous lines). In Freihaut's experiment, coal particles are heated at 1000 K/s to the designated final temperature, and then cooled immediately to room temperature (zero hold time). Coefficients determined from this fit to the data are $L_0 = 0.311$, $c_0 = 0.138$, and $f_{\infty} = 0.305$.

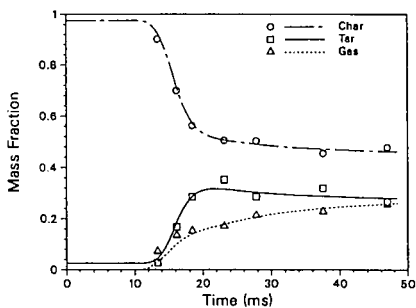


Figure 2. Results of least squares fit to Serio, et al. [5] devolatilization data (points) using the CPD model (continuous lines). In this experiment, Illinois #6 hvb bituminous coal particles are heated in an entrained flow reactor to 1040 K. The model calculations were made using $h_0 = 0.3$ and $E_p = 3,000$ cal/mole.

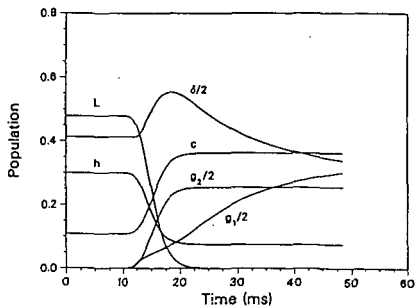


Figure 3. Predictions of dynamic variables used in the CPD model for the Illinois #6 coal, $h_0 = 0.3$, $E_p = 3000$ cal/mole. Variables δ , g_1 and g_2 are scaled by a factor of 2.

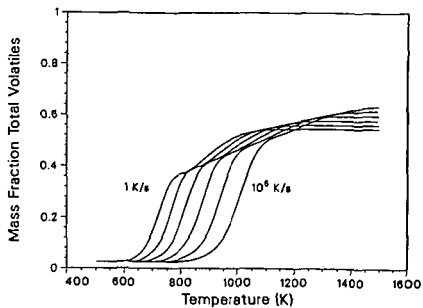


Figure 4. Predicted effect of heating rate on total volatiles yield from Illinois #6 hvb bituminous coal. Numerical experiments performed by heating at the designated rate to 1500 K (zero hold time).

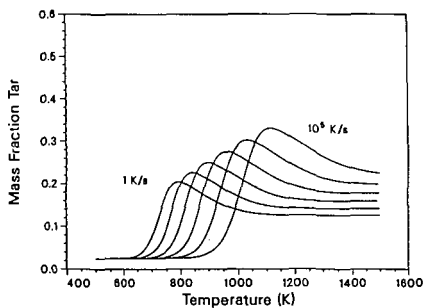


Figure 5. Predicted effect of heating rate on tar yield from Illinois #6 hvb bituminous coal. Numerical experiments performed by heating at the designated rate to 1500 K (zero hold time).

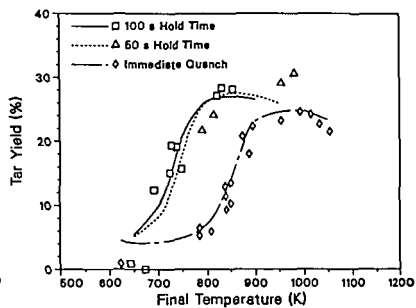


Figure 6. Comparison of CPD model calculations (curves) with Freihaut Pittsburgh #8 coal devolatilization data [10] at different hold times. Experiments were conducted by heating the coal at 1000 K/s to the final temperature and holding for 0, 50, and 100 s before quenching.

NETWORK MODELS OF COAL THERMAL DECOMPOSITION

P.R. Solomon, D.G. Hamblen, and Z.Z. Yu
Advanced Fuel Research, Inc., 87 Church Street, East Hartford, CT 06108

INTRODUCTION

Many recent studies have proposed that coal can be thought of as having a macromolecular network structure to which concepts of crosslinked polymers can be applied (1-10). These concepts have been employed to understand and model such properties of coal as: i) the insolubility; ii) the equilibrium swelling and penetration of solvents; iii) the viscoelastic properties; iv) similarities between the parent coal and products of hydrogenolysis, or mild oxidation; v) crosslinking during char formation (11,12); and vi) the formation of coal tar in pyrolysis (13-17). With the success of these concepts in describing coal properties, it appears logical to extend macromolecular network concepts to completely describe coal thermal decomposition behavior. This has been done by applying statistical methods to predict how the network behaves when subjected to thermally induced bond breaking, crosslinking, and mass transport processes (17-30).

In applying network models to coal thermal decomposition, one considers the coal to consist of aromatic ring clusters linked together by bridges in some geometry designated by the coordination number ($1 + \sigma$) which is the total number of allowable bridges per cluster. When the coal is heated, the bridges can break and new bridges can form. Various statistical methods can be employed to predict the concentration of single aromatic ring clusters (monomers) and linked clusters (oligomers of n clusters, "n-mers") up to a totally linked network. By assigning an average or distribution of molecular weights to the monomers, the amounts of tar, extractables, liquids or char can then be defined from the distribution of oligomer sizes. The models vary in the assumed chemistry of bond breaking and crosslinking, in the definition of tar, extracts, liquids, and char and in the statistical methods used.

Gavalas et al. employed statistical methods to predict the release of monomers from a randomly connected network (20). The model of Niksa and Kerstein employed percolation theory in a model called DISARAY (28) which extended their previous model built on chain statistics (24,25). Grant et al. employed percolation theory in a model called Chemical Percolation Devolatilization (CPD) (30). Solomon et al. employed Monte Carlo methods in a network model called the Depolymerization, Vaporization, and Crosslinking (DVC) model (21-23,27). This was an extension of their previous model for linear polymers (17,20). The DVC model was recently combined with their Functional Group (FG) model (27,29) to produce the general FG-DVC pyrolysis model. This model is currently being applied to predict the fluidity of coals (31). Other statistical methods for network behavior have been employed in the polymer literature (32-37).

In view of the importance of macromolecular network models to the accurate predictions of coal processing behavior, this paper assesses the assumptions and limitations of the proposed models. It appears that the way one performs the statistics (Monte Carlo, percolation theory, or other statistical methods) makes little difference. For example, we have substituted percolation theory methods for Monte Carlo calculations in the FG-DVC model and obtained comparable predictions for appropriately restricted cases. The important differences among models are in the assumptions for: 1) the network geometry; 2) the chemistry of bond breaking; 3) the chemistry of crosslink formation; 4) hydrogen utilization; and 5) mass transport. The paper compares the models and considers how the assumed network properties relate to behavior observed for coal.

MACROMOLECULAR NETWORKS

GENERAL PROPERTIES OF NETWORK - Figures 1 and 2 present the networks employed in the FG-DVC Monte Carlo calculations and percolation theory, respectively. For the FG-DVC Monte Carlo calculation, oligomers of ϵ clusters of a molecular weight distribution defined by M_{avg} and deviation (shown as the horizontal chains of clusters) are linked by m_0 crosslinks per monomer (shown as the vertical double lines) (26,29). The crosslinks are the branch points in the network where more than two bridges connect a cluster. During thermal decomposition, bridges break, crosslinks are added and the molecular weight of the oligomers is calculated by randomly distributing these changes.

For the percolation theory, a Bethe lattice is employed (28,30,39). Lattices are characterized by the coordination number ($\sigma + 1$), which is the number of possible bridges per cluster. Figure 2 shows lattices for $\sigma + 1 = 2.2$ and $\sigma + 1 = 4$. The Bethe lattice has no loops, but it has been demonstrated that this lattice is a good approximation to a lattice of equivalent coordination number containing loops (39).

The loop free geometry of the Bethe lattice allows for the number of free oligomers to be analytically expressed as a function of σ and the probability p of bonds being unbroken. This is the feature which makes the percolation theory so attractive from the stand point of computer efficiency and for understanding the behavior of networks under conditions of varying bridge populations. In Fig. 3 we present calculations using percolation theory for three values of $\sigma + 1$ for the monomer, the sum of oligomers up to 3, up to 10, and the sum of all free oligomers as a function of the number of unbroken bonds per ring cluster α , where $\alpha = 1/2 p (\sigma + 1)$. If σ remains constant during pyrolysis, the molecular weight distribution is a single valued function of α . For ring clusters of molecular weight 300 amu, the sum of 1 to 3 oligomers corresponds roughly to the potential tar fraction (up to 900 amu), the sum of 1-10 corresponds to the extractable fraction (up to 3000 amu), and the sum of all oligomers corresponds to the liquids fraction (all free oligomers). It can be seen that with increasing σ , more broken bonds are required to achieve equivalent fractions of free oligomers. Also the relative amounts of tar, extracts, and liquids vary with σ .

NETWORK GEOMETRIES REPRESENTATIVE OF COAL - The three important parameters of the network are the average ring cluster size M_{avg} , the coordination number ($\sigma + 1$), and the starting probability, p_0 . For comparing networks of different coordination numbers, it is convenient to use α rather than p .

Ring Cluster Size - Ring cluster sizes have been estimated from NMR alone (40), NMR and FT-IR (41), mild degradation (42), and molecular weight distribution of tar (15,16,29). Based on these results, the average ring cluster size for coals with less than 90% carbon is expected to be between 2 and 3 aromatic rings or a total molecular weight per cluster including peripheral groups of 200-400 amu.

DISARAY assumes a value of 1400 amu for the monomer which can split into two 700 amu tar fragments. CPD does not specify the monomer molecular weight. For coals with less than 90% carbon, FG-DVC employs a distribution of monomers with an average M_{avg} of 256 amu.

Coordination Number - Information on the coordination number comes from estimates from solvent swelling measurements of the average molecular weight between crosslinks, M_c (2-9) and recent estimates made using NMR of the number of non-peripheral group attachments to the cluster (40). The M_c determinations suggest that there are between 4 and 8 repeating units between crosslinks (or branch points). This indicates a value for $\sigma + 1$ between 2.13 and 2.25. The NMR data suggest that there are between 2 and 3 bridge or loop attachments per cluster (see Fig. 8 of Ref. 40). This suggests $\sigma + 1$ is between 2 and 3. Based on these two above measurements, the coordination number for the starting coal for describing the break up of the network by bridge cleavage should be less than 3, and probably between 2.2 and 2.5. A different value of $\sigma + 1$ might be appropriate for describing crosslinking as discussed later.

To model a high volatile bituminous coal, the different models used networks with $(\sigma + 1) = 3.25$ (DISARAY), 4.6 (CPD), and ≈ 2.1 (FG-DVC).

Initial Bond Population - The starting macromolecular network for FG-DVC is chosen to match the measured extract yield and molecular weight between crosslinks by picking two parameters: i) the length of the oligomer chain, ℓ , ii) the number of initial crosslinks per monomer, m_0 . First m_0 is picked such that $m_0 = M_{avg}/M_c$ where M_{avg} is the average monomer molecular weight and M_c is the molecular weight between crosslinks determined from solvent swelling (2-9). Then ℓ is chosen so that when the molecule is randomly constructed, the weight percent of oligomers less than 3000 amu matches the measured extract yield. There is the implicit assumption that the extract yield is due to the unpolymerized fraction of a homogeneous network. Exinites and polymethylenes should really be treated as separate components but are not. The initial value of α is approximately $((\ell - 1)/\ell + m_0)$ which for the Pittsburgh Seam coal modeled in Ref. (29) is $\alpha_0 \approx 0.95$. This initial

value is indicated in Fig. 3a.

In DISARAY, $\sigma + 1$ is set equal to 3.25 and p_o is set equal to 1 ($\alpha_o = 1.63$). This is illustrated in Fig. 3b.

The starting macromolecular network in the CPD model is chosen by picking two parameters: i) the coordination number $\sigma + 1$, picked to match the average number of attachments (bridges and peripheral groups) per ring determined by NMR (30,40); and ii) p_o , the starting probability of unbroken bonds. For the high volatile bituminous coal simulated in Ref. (30) $\sigma + 1 = 4.6$, $\alpha_o = 1/2 p_o (\sigma + 1) = 1.36$. This initial value is indicated in Fig.3c.

PROCESSES CONTROLLING THE NETWORK DECOMPOSITION

BOND BREAKING AND HYDROGEN UTILIZATION - Both the FG-DVC and CPD models assume similar (within a factor of 3) bond breaking rates, $0.86 \times 10^{15} \exp^{-65,400/RT} \text{ sec}^{-1}$ for FG-DVC[†] and $2.6 \times 10^{15} \exp^{-65,400/RT} \text{ sec}^{-1}$ for CPD. Both models employ rank independent kinetics. The FG-DVC model rate was determined in experiments in which particle temperatures were directly measured (43). The rate was recently confirmed within a factor of 2 by Fletcher et al. in a second experiment which directly measures particle temperatures (44).

There are some minor differences in FG-DVC and CPD assumptions for bond breaking. The FG-DVC model includes three kinds of bonds: labile bridges, unbreakable bridges, and crosslinks. For each broken labile bridge, FG-DVC requires that hydrogen be available to stabilize the free radicals. It is assumed that all the donatable hydrogen (aliphatic plus hydroaromatic) is located in the labile bridges, so that only half the labile bridges can break with the other half becoming unbreakable with the donation of their hydrogen (i.e., there is a 1:1 ratio between bond breaking and the formation of additional unbreakable bridges). The weight fraction of the initial bridges in the chain of length ϵ which are labile is given by the parameter W_B ; the rest are assumed to be unbreakable bonds. W_B is a fitting parameter chosen to make the model fit the pyrolysis data.

In a similar manner, in CPD, there are both unbreakable bridges with probability c_o and labile breakable bridges with probability d_o ($d_o + c_o = p_o$). As pyrolysis proceeds, the labile bridges can break and react by two possible routes to form unbreakable "char" bridges or broken bridges. CPD assume a 0.9:1.0 ratio for the ratio of bond breaking to char bridge formation. That assumption is almost identical to the FG-DVC 1:1 ratio required for hydrogen availability.

The DISARAY model assumes a bridge disassociation rate of $6 \times 10^8 \exp^{-30,000/RT} \text{ sec}^{-1}$ [†] which can produce monomers. The monomers subsequently decompose at $1.4 \times 10^7 \exp^{-31,000/RT} \text{ sec}^{-1}$ to form tar. These rates have activation energies which appear to be too low to describe chemical processes.

CROSSLINKING - CPD does not assume any crosslinking processes. The char forming processes are only those occurring as one possible end of the bridge breaking reaction.

DISARAY assumes char formation occurs at a rate $2 \times 10^8 \exp^{-24,600/RT}$. Char formation is assumed to occur by monomers attaching to the original lattice or to each other.

FG-DVC assumes two independent crosslinking reactions, in addition to the unbreakable bond formation accompanying hydrogen donation. One occurs at low temperature (below that for bond breaking) for low rank coals and is associated with oxygen functional groups (COOH or OH) and probably CO_2 evolution (11,12,45). Crosslinking also occurs at moderate temperatures, slightly higher than bond breaking and appears to be associated with the evolution of CH_4 or other peripheral groups (e.g., ethyl, propyl).

MASS TRANSPORT - A combination of chemistry and mass transport controls the production of the tar in pyrolysis. The motivation for including mass transport processes in tar formation is the observation that tar yields are strongly influenced by external pressure (29,46,47).

[†] both FG-DVC and DISARAY employ distributed activation energy expressions. The rates quoted above are for the center of the distribution

In FG-DVC, the Monte Carlo calculation is employed to determine the molecular weight distribution in the decomposing char. Then a mass transport equation is applied to determine the probability of the light n-mers evolving as tar. The transport equation assumed that a molecular weight dependent vapor pressure controls the appearance of these molecules in the gas phase and that they escape the coal particles by convective transport of the gas (29). Tar is thus the light end of the molecular weight spectrum, i.e., those with sufficiently high vapor pressures. This produces tar with number average molecular weights of 300-400 amu and maximum weights of 800-1000 amu. Thus in FG-DVC, tar is approximately the sum 1-3 in Fig. 3a. Extractable material is defined as all molecules up 3000 amu (sum 1-10) and liquids are defined as all molecules not attached to the starting molecule.

In DISARAY, tar is defined as half the monomer, and the monomer is taken as 1400 amu. So the tar would be defined as some fraction of the monomer curve in Fig. 3b.

No transport equations were employed in CPD. Tar was defined as all molecules not attached to the infinite lattice. Thus tar is represented by the highest line in Fig. 3c.

One advantage of the Monte Carlo method over the percolation theory is that when tar is produced, molecules can be removed from the network. In percolation theory, there is no mechanism for removing molecules from the network. If there are crosslinking events, as in FG-DVC, all the small molecules can reconnect to the network. CPD avoids this problem by excluding any independent crosslinking which would reconnect oligomers. This presents the limitation that independent crosslinking and mass transport cannot be treated with the exact percolation theory expressions.

EXAMPLES OF MODEL CALCULATIONS

FORMATION OF PYROLYSIS PRODUCTS - The evolution of the macromolecular network in the CPD model is illustrated in Fig. 4. Figure 4a shows the percolation theory predictions for the total of unattached oligomers (defined to be the tar) as a function of α . The coal is represented at $\alpha_0 = 1/2 p_0 (\sigma + 1) = 1.36$. During pyrolysis the labile bridges form either broken bridges or unbreakable char bridges in the ratio 0.9 to 1.0. Figure 4b shows how α changes during pyrolysis. Pyrolysis proceeds until α_{\min} is reached where $\alpha_{\min} = 1/2 (\sigma + 1) (c_0 + (1.0/1.9)\delta_c) = 0.83$. Thus the change in α during pyrolysis was 0.53.

The evolution of the macromolecular network for FG-DVC computed using the Monte Carlo method for a bituminous coal is illustrated in Fig. 5. Figure 5a shows the calculated extract yield as a function of α . The initial probability of unbroken bridges, α_0 , starts out at close to 1.0 to produce the measured extract yield (30%). Figure 5b shows the computed value of α with its contributions from the initial crosslinks m_0 , the conversion of labile bridges to broken bonds and unbreakable bonds and the added crosslinks. For the bituminous coal, the added crosslinks are almost all due to CH_4 related processes. Note that α goes back up in the FG-DVC model to resolidify the lattice. This is necessary to model fluidity effects (31).

Results of the FG-DVC model applied to a lignite are presented in Fig. 6. The formation of CO_2 crosslinks prevents α from being reduced and no additional extract is produced.

UTILIZATION OF DONATABLE HYDROGEN - As discussed above, W_B , the initial fraction of labile bridges is a parameter of the FG-DVC model. This parameter is related to the fraction of donatable hydrogen by $H(d) = 2/28 W_B$; i.e., there are two donatable hydrogens per labile bridge. This parameter has a strong affect on α_{\min} and hence the yield of tar, extracts, and liquids.

There are two ways to estimate the amount of hydrogen donated. During pyrolysis, the donation of hydrogen converts two aliphatic or hydroaromatic hydrogens into a donated aliphatic hydrogen plus a newly formed aromatic hydrogen. We can measure both the increase in aromatic hydrogen in the pyrolysis products and the increase in aliphatic hydrogen in the tar using quantitative FT-IR analysis (48,49). The results for a Pittsburgh Seam coal are summarized in Fig. 7. They show that the aromatic hydrogen in the total pyrolysis products increased from 2.1 to 2.4% or an increase of 0.3% on a starting coal basis. This increased aromatic content is all in the char. The aromatic content in the tar remains about the same. The tar, which is approximately 30% of the starting coal increases

its aliphatic hydrogen content by about 1% or 0.3% on the starting coal basis. The two numbers are thus consistent; 0.6% donatable hydrogens in the coal are converted to 0.3% new aromatics plus 0.3% donated aliphatics. If it is assumed that a monomer has a molecular weight of 300 amu, then one breakable bridge per monomer with four aliphatic carbons is 1.33% donatable hydrogen. Half the bridges can break (0.67%) and the other half can donate hydrogen (0.67%) in reasonable agreement with the experimentally estimated value of 0.6% hydrogens actually donated. The value assumed in FG-DVC for H(d) for the Pittsburgh Seam coal is 0.67% (29).

The value of H(d) has implications for the CPD model, if $\Delta\alpha$ is limited to 0.33 rather than 0.53, then the value of $\sigma + 1$ would have to be reduced to match the data. Also, the average molecular weight for the unattached molecules is too high to be identified as tar. If a more reasonable definition of tar is used (e.g., the sum of oligomers up to 3) then $\sigma + 1$ would have to be reduced still further.

COMPARISON OF MONTE CARLO CALCULATION WITH PERCOLATION THEORY - To further illustrate some of the differences between the FG-DVC Monte Carlo model and percolation theory calculations, the extract yield calculated for a case similar to that in Fig. 5a, but with tar evolution not permitted is plotted in Fig. 8 along with the predictions of percolation theory for several values of α . The FG-DVC Monte Carlo predictions are not a single valued function of α . As pyrolysis proceeds, the increase in extract yield follows $\sigma + 1 \approx 2.2$ while the decrease in extract yield follows $\sigma + 1 \approx 4$.

It is important to know whether this result is an artifact of the Monte Carlo calculation or a real feature of pyrolysis. Based on what is happening in pyrolysis, the result does make sense. For a bituminous coal, the initial process occurring in pyrolysis is bond breaking. This occurs by breaking bridges in the network described by $\sigma + 1$ between 2.1 and 2.5. No crosslinking is occurring initially as the solvent swelling ratio is observed to increase during this period (45). Eventually crosslinks start forming, resulting in an increase in the coordination number and in α . The network thus cannot adequately be described by a single coordination number. There is a coordination number for labile bridges and a separate coordination for crosslinks. This observation motivated the development of a more general percolation network with two coordination numbers discussed below.

LATTICE MODEL WITH TWO BOND TYPES

Two- σ Model - In order to deal with a structure with a time dependent coordination number, we consider a Bethe lattice with two types of bonds, with coordination numbers and probabilities of occupation given by $\sigma_1 + 1$, p and $\sigma_2 + 1$, q for the two types, respectively. Such a lattice for $\sigma_1 = \sigma_2 = 1$ is illustrated in Fig. 9. The analysis can be carried through using the same procedures as Fisher and Essam (39) or Ref. 30, but with extensions to deal with the extra variables. The probability $F_{s,u}(p,q)$ that a site is a member of a cluster of n sites with s type 1 bridges and u type 2 bridges is given by

$$F_{s,u}(p,q) = a_{s,u} p^s (1-p)^\tau q^u (1-q)^\nu \quad (1)$$

where

$$\begin{aligned} n &= u + s + 1 \\ \tau &= (\sigma_1 + 1) n - 2s \\ \nu &= (\sigma_2 + 1) n - 2u \end{aligned} \quad (2)$$

and τ , ν are the number of broken bridges of type 1 and 2, respectively, on the perimeter of the cluster, and $a_{s,u}$ is the number of different ways to form such a cluster. Following the same procedure used by Fisher and Essam, we can derive an expression for the configuration coefficient

$$a_{s,u} = \left(\frac{\sigma_1 + 1}{s + \tau} \frac{\sigma_2 + 1}{u + \nu} \right) \binom{s + \tau}{s} \binom{u + \nu}{u} (u + s + 1) \quad (3)$$

Note that for $u = 0$ (no type 2 bonds), this reduces to the quantity nb_n in Ref. (30). To determine the probability, $F_n(p,q)$ that a given site is a member of a cluster of n sites, i.e., the fraction of n-mers, we must sum Eq. 1 over all possible values of s and u that give an n-site cluster:

$$F_n(p,q) = \sum_{s=0}^{n-1} a_{s,u} p^s (1-p)^r q^u (1-q)^y; \quad u = n - s - 1 \quad (4)$$

The total fraction of sites, $F(p,q)$ in finite clusters is the sum over all s and u

$$F(p,q) = \sum_{s=0}^{\infty} \sum_{u=0}^{\infty} F_{s,u}(p,q) = \left(\frac{1-p}{1-p^*} \right)^{\sigma+1} \left(\frac{1-q}{1-q^*} \right)^{\sigma+1} \quad (5)$$

where p^* and q^* are obtained by finding the least roots of

$$\begin{aligned} p^* (1-p^*)^{\sigma-1} (1-q^*)^{\sigma+1} - p(1-p)^{\sigma-1} (1-q)^{\sigma+1} &= 0 \\ q^* (1-q^*)^{\sigma-1} (1-p^*)^{\sigma+1} - q(1-q)^{\sigma-1} (1-p)^{\sigma+1} &= 0 \end{aligned} \quad (6)$$

The critical point, where an infinite lattice begins to form (i.e., $F(p,q)$ begins to decrease) becomes a critical curve which divides the p - q plane into two regions. Note that for $q = 0$, the equations all reduce to the single σ case given in Ref. 30.

Application of Two- σ Model - Figure 10 presents a comparison of the prediction for pyrolysis assuming the FG-DVC chemistry using: a) the Monte Carlo calculation, b) the two- σ percolation calculations ($\sigma_1 = 1, \sigma_2 = 1$) and c and d) two cases of the one- σ percolation calculation ($\sigma = 2.2$ and $\sigma = 3.2$). The calculations are made under the assumption that no tar is evolved. The tar values in Fig. 10 are the sum of 1-3 n-mers remaining in the char. The Monte Carlo calculation in Fig. 10a is matched best by the two- σ model if liquids are assumed to be the sum of the first 100 n-mers (i.e., up to 300,000 amu). The two- σ model has a reasonable value for the initial extract yield but predicts slightly more initial tar. Neither of the one- σ cases is a good match. Use of $\sigma = 2.2$ is good at low temperature but over predicts the maximum values of extracts and liquids. Use of $\sigma = 3.2$ does a much better job on predicting the maximum values but the initial ratio of tar to extract is not consistent with what is observed for coal and the rate of increase of n-mers is too slow. It thus appears that the two- σ model can be used instead of the Monte Carlo calculations when no tar is evolved, while one- σ calculations are less accurate.

The real test, however, is how well the models fit the data for coal. A comparison of tar yield is not a sufficient test since α_0 and $\Delta\alpha$ can always be selected in conjunction with the network geometry to fit the data. A critical test requires a careful comparison of how α_0 and $\alpha(t)$ match with measurement of functional group changes in the char (e.g., the transformation of hydrogen functional groups and bridges), solvent swelling behavior (i.e., crosslink density), and the complete molecular weight distribution as reflected in the amounts of tar, extracts, and fluidity.

COMPARISON OF NETWORK MODELS

A summary of the processes predicted by the three recent network models, CPD, DISARAY and FG-DVC is presented in Table I. All the models predict their primary objective, the variations in tar and gas yield with time and temperature. All three are capable of predicting variations of tar yield with heating rate, but CPD has not yet done this. All three models are capable of predicting the complete molecular weight distributions of fragments, but only FG-DVC uses this information to predict the extract yield, the tar yield and the tar molecular weight distribution. DISARAY uses only the prediction for monomers (defined as tar precursor) and CPD uses only the prediction for all oligomers (defined as tar). In a paper presented at this conference, the total oligomer population computed by the FG-DVC model is used to predict coal fluidity behavior (31). Only FG-DVC employs a mass transport equation which is necessary to predict tar molecular weights and the variations of yield and molecular weights with pressure. Only FG-DVC predicts the solvent swelling ratio.

CONCLUSIONS

- 1) The extension of macromolecular network concepts to describe coal thermal decomposition

appears to be very successful and versatile in allowing the prediction of tar, extract yield, and total liquids.

- 2) A complete model requires a description of: i) labile bridge breaking with hydrogen utilization; ii) rank dependent crosslinking processes; and iii) mass transport.
- 3) Monte Carlo methods for computing the network statistics are the most versatile but are computationally demanding.
- 4) The use of percolation theory is computationally efficient and helps provide insight into network behavior, but the use of a fixed coordination number may be inadequate to accurately describe coal thermal decomposition. The network appears to require a coordination number between 2.2 and 2.5 for labile bridge breaking and greater than 3 for crosslinking.
- 5) An expanded percolation theory for a network with two coordination numbers was developed.
- 6) When the two- σ percolation model is applied using the FG-DVC chemistry to cases in which tar is not removed, it gives results which are comparable to the Monte Carlo calculation. Applying percolation theory to cases where tar is removed requires additional approximations.
- 7) Of the three models which were compared (CPD, DISARAY, and FG-DVC), FG-DVC is the most complete in treating the molecular weight of network fragments and vaporization and mass transport to define tar, tar molecular weight distribution and extract yield.
- 8) Of the three models, FG-DVC is the most closely related with the previous concepts of coal as a macromolecular network by requiring that the network predict the coal and, char solvent swelling ratios and measured extract yields. The assumption which define the parameters of the starting network are open to question and must be explored.
- 9) Future effort should focus on identifying the chemistry for the processes of bond breaking, low temperature crosslinking, moderate temperature crosslinking, and hydrogen utilization.

ACKNOWLEDGEMENT

The authors gratefully acknowledge the support for the work provided by the Morgantown Energy Technology Center of the Department of Energy under Contract No. DE-AC21 86MC23075.

REFERENCES

1. Van Krevelen, D.W., Coal, Elsevier, Amsterdam, (1961).
2. Green, T.K., Kovac, J., and Larsen, J.W., *Fuel*, **63**, 935 (1984).
3. Green, T.K., Kovac, J., and Larsen, J.W., in "Coal Structure," R.A. Meyers, Ed., Academic Press, NY (1982).
4. Lucht, L.M. and Peppas, N.A., *Fuel*, **66**, 803, (1987).
5. Lucht, L.M., Larsen, J.M., and Peppas, N.A., *Energy & Fuels*, **1**, 56, (1987).
6. Larsen, J.W., *ACS Fuel Chem. Div. Preprints*, **30**, (4), 444, (1985).
7. Green, T., Kovac, J., Brenner, D., and Larsen, J., Coal Structure, (R.A. Meyers, Ed.), Academic, NY, p 199, (1982).
8. Hall, P.J., Marsh, H., and Thomas, K.M., *Fuel*, **67**, 863, (1988).
9. Sanada, Y. and Honda, H., *Fuel*, **45**, 295, (1966).
10. Suuberg, E.M., Yoshi, O., and Deevo, S., *ACS Div. of Fuel Chem. Preprints*, **33**, (1), 387, (1988).
11. Suuberg, E.M., Lee, D., and Larsen, J.W., *Fuel*, **64**, 1668, (1985).
12. Suuberg, E.M., Unger, P.E., and Larsen, J.W., *Energy & Fuels*, **1**, 305, (1987).
13. Brown, J.K., Dryden, I.G.C., Dunevein, D.H., Joy, W.K., and Pankhurst, K.S., *J. Inst. Fuel*, **31**, 259, (1958).
14. Orning, A.A. and Greifer, B., *Fuel*, **35**, 318, (1956).
15. Solomon, P.R. and Hamblen, D.G., Chemistry in Coal Conversion, (R.H. Schlosberg, Ed.),

- Plenum, New York, p. 121, Chapter 5, (1985).
16. Solomon, P.R., New Approaches in Coal Chemistry, ACS Symposium Series 169, ACS, Washington, DC p. 61, (1981).
 17. Solomon, P.R., and King, H.H., *Fuel*, **63**, 1302, (1984).
 18. Gavalas, G.R., Coal Pyrolysis, Elsevier, NY, p. 51, (1982).
 19. Gavalas, G.R., Cheong, P.H., and Jain, R., *Ind. Eng. Chem. Fundam.*, **20**, 122, (1981).
 20. Squire, K.R., Solomon, P.R., Carangelo, R.M., and DiTaranto, M.B., *Fuel*, **65**, 833, (1986).
 21. Squire, K.R., Solomon, P.R., DiTaranto, M.B., and Carangelo, R.M., *ACS Di. of Fuel Chem. Preprints*, **30**, (1), 386, (1985).
 22. Solomon, P.R., Squire, K.R., and Carangelo, R.M., *Proceedings of the Int. Conf. on Coal Science*, Pergamon: Sydney, Australia, p. 945, (1985).
 23. Solomon, P.R., and Squire, K.R., *ACS Div. of Fuel Chem. Preprints*, **30**, (4), 347, (1985).
 24. Niksa, S., and Kerstein, A.R., *Combustion and Flame*, **66**, 95, (1986).
 25. Niksa, S., *Combustion and Flame*, **66**, 111, (1986).
 26. Solomon, P.R., Hamblen, D.G., Deshpande, G.V. and Serio, M.A., A General Model of Coal Devolatilization, International Coal Science Conference, The Netherlands, October 1987.
 27. Solomon, P.R., Hamblen, D.G., Carangelo, R.M., Serio, M.A., and Deshpande, G.V., *Combustion and Flame*, **71**, 137, (1988).
 28. Niksa, S. and Kerstein, A.R., *Fuel*, **66**, 1389, (1987).
 29. Solomon, P.R., Hamblen, D.G., Carangelo, R.M., Serio, M.A. and Deshpande, G.V., *Energy and Fuels*, **2**, 405, (1988).
 30. Grant, D.M., Pugmire, R.J., Fletcher, T.H., and Kerstein, A.R., *Energy & Fuels*, **3**, 175, (1989).
 31. Solomon, P.R., Best, P.E., Yu, Z.Z., and Deshpande, G.V., "A Macromolecular Network Model for Coal Fluidity", *ACS Div. of Fuel Chem. Preprints*, **34**, paper presented at this meeting, (1989).
 32. Nielsen, L.E., Mechanical Properties of Polymers and Composites, Vol. 2, Marcel Dekker, Inc. NY, (1974).
 33. Bartels, C.R., Crist, B., Felters, L.J., and Graessley, W.W., *Macromolecules*, **19**, 785, (1986).
 34. Nazem, F.F., *Fuel*, **59**, 851, (1980).
 35. Macosko, C.W., *Brit. Polymer Journ.*, **17**, 239, (1985), and references therein.
 36. Flory, P.J., *J. Am. Chem. Soc.*, **63**, 3083, 3097, (1941); see also Principles of Polymer Chemistry, Cornell University Press, Ithaca, NY, Chapter 9, (1953).
 37. Stockmayer, W.H., *J. Chem. Phys.*, **11**, 45, (1943); also **12**, 125, (1944).
 38. Serio, M.A., Solomon, P.R., Yu, Z.Z., Deshpande, G.V., and Hamblen, D.G., *ACS Div. of Fuel Chem. Preprints*, **33**, (3), 91, (1988).
 39. Fisher, M.E., and Essam, J.W., *J. Math. Phys.*, **2**, 609, (1961).
 40. Solum, M., Pugmire, R.J., and Grant, D.M., *Energy & Fuels*, **3**, 40, (1989).
 41. Gerstein, B.C., Murphy, D.P., and Ryan, L.M., Coal Structure, (R.A. Meyers, Ed.), Academic Press, NY, p. 87, Chapter 4, (1982).
 42. Hooker, D.T., II, Lucht, L.M., and Peppas, N.A., *Ind. Eng. Chem. Fundam.*, **25**, 103, (1986).
 43. Solomon, P.R., Serio, M.A., Carangelo, R.M., and Markham, J.R., *Fuel*, **65**, 182, (1986).
 44. Fletcher, T.H., "Time Resolved Temperature Measurements of Individual Coal Particles During Devolatilization", Submitted to *Combustion Science and Technology*.
 45. Deshpande, G.V., Solomon, P.R., and Serio, M.A., *ACS Div. of Fuel Chem. Preprints*, **33**, (2), 310, (1988).
 46. Unger, P.E. and Suuberg, E.M., 18th Symposium (Int) on Combustion, The Combustion Institute, Pittsburgh, PA, p. 1203, (1981).
 47. Suuberg, E.M., Unger, P.E., and Lilly, W.D., *Fuel*, **64**, 956, (1985).
 48. Solomon, P.R. and Carangelo, R.M., *Fuel*, **61**, 663, (1982).
 49. Solomon, P.R. and Carangelo, R.M., *Fuel*, **67**, 949, (1988).

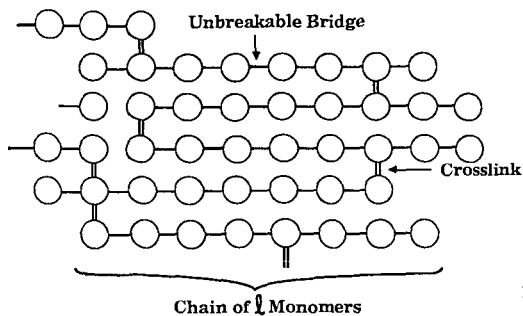


Figure 1. Macromolecular Network Used in Monte Carlo Simulation.

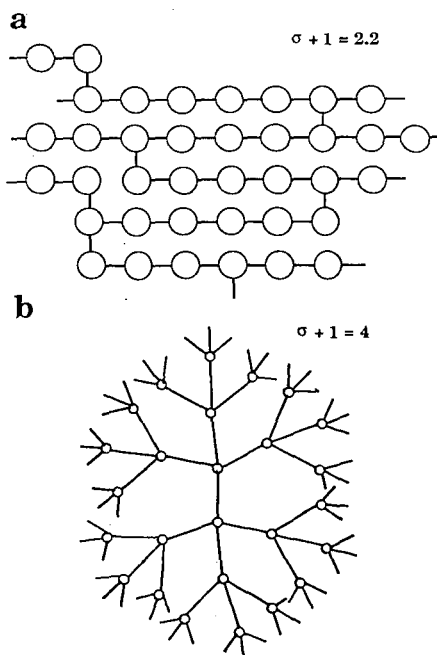


Figure 2. Bethe Lattice for a) Coordination Number 2.2 and b) Coordination Number 4.

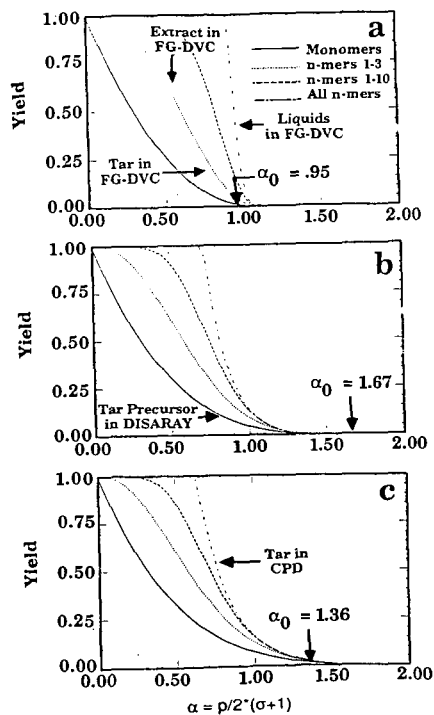


Figure 3. Percolation Theory Predictions for Pyrolysis Products (monomers, tar, extracts and total liquids) for Three Values of the Coordination Number ($\sigma + 1$). a) $\sigma + 1 = 2.2$, b) $\sigma + 1 = 3.25$ and c) $\sigma + 1 = 4.6$.

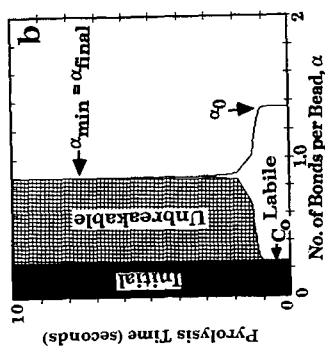
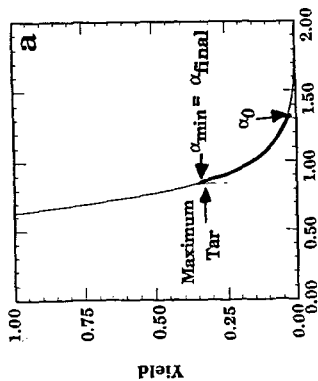


Figure 4. Tar Yield for a Bituminous Coal by the CPD Model. a) Tar Yield vs. α , b) Variation in α with Time Heating at 450°C/min to 936K.

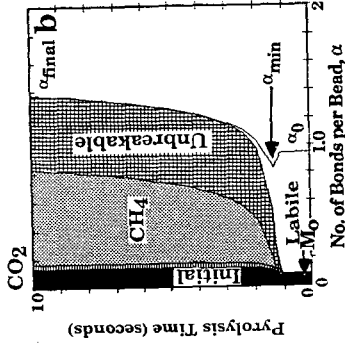
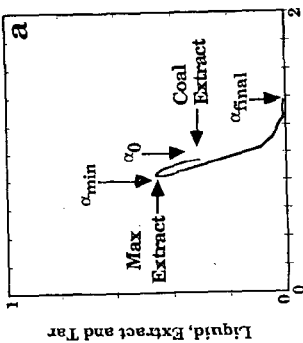


Figure 5. Extract Yield for a Bituminous Coal Predicted by the FG-DVC Model. a) Extract Yield vs. α and b) Variation in α with Time Heating at 450°C/min to 936K.

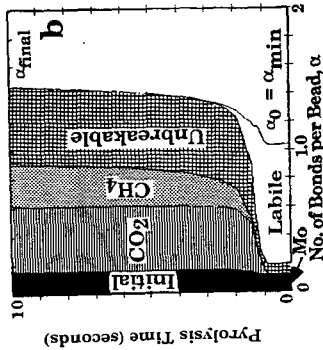
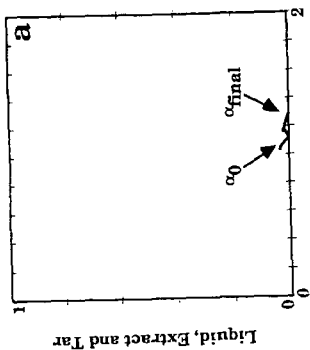


Figure 6. Extract Yield for a Lignite Predicted by the FG-DVC Model. a) Extract Yield vs. α and b) Variation in α with Time Heating at 450°C/min to 936K.

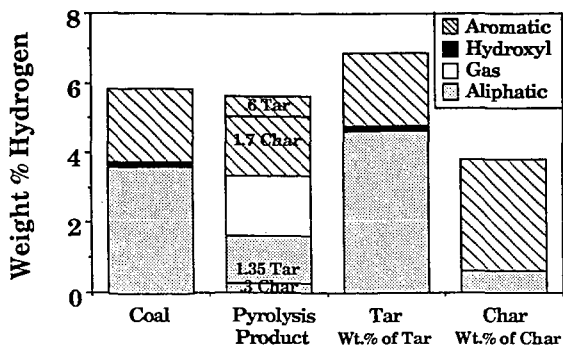


Figure 7. Distribution of Hydrogen in Coal and Pyrolysis Products. Pyrolysis Produced Approximately 53% Char, 30% Tar and 21% Gas.

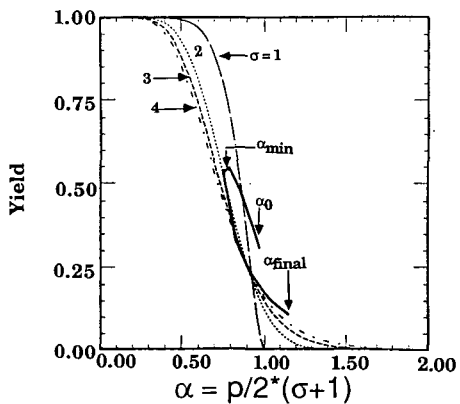


Figure 8. Comparison of Extract Yield in FG-DVC Model with Percolation Theory for $\sigma = 1, 2, 3$ and 4 . FG-DVC is for Pittsburgh Seam Coal Heated at $450^\circ\text{C}/\text{sec}$ to 936K with No Tar Evolved.

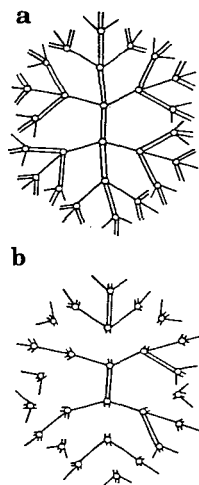


Figure 9. Bethe Lattice for Two- σ Model with $\sigma_1 = 1$ (shown as single bonds) and $\sigma_2 = 1$ (shown as double bonds). a) Fully Linked Case ($p = q = 1$) is Like One- σ Model with $\sigma = 3$. b) With Most Double Bands Representing the Crosslinks Not Yet Formed to Represent the Starting Coal. The Lattice is Like a One- σ Model with $\sigma = 1$, Linear Chains.

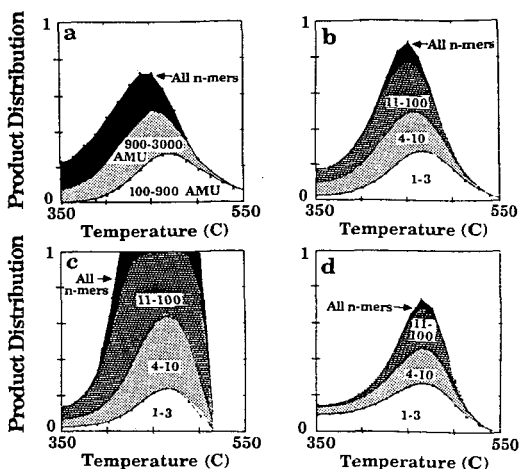


Figure 10. Comparison of Distribution of n -mers for Pyrolysis at 450°C/sec to 936K. a) Monte Carlo Calculation, b) Two- σ Model ($\sigma_1 = 1, \sigma_2 = 1$), c) One- σ Model ($\sigma = 1.2$) and d) One- σ Model, $\sigma = 2.2$.

Table 1 - Comparison of Network Models.

	CPD	DISARAY	FG-DVC Monte-Carlo or 2 σ	Relevant Model Process
Tar Yield vs Time	Yes	Yes	Yes	Bond breaking
Extract Yield vs Time	No ^a	No	Yes	Bond breaking
Gas Yield vs Time	Yes	Yes	Yes	From peripheral groups
Tar Yield vs Heating Rate	Not Yet	Yes	Yes	Relative rates of bond breaking and crosslinking
Variation of Tar Molecular Weight with Heating Rate	No	No	Yes	Relative rates of bond breaking and crosslinking
Molecular Weight of Tar	No	No	Yes	Mass transport Limitation
Tar Yields vs Pressure	No	No	Yes	Mass transport Limitation
Molecular Weight vs Pressure	No	No	Yes	Mass transport Limitation
Solvent Swelling of Char	No	No	Yes	Crosslinking

^a All oligomers are defined as tar

INTERPRETING COAL DEVOLATILIZATION AS A FLASH DISTILLATION DRIVEN BY COMPETITIVE KINETICS FOR DEPOLYMERIZATION AND REATTACHMENT

Stephen Niksa
Mechanical Engineering Department
Stanford University
Stanford, CA 94305

Alan R. Kerstein
Combustion Research Facility
Sandia National Laboratories
Livermore, CA 94550

Introduction

According to the most recent theories¹⁻⁴, the evolution rates, distribution, and molecular characteristics of the volatile products of coal devolatilization express the independent influences of chemical reaction rates and macromolecular configuration. Generally speaking, these approaches firm up the connections between the modeling species associated with the reactant and coal's structural features and functional groups inferred from chemical analyses. Obviously such connections are essential to systematic interpretations of the behavior of various coals. But chemical kinetics and configurational probabilities alone cannot account for the reduced tar yields and smaller tar fragments from devolatilization at elevated pressures. Reduced tar yields have long been attributed to redeposition of tar from the gas phase on the time scale for transport of volatiles through the particle surface, although an alternate scheme⁵ based on flash distillation correlates yields as well as tar molecular weight distributions (MWDs) without invoking any finite-rate, mass transport mechanism.

The theory introduced in this paper extends the development of models based on chemical kinetics, macromolecular configuration, and flash distillation, and is called FLASHCHAIN. Like DISCHAIN¹ and DISARAY², it comprises simplified kinetic mechanisms and analytical expressions to account for configurational effects, and to describe their evolution in time. However, the complete size distributions of all fragments are now determined. And like FLASHTWO³, this theory invokes a phase equilibrium among intermediates in the condensed phase and tar components in the vapor to rationalize the pressure dependence. Whereas the fragment distribution in FLASHTWO is assumed a priori, it is now computed from the configurational model.

In the sections which follow, the main features of the theory are outlined briefly, largely to explain the various modeling parameters. Then model correlations are presented for the devolatilization of high volatile bituminous coals, including the proportions of tar and noncondensable gases, and tar molecular weights for broad ranges of temperature, heating rate, reaction time, and pressure.

Overview of the Theory

Coal is modeled a distribution of linear chains composed of refractory aromatic nuclei interconnected pairwise by two types of linkages, labile bridges and refractory char links. The initial coal constitution is specified by the proportions of labile and broken bridges and char links, and the probability that peripheral groups appear on the ends of fragments. Initially and throughout pyrolysis, the condensed phase species are subdivided into reactant, intermediate, and metaplast lumps, in order of decreasing size.

Although the cutoff sizes are arbitrary, their proportions are described by analytical expressions for the complete size distribution as a function of the instantaneous numbers of bridges, char links, and ends. Consequently, for the initial coal reactant species, the sizes in the fragment distribution shift toward smaller values as the initial fraction of broken bridges is increased, and more of the coal appears as a lighter mobile phase which is taken to be the initial amount of metaplast.

Labile bridges either dissociate during pyrolysis or spontaneously decompose into char links. Consequently, bridge dissociation initiates two distinct reaction pathways, either to generate smaller fragments with new peripheral groups on the newly-created fragment ends, or to form a new char link and noncondensable gases. These pathways are designated as bridge scission and spontaneous condensation, respectively. Bridge scissions increase the amount of metaplast, at the expense of the reactant and intermediate, but spontaneous char formation tends to retain more of the coal mass in the heavier lumps, by lowering the number of sites available for fragmentation. Both reaction rates are based on the same Gaussian distribution of activation energies, and a stoichiometric coefficient specifies the selectivity between these two pathways.

Additional char links and noncondensable gases may also form by bimolecular recombination, but only within a restricted range of fragment sizes. Neither the reactant nor the intermediate species participate in bimolecular recombination, but nevertheless accumulate char links by spontaneous condensation. Recombinations among the ends of metaplast fragments produce additional char links, and also additional gases if peripheral groups are present on the ends which participate.

Tar formation is also developed from the metaplast only, using the flash distillation analogy; i. e., a phase equilibrium relates the instantaneous mole fractions of like fragments in the tar vapor and metaplast. Representing the equilibrium with Raoult's law for continuous mixtures characterizes the impact of fragment size on the phase change. While no finite mass transport rates appear, all volatile species are presumed to escape by a convective flow process, so that the evolution rate of tar is proportional to that of noncondensibles when weighted by the ratio of their respective mole fractions.

Tar quality is expressed in terms of its molecular weight distribution, and the proportions of peripheral groups, labile and refractory links, as a coarse scale for aromaticity. Tar quality varies throughout the process, due in part to the greater impact of bimolecular recombination during the later stages.

Guidelines for the Data Correlations and Model Parameters

Taken together, the four laboratory studies⁶⁻⁹ selected for the model evaluation depict the behavior for wide ranges of the relevant operating conditions, and all coal samples were Pittsburgh Seam HVA bituminous coals; ultimate and proximate analyses appear in the primary references. Among the results reported by Oh, only those which include tar yields and close the mass balance to within 5 wt% are included here. Wire-grid heaters in which the sample was dispersed in a layer which is only a few particles deep were used in all cases. Process temperatures were determined with fine-wire thermocouples and are regarded as the actual reaction temperature. One study featured forced rapid quenching, although decomposition during cooling is included in all simulations using the reported cooling rates.

All simulations in this study are based on the parameters in Table 1. The molecular weight of aromatic nuclei, and the MW ratios for bridges and peripheral groups were assigned from ¹³C NMR analyses of HVA bituminous coals¹⁰, to match the carbon

aromaticities and measured average molecular weights of noncondensibles (25g/g-mole). At the tabulated initial probability for all links, there is 9.4 wt % of metaplast in the reactant, which is similar to the amounts of THF extracts from such coals. All other values and the rate parameters were assigned to match the transient product distributions and tar molecular weights for atmospheric pyrolysis at 10^3 K/s. Once assigned, only the operating conditions of pressure, temperature, heating rate, and/or time were varied to match those in all other experiments. While the pressure is usually assigned as the ambient pressure, simulations of vacuum pyrolysis are based on a pressure of 0.025 MPa.

A simulation of each thermal history requires about 2 minutes on a 386 personal computer operating at 20 MHz, with an 8-Bit Fortran compiler.

Data Correlations

The predicted distribution of all reaction species for atmospheric pyrolysis is compared with measured weight loss and tar yields in Fig. 1. The thermal histories consist of uniform heating at 10^3 K/s to the stated temperatures immediately followed by cooling at 10^2 K/s. The correlations of both weight loss and tar yields are within the experimental uncertainty throughout. Note that the proportions of tar to gas decrease continuously, and that tar formation is completed by about 900K, but gas evolution persists through higher temperatures.

The largest fragments in the coal, the reactant lump, are rapidly converted into intermediates up to about 950K. Note that, due to spontaneous char formation, not all of the reactant fragments dissociate into either of the smaller lumps. The intermediate accumulates continuously, initially by fragmentation of the reactant and ultimately by bimolecular recombination of metaplast. The predicted amount of metaplast is maximized at 800K, then falls during the most rapid stage of tar evolution; its disappearance coincides with the end of tar formation.

The predicted number-average molecular weight of tar for vacuum and atmospheric pressure are compared with Oh's measurements in Fig. 2. The predicted values for vacuum are within the experimental uncertainty, but seem low by several percent for the atmospheric tars. Notwithstanding, the theory captures the observations that (1) the first tar fragments are somewhat lighter than the bulk of the tar fraction; and (2) increasing the pressure shifts the tar to substantially lower molecular weights. Both of these features are tied to the flash distillation mechanism. Although predicted distributions are omitted here, they all are of the form of Gamma-distributions.

Variations in the thermal history for nearly-atmospheric pyrolysis are examined in Fig. 3. These three cases depict the influence of extended reaction times at constant temperature following uniform heating, and variations in heating rate of three orders of magnitude. For the case of heating at 10^3 K/s with immediate quenching, the predictions are within the experimental uncertainty, except at the highest temperatures. The predicted impact of a 30 s reaction period at each temperature is qualitatively correct, in that most of the weight loss is observed at temperatures between 650 and 900K. But the predicted ultimate yields above 900 K are consistently lower than the data by about 6 wt %. As these investigators acknowledge, their ultimate yields are higher than the bulk of reported values for atmospheric pyrolysis, which are represented by the data in Fig. 1.

Similarly, the predicted variation due to lowering the heating rate from 10^3 K/s to 1K/s is qualitatively accurate, and also within the experimental uncertainty for temperatures up to 800K. But at higher temperatures the predicted weight loss is about 12% lower than the data. We have not yet determined that raising the predicted yields at

10³K/s would bring the predictions for 1K/s into quantitative agreement, although it would certainly improve the correlation.

This theory omits both gas-phase tar deposition and mass transport limitations which have long been regarded as the mechanistic basis for the pressure effect; instead, it relies on the phase equilibrium between metaplast and tar to retain more light fragments in the condensed phases as the pressure increases. This mechanism strongly influences the tar yields, especially at pressures up to several atmospheres. In Fig. 4, predicted tar yields at three pressures are validated by the available data.

An evaluation over a much wider pressure range, in Fig. 5, involves weight loss for extended reaction periods following heatup at 10³K/s to 1025K. The quantitative discrepancies for pressures less than 5 atm are generally within 5 wt % of the data. Perhaps more importantly, the predicted approach to a near-asymptotic weight loss at pressures above 10 atm is clearly consistent with the data. The predicted tar yields (not shown) decrease with increasing pressure, but remain substantial at the highest pressures; e. g., at 10 atm, the predicted tar yield is 16 wt%. Predicted gas yields increase with increasing pressure, in accord with an established trend.

Discussion

Qualitatively, this theory captures the influences of all of the important operating conditions on the devolatilization behavior of high volatile bituminous coals, and in most cases the quantitative agreement is within the experimental uncertainties. But its greatest potential lies in the formalism to rationalize the behavior of different coals. In this study, only the connection to the structural parameters from ¹³C NMR analyses has been demonstrated, and the general reliability of the predictions is encouraging. Future reports will evaluate the predicted behavior for variations in the parameters which describe the initial constitution of the coal.

Acknowledgement

We are happy to acknowledge the U. S. Department of Energy for financial support. Partial support for S. Niksa and the computational facilities were provided by the Advanced Research and Technology Development Program administered by the Pittsburgh Energy Technology Center. Partial support for A. R. Kerstein was provided by the Office of Basic Energy Sciences.

References

1. Niksa, S. and Kerstein, A. R., *Combust. Flame* 66:95 (1986).
2. Niksa, S. and Kerstein, A. R., *Fuel* 66:1389 (1987).
3. Solomon, P. R. et al., *Energy Fuels* 2:405 (1988).
4. Grant, D. M. et al., *Energy Fuels* 3:175 (1989).
5. Niksa, S., *AIChE J.* 34:790 (1988).
6. Oh, M. S., "Softening Coal Pyrolysis", Sc. D. thesis, Department of Chemical Engineering, MIT, 1985.
7. Gibbins-Maltham, J. and Kandiyoti, R., *Energy Fuels* 2:505 (1988).
8. Suuberg, E. M., Unger, P. E., and Lilly, W. D., *Fuel* 64:966 (1985).
9. Bautista, J. R., Russel, W. B., and Saville, D. A., *Ind. Eng. Chem. Fundam.* 25:536 (1986).
10. Solum, M. S., Pugmire, R. J., and Grant, D. M., *Energy Fuels* 3:187 (1989).

TABLE 1. MODEL PARAMETERS

Coal Characteristics		
MW of Aromatic Nuclei	186 g/g-mole	
MW Ratio, Bridges to Nuclei	0.785	
MW Ratio, Char Links to Nuclei	0.300	
MW Ratio, Peripheral Groups to Nuclei	0.134	
Initial Fraction of Total Links	0.912	
Initial Fraction of Labile Bridges	0.600	
Rate Parameters		
Reaction	A-Factor, s ⁻¹	Ea, kJ/mole
Bridge Dissociation	3×10^{11}	176 ($\sigma = 25$)
Recombination	4×10^{14}	209
Per. Group Elim.	1×10^{15}	230
Selectivity Coefficient for Bridge Scission 0.35		
$p_{\text{metaplast}}^{\text{SAT}}(T, \text{MW}) = 1.5 \times 10^3 \exp(-165 \text{MW}^{0.6}/T)$, MPa		

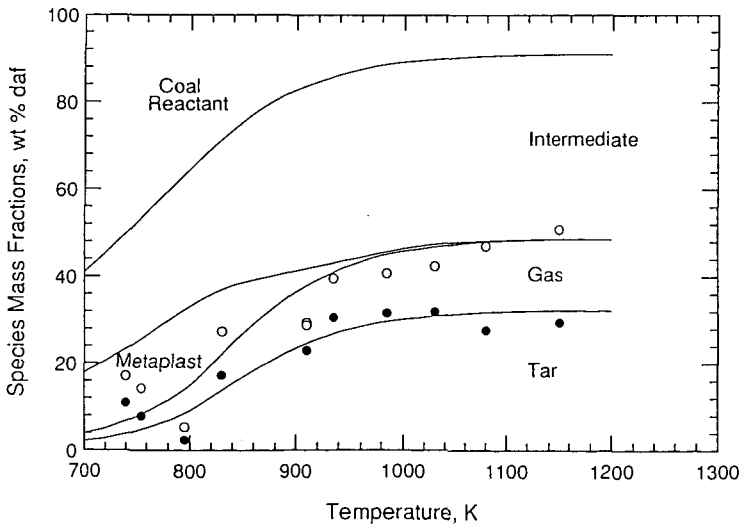


Fig. 1. The predicted distribution of reaction species for atmospheric pyrolysis for heating at 10³ K/s followed by immediate cooling at 100K/s, compared to Oh's⁶ measurements of weight loss and tar yields.

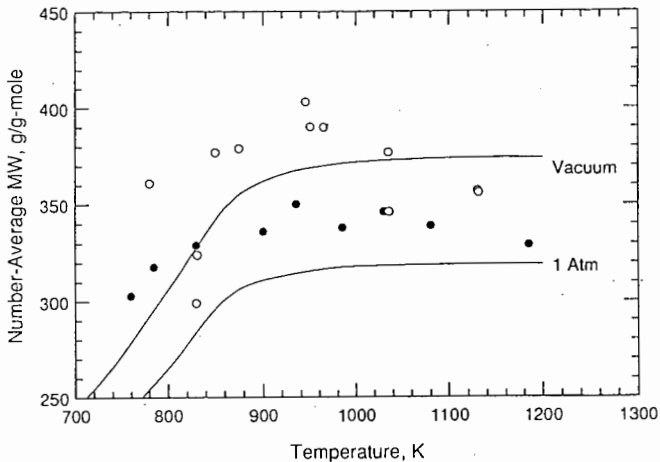


Fig. 2. An evaluation of the predicted number average molecular weights of tar for vacuum and atmospheric pyrolysis against Oh's⁹ GPC determinations. Thermal histories are the same as in Fig. 1.

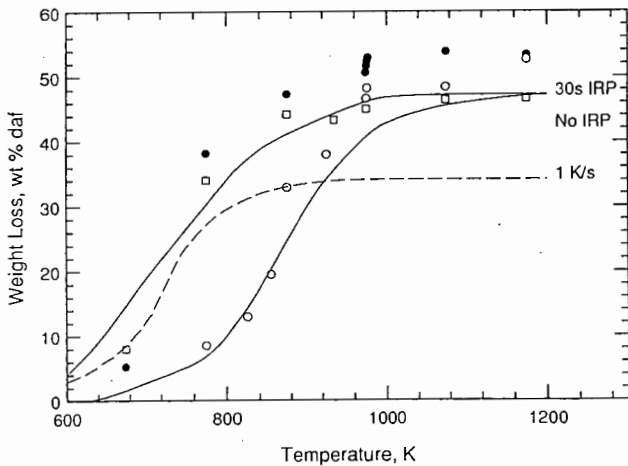


Fig. 3. An evaluation of the predicted weight loss for various thermal histories against the data recorded at 0.12 MPa⁷. Both solid curves are for a heating rate of 10³ K/s, with different reaction times at constant temperature of 30s (upper curve and filled circles) and 0s (open circles). The dashed curve and open squares depict the behavior at 1 K/s.

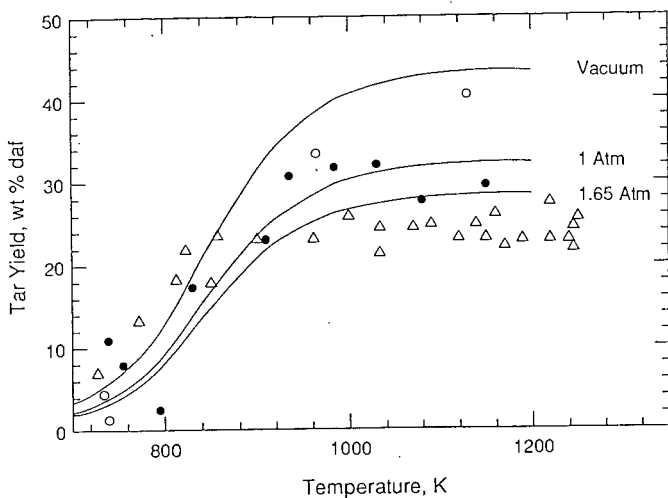


Fig. 4. An evaluation of the predicted tar yields for vacuum and atmospheric pyrolysis, with data from Oh⁶, and for pyrolysis at 0.165MPa, with data from Suuberg et al.⁸ The thermal histories are the same as in Fig. 1.

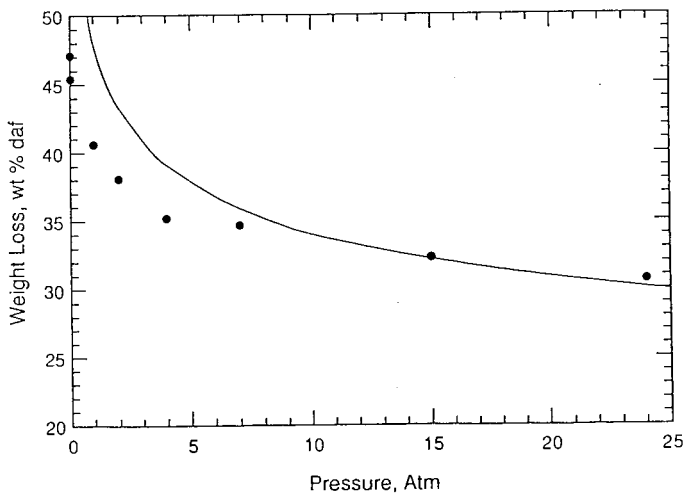


Fig. 5. An evaluation of the predicted weight loss at various pressures for heatup at 10³K/s to 1025K with 10s reaction times. The data are from Bautista et al.⁷

Approximating Rapid Pyrolysis of Coal Particles
with Shrinking Core Model

Mohammad R. Hajjaligol and Sung C. Yi
Philip Morris U.S.A.
Research Center, P.O.Box 26583
Richmond, Va 23112

INTRODUCTION

Coal pyrolysis is a complex phenomenon and when it is accompanied with rapid heating conditions, it becomes even more complex. A robust but mathematically simple approach is needed when such complexities are encountered. Literature on coal pyrolysis modeling are extensive. Part of this literature describes empirical approaches (1-2), while others include phenomenological and/or physico-chemical approaches (3-6) toward modelling this complex system. Due to these complexities the outcomes of the models appear to be more of a mathematical correlation than mechanistic relations. Accurate knowledge of pyrolysis temperature is one of the essentials in these studies. This becomes more dominant when heating rates approach extremely high values. According to Hajjaligol et al. (7,8) and others (2,9,15), at lower heating rates, pyrolysis occurs volumetrically and there exist conditions where pyrolysis is controlled by chemical kinetics. With higher heating rates pyrolysis becomes controlled by heat transfer to the particle that eventually enters an ablation regime (9). On the other hand there are indications that pyrolysis kinetics is influenced by heating rate (11). Since pyrolysis occurs at higher temperatures for higher heating rates, the mechanism of reaction might have been altered. These complexities have led some investigators to believe that pyrolysis has to be explained with a scheme different than chemical reactions (12).

The focus of this study is to show that for high heating rates ($> 10^5$ K/s), pyrolysis in a particle occurs according to a shrinking core model rather than a volumetric model in which temperature gradient is the driving force. Quite simply it is shown that temperature at pyrolysis front is different than that of particle surface temperature under this extreme heating condition. This temperature is uniquely dependent upon the pyrolysis kinetics, but not on the external heating conditions nor on the thermal properties of the particle. This study provides information on the primary pyrolysis kinetics of coal which can be estimated under these heating conditions.

MATHEMATICAL ANALYSIS

Pyrolysis is modelled for a single spherical coal particle which is pyrolyzed via a single first-order reaction with Arrhenius kinetics

$$\frac{dV}{dt} = (V^* - V) k_0 \text{EXP}(-E/RT) \quad (1)$$

Thermophysical properties of the particle can be constant or variable and depend on the temperature. Heat is transmitted into the particle by conduction. Other modes of heat transfer are shown to be less significant under these heating conditions. A standard heat balance on

the particle leads to the following governing partial differential equations

$$\rho C_p \frac{\partial T}{\partial t} = \frac{1}{r^2} \frac{\partial}{\partial r} (r^2 \lambda \frac{\partial T}{\partial r}) - \rho u C_p \frac{\partial T}{\partial r} + (-\Delta H) \rho (V^* - V) k_o \text{EXP}(-E/RT) \quad (2)$$

$$\frac{\partial \rho}{\partial t} = - \frac{1}{r^2} \frac{\partial}{\partial r} (r^2 \rho u) + \rho (V^* - V) k_o \text{EXP}(-E/RT) \quad (2a)$$

Equation (2) is solved numerically for the particle temperature field with following initial and boundary conditions. The initial condition is a uniform temperature, T_o , throughout the particle

$$T = T_o \text{ for } t \leq 0 \text{ and all } r \quad (3a)$$

The first boundary condition is the mathematical expression for center-line symmetry of the particle temperature field

$$\frac{\partial T}{\partial r} = 0 \text{ at } r = 0 \text{ for all } t \quad (3b)$$

Second boundary condition can be chosen as a heating rate condition greater than 10^5 K/s or a heat flux density greater than 100 watt at the surface to a desired final temperature as follows:

case a)

$$\begin{aligned} T &= T_o + mt & \text{at } r = R_p, t \leq t_1 \\ T &= T_s & \text{at } r = R_p, t > t_1 \end{aligned} \quad (3c)$$

case b)

$$\begin{aligned} -\lambda \frac{\partial T}{\partial r} &= q & \text{at } r = R_p, t \leq t_1 \\ T &= T_s & \text{at } r = R_p, t > t_1 \end{aligned} \quad (3d)$$

The solution to Equation (2) is prediction of the temperature field throughout the particle. This information is then used to compute the instantaneous conversion at any given point to monitor, (i) the pyrolysis front within the particle (points of > 98% conversion) (ii) the temperature where 98 % of conversion has been reached at that point, and (iii) the particle fractional conversion and the total pyrolysis time for the conversion.

RESULTS AND DISCUSSION

Either boundary condition prescribed by a heat flux density (3d) or a surface heating rate (3c) to provide a surface heating time of 1 ms. is used in the above analysis to predict pyrolysis behavior under these thermal conditions. Unless stated, the following numerical values were used for the analysis: $\rho=1.3\text{g/cm}^3$, $\lambda=0.0006 \text{ cal/cm-s-K}$, $C_p=0.4\text{cal/g-K}$, $\Delta H=1000\text{cal/g}$, $k_o=10^{13} \text{ sec}^{-1}$, and $E=50\text{Kcal/mole}$.

Figure 1 shows the effects of pyrolysis time on the radial position, and the shape of the pyrolysis front for a 100 μm diameter particle. It clearly demonstrates that under these heating conditions the region

where 98 % conversion has occurred is confined in a thin layer which moves inward with a velocity that depends on the thermo-chemical properties of the particle and external heating loads imposed on the particle. Figure 2 presents the effects of different surface temperatures for a given pyrolysis time on the shape and position of the pyrolysis front. As expected, the higher the surface temperature, the larger the driving force (ΔT), thus the higher the velocity of a pyrolysis front and the shorter the pyrolysis time. Figure 2 also shows that the shape of the pyrolysis front (region with 98 % conversion) does not change with the surface temperature. This is true unless the surface temperature drops below a threshold value.

Results from Figures 1, 2 as well as results for other particle diameters (up to 2 mm) show that regardless of the position of pyrolysis front, particle diameter and surface temperature, the temperature of the pyrolysis front is constant. As will be discussed further, when thermal properties of the particle were changed (λ , ΔH , etc.) or variable thermal properties were assumed or other heating rates (10^5 K/s) were applied, the temperature at the pyrolysis front (where 98 % conversion is reached) did not change. Analysis shows that this temperature (T_i) is a unique function of pyrolysis kinetics, i.e., if K_o or E were to change, the temperature would change accordingly. This is what we called threshold value for temperature.

All the above observations indicate that the pyrolysis under these circumstances could be approximated by a shrinking unreacted core model. Following Szekly et al. (13), but exchanging heat for mass diffusion in their description leads to

$$t = \left[k_o e^{-\frac{E}{RT_i}} \right]^{-1} p(x) + \frac{R_p^2 \rho \left[C_p (T_i - T_o) + \Delta H \right]}{\lambda (T_s - T_i)} g(x) \quad (4)$$

where $p(x)$ and $g(x)$ are given elsewhere (13). It can be shown that under rapid heating conditions, the first term on the right hand side (which describes the kinetic effects) is insignificant and thus pyrolysis is controlled by diffusional resistance (second term). In order to observe the validity of this hypothesis, a parametric study was conducted using Equation (2). The pyrolysis time for complete conversion was compared with that of Equation (4). Given T_s , E , K_o , and ΔH , when λ or R_p is varied, pyrolysis time will scale with λ and increase with the square of R_p (Figure 3). As can be seen this matches well with Equation (4). When ΔH or T_s varied, the results from Equation (2) did not match well with what predicted from Equation (4), although they did show the same trend (Figure 4). ΔH in the range of 0 to 1000 cal/g does not have a significant effect on Equation (2). This is due to the fact that under these heating conditions the ratio of heat transmitted into the particle to the heat consumed by the pyrolysis at the front is high. When higher values of ΔH (>10000 cal/g) were examined (a hypothetical case) the pyrolysis time and ΔH correlation would come out the same from both Equations (2) and (4). Part of the heat which is transmitted into the particle will also be used to heat up that part of the particle through which the pyrolysis front will pass, this effect becomes less noticeable with increasing T_s as predicted by Equation (4). Again for the very large T_s or $(T_s - T_i)$ where the portion

of total heat which is needed for sensible heat of particle is very small in comparison to the total heat transmitted into the particle, prediction of Equations (2) and (4) are exactly the same.

As presented above when any combination of E and k_0 according to Nsakala et al. (14) were chosen, regardless of T_s , λ , ΔH , R_p , the temperature at the pyrolysis front (T_i) showed a dependency only on k_0 and E . Results can be seen in Figure 5 where k_0 is constant and T_i increases as E increases. When dimensionless time ($t = \alpha t / R_p^2$) was plotted against the pyrolysis rate constant ($k_0 e^{-E/RT_i}$), the results fall on a single line for any given T_s (Figure 6). This indicates a unique correlation between pyrolysis kinetics and the total pyrolysis time. This is due to the strong functionality of pyrolysis time with λ and R_p (embedded in dimensionless time) and pyrolysis kinetics as discussed above. Furthermore, the results of pyrolysis time for total conversion are consistent with Essenhigh (10,14) and others. Effects of T_s can be calculated from Figure 4 and presented with families of curves in Figure 6 using T_s as a parameter.

Effects of variable thermal properties were also studied. For instance, if a variable $\lambda(t) = 1.226 \times 10^{-5} [1.3 + 0.96x(V/V^*)]^{3.5} T^{1/2}$ was assumed instead of $\lambda = 0.006$ cal/cm-s-k the total pyrolysis time would have changed only by 10%. This is because the effective thermal conductivity is controlled by the char thermal conductivity (outer layer of pyrolysis front) and that is relatively constant for the temperature range studied (1200 - 1500 K). This effect is even less significant for heat of pyrolysis, as discussed above where ΔH was varied from 0 to 1000 cal/g.

The practical implication of these results is that by measuring pyrolysis time for a given particle diameter and surface temperature, one could use Figure 6 to estimate T_i and k . This T_i and k can be used along with Figure 5 to estimate the kinetic parameters for primary pyrolysis of coal under severe thermal conditions.

CONCLUSIONS

1. For the rapid heating rates ($>10^5$ K/s), pyrolysis is confined to a thin layer and reaction occurs according to the shrinking core model rather than a volumetric reaction model.
2. Under these heating conditions pyrolysis occurs totally under diffusional limitations (in the ablation regime).
3. Activation energy (E) and thermal conductivity (λ) are the most stringent parameters on pyrolysis followed by heat of reaction and the surface temperature.
4. Temperature at the pyrolysis front is different from the surface temperature and is uniquely correlated to the pyrolysis kinetics.
5. Intrinsic pyrolysis kinetics under these heating conditions can be estimated using results of existing analysis.

ACKNOWLEDGEMENTS

Authors gratefully acknowledge Dr. Bruce Losee and Dr. Sarajini A. Deevi of Philip Morris U.S.A. for their helpful comments.

NOMENCLATURES

C_p	heat capacity, [Cal/g-K]
E	activation energy, [Cal/gmole]
k_o	frequency factor, [1/s]
m	heating rate, [K/s]
$g(x), p(x)$	conversion functions [-]
q	heat flux density, [Cal/cm ² -s]
r	radius, [cm]
R_c	pyrolysis front, [cm]
R_p	particle radius, [cm]
T	temperature [K]
T_o	initial temperature [K]
T_i	temperature at pyrolysis front [K]
T_s	surface temperature [K]
t	time [s]
u	volatiles velocity [cm/sec]
V	percent weight loss
V^*	ultimate weight loss
ΔH	heat of pyrolysis [Cal/g]
λ	thermal conductivity [Cal/cm-s-K]
ρ	density [g/cm ³]
τ	dimensionless time [-]

REFERENCES

- Howard, J.B., Chemistry of Coal utilization, 2nd supplementary volume, chapter 12, Elliot M.A., Ed., Wiley-Interscience, NY 1981.
- Galvalas, G.R., Coal pyrolysis, Elsevier Scientific, NY 1982.
- Solomon, P.R., Hamblen, D.G., Carangelo, R.M., Serio, M.A., and Deshpande G.V., ACS, Div. Fuel Chem. prep., 32(3), 83, 1987.
- Niksa, S., Combustion and Flame, 66, 111, 1986.
- Niksa, S., AIChE J., 34, 5, 790, 1988.
- Suberg, E.M., in Chemistry of Coal Conversion, R. Schlosberg, Ed., 67 Plenum, 1985.
- Hajjaligol, M.R., Peters, W.A. and Howard, J.P., Energy and Fuels, 2, 430, 1988.
- Hajjaligol, M.R., Peters, W.A. and Howard, J.P., to be submitted to AIChE, 1989.
- Villiermaux, J., Antoine B., Lede J., and Soullignac, F., ACS Div. Fuel Chem. prep., 28(5), 390, 1983.
- Misra M.K., and Essenhigh, R.H., ACS Div. Fuel Chem. prep., 32(2), 59, 1982.
- Ko, C.H., Sanchez, D.M., Peters, W.A. and Howard, J.P., ACS, Div. Fuel Chem. prep., 33(2), 112, 1988.
- Hertzberg, M., Zlochower I.A., Conti, R.S. and Cashdollar K.L., ACS Div. Fuel Chem. prep., 32(3), 24, 1987.
- Szekely, J., Evans, J.W., and Sohn, H.Y., Gas-Solid Reactions, Academic Press, N.Y., 1976.
- Nsakala N., Essenhigh, R.H., and Walker, P.L., Combustion Sci. Tech., 16, 153, 1977.
- Wanzl, W., Kabler P., Van Heck K.H., and Junten H., ACS Div. Fuel Chem. prep., 32(3), 125, 1987.

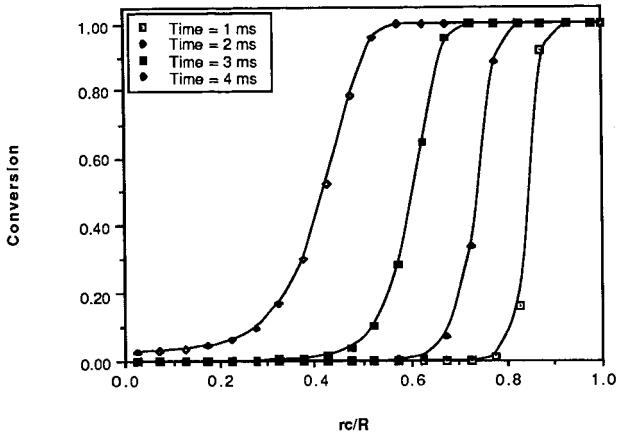


Figure 1. Effect of pyrolysis time on the position and shape of pyrolysis front ($T_s=1500$ K, $R_p=50\mu\text{m}$)

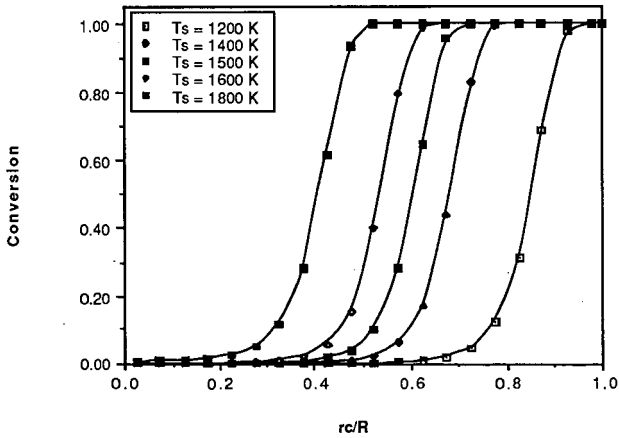


Figure 2. Effect of surface temperature on the position and shape of pyrolysis front ($R_p=50\mu\text{m}$, 5ms)

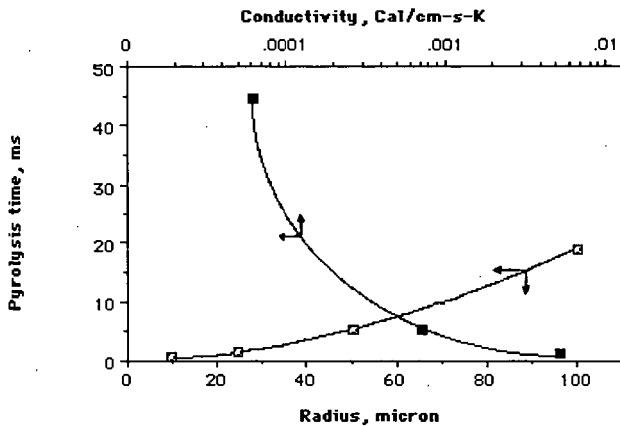


Figure 3. Effect of thermal conductivity and radius on the total pyrolysis time ($T_s=1500$ K, $R_p=50\mu\text{m}$)

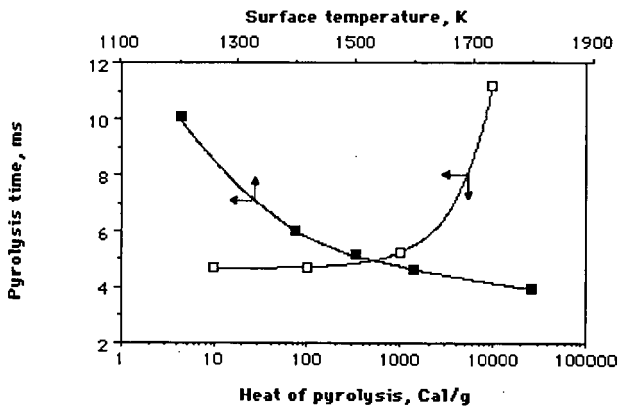


Figure 4. Effect of heat of pyrolysis and surface temperature on the total pyrolysis time ($T_s=1500$ K, $R_p=50\mu\text{m}$)

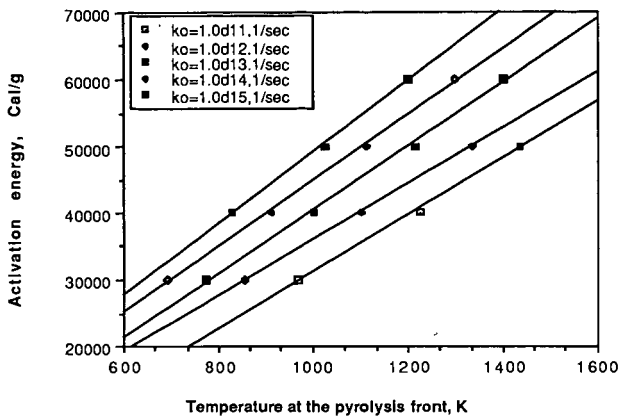


Figure 5. Correlation between activation energy (E), frequency factor (k_0) and the temperature at the pyrolysis front (T_i)

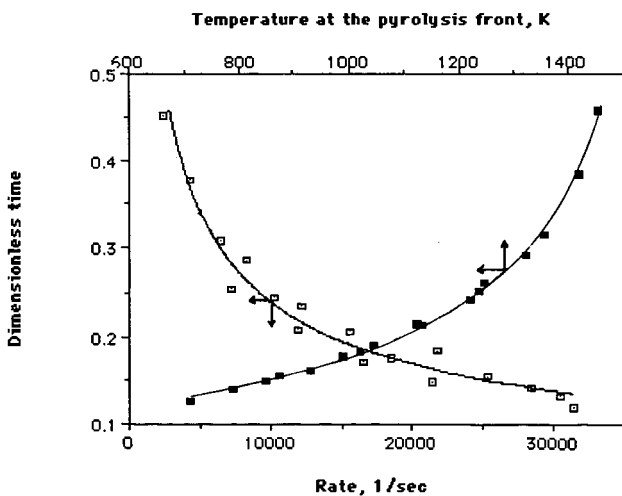


Figure 6. Effect of pyrolysis kinetic and temperature on the pyrolysis dimensionless time

ESTIMATION OF COAL DEVOLATILIZATION MODELING PARAMETERS FROM THERMOGRAVIMETRIC AND TIME-RESOLVED SOFT IONIZATION MASS SPECTROMETRIC DATA

Yongseung Yun, Wallace Maswadeh, Henk L.C. Meuzelaar, Norbert Simmleit* and Hans-Rolf Schulten**

Center for Micro Analysis & Reaction Chemistry, University of Utah
Salt Lake City, Utah 84112

*Institut Fresenius, Chemical and Biological Laboratories
D-6204 Taunusstein-Neuhof, F.R.G.

** Fachhochschule Fresenius, Dept. Trace Analysis
D-6200 Wiesbaden, F.R.G.

INTRODUCTION

Nowadays it is widely recognized that the initial pyrolysis step in coal conversion processes has a profound effect on the yield and distribution of end products such as coal-derived liquids, gases, coke, or pollutant emissions. Two general approaches for modeling coal pyrolysis reactions can be distinguished, namely: (a) phenomenological modeling and (b) chemical modeling [1]. The phenomenological modeling approach is useful in conversion processes such as high temperature gasification where detailed chemical information may be advantageous but is probably not indispensable. Other conversion processes, however, e.g., liquefaction and hydrolysis, may require more detailed chemical information to predict the distribution of final products [2]. Whether pyrolysis ("devolatilization") models for pulverized coal combustion processes require detailed information on coal structure and reactivity or can be based primarily on a phenomenological approach is still a matter of considerable debate [3].

Heated screen pyrolysis techniques have been widely used to provide modeling parameters for phenomenological models based on the thermal behavior of light gas components detected by gas chromatography, mass spectrometry (MS) and other spectroscopic techniques [4]. Due to limitations of the analytical techniques used, tar components are generally lumped into a single component.

Since time-resolved mass spectrometry (TR-MS) data can be used to analyze single mass profiles or mass spectra as a function of temperature, TR-MS results from thermogravimetry/low-voltage electron impact mass spectrometry (TG/EIMS) [5] and pyrolysis-field ionization mass spectrometry (Py-FIMS) [6] can provide detailed chemical information on gas and tar products [5].

The aim of this study is to present several possibilities for estimating kinetic parameters to model coal pyrolysis phenomena from TR-MS data. Our estimations will be based on the chemical assignment of tar components observed in soft ionization mass spectra in combination with kinetic evaluation or temperature-resolved intensity profiles of single mass peaks and measured or simulated thermogravimetric weight loss curves.

EXPERIMENTAL

Three -100 mesh Argonne Premium coal samples of different rank (Pocahontas #3, 1vb; Pittsburgh #8, hvAb; and Beulah-Zap, lignite) were analyzed by vacuum TG/EIMS and Py-FIMS. Conventional characterization data on the coal samples can be found elsewhere [7].

The TG/EIMS system consists of a Mettler TA1 Thermoanalyzer directly interfaced to a Finnigan MAT 3200 quadrupole mass spectrometer. Devolatilization was performed directly in front of the ion source in order to avoid

recombination reactions and/or secondary decomposition of reactive compounds as well as to reduce the loss of polar compounds through adsorption and condensation. Sample aliquots of 4-5 mg were heated under vacuum ($3-6 \times 10^{-7}$ torr) as the sample temperature was increased from 60 C to 730 C at 25 C/min. MS conditions were as follows: electron energy 14 eV (set value), mass range scanned m/z 33-200, total number of scans 80, and total scanning time 27 minutes.

For temperature-programmed pyrolysis in combination with TR-FIMS, about 100 μ g samples were transferred into a commercially available quartz crucible and introduced into the high vacuum (10^{-7} torr) of the ion source (200 C). The instrumental setup using a Finnigan MAT 731 double-focussing mass spectrometer, a combined EI/FI/FD/FAB ion source and a AMD Intetra direct introduction system has been previously described in detail [6]. The samples were heated linearly from 50 C to 750 C at a rate of 100 C/min. The crucible temperature was measured with a thermocouple at the bottom of the oven. In general, 34 FI mass spectra were recorded in the m/z 50-900 mass range. The mass signals and the total ion intensities (TII) of the mass spectral series were used to calculate tar weight loss curves [8].

A three parameter kinetic fitting procedure, based on Marquardt's algorithm [9], was employed after scaling the activation energy, pre-exponential factor, and reaction order to similar orders of magnitude. The distributed activation energy kinetic model used was based on Gaussian distributed activation energies with a fixed pre-exponential factor and a reaction order of 1 [10].

RESULTS AND DISCUSSION

From the vacuum TG observations, char yields at 25 C/min and maximum temperature of 730 C were found to be 71, 48, and 58 wt% (based on as received samples) for Pocahontas #3, Pittsburgh #8, and Beulah-2ap coals respectively. Consequently, the (gas+tar) yield of the three coals under vacuum TG conditions can be put at 29, 52 and 42 wt %, respectively.

Figure 1 shows temperature profiles of low molecular weight (MW) tar products recorded by means of vacuum TG/EIMS. Since the data plotted in the figure show the rate profile versus temperature, kinetic parameters can be calculated for each mass signal. Although each of the mass profiles shown at m/z 56, 108 and 124 can be expected to originate from several different sources the most abundant ion species at these m/z values in coal pyrolyzates are thought to represent butenes ($C_4H_8^+$; m/z 56), cresols (C_7H_8O ; m/z 108) and methyl-dihydroxybenzenes ($C_7H_8O_2$; m/z 124) [11].

The results of the kinetic estimates are also presented in Figure 1. First the normalized raw data (total weight loss fraction due to single mass signal ≈ 1) have been fitted to a 1st order Arrhenius model ($n=1$) yielding apparent activation energies E , pre-exponential factors A and in general a good fit of the ascending part of the temperature/nominal mass signal profile (Figure 2). In a second step, maintaining E and A constant, the fit of the descending part of the curve was improved by varying the reaction order n . Similar combinations of reaction orders, activation energies and pre-exponential factors could also be obtained in a single step by nonlinear regression based on Marquardt's algorithm. In most cases studied this led to a satisfying result (Figure 2a). In other cases, however, no satisfying fit could be achieved with any of the methods applied (Figure 2b). This is probably due to the presence of two or more overlapping processes [5]. In an independent third step the normalized raw data were fitted to a distributed activation model (DAE, $n=1$) yielding a frequency factor A , the mean activation energy E_0 and the standard deviation of the activation energy σ_E . For the EI mass signal m/z 124 evolved from Pocahontas coal it was not possible to apply the DAE model due to a poor signal-to-noise ratio.

With the exception of mass signal m/z 124 of the Beulah Zap coal apparent activation energies estimated by 1st order Arrhenius model are not in the range of the corresponding activation energies $E_0 + 36E$ estimated by the DAE model. The kinetic parameters E_0 and A derived from the DAE model are higher and in particular A is several orders of magnitude higher when estimated by the DAE model. The mean activation energy E_0 is higher due to the effect of distribution functionality. Accordingly, A has to be much higher due to the compensating effect between E and A . The data in Figure 1 show that most of the reactions studied are not of reaction order $n=1$. With exception of the mass signal m/z 56 of Beulah Zap coal the reaction order ranges between 1.3 and 1.8 apparently indicating the occurrence of intermolecular reactions, e.g., char formation, at higher temperatures. In general, apparent and distributed activation energies, and consequently the pre-exponential factors, increase with coal rank, i.e., with higher degree of condensation. During pyrolysis of Pittsburgh and Pocahontas coals the activation energies decrease with increasing polarity of the thermal degradation products. The opposite effect is observed for the lignite coal (Beulah Zap). Presumably, this indicates an effect of amount and availability of thermal degradation products formed during pyrolysis of the three coals of different rank.

Figures 3-5 show Py-FIMS results of the three ANL coals of different rank. The upper left corner figures (3a-5a) are thermograms which illustrate with increasing temperature the total ion intensity of each spectrum scanned. The upper right corner figures (3b-5b) are the time-integrated mass spectra obtained by summing all spectra scanned on each coal indicating that much higher MW compounds are released during coal pyrolysis than detected under the conditions of the TG/EIMS experiment. The bottom left hand side figures (3c-5c) show calculated weight loss curves for selected mass ranges. Due to the absence of significant mass spectrometric fragmentation and relatively uniform response factors for aromatic and hydroaromatic compounds, FIMS provides reliable information on the (MW) distribution of most types of tar products detected. The product of an m/z -value and its corresponding FI signal intensity equals the calculated weight loss of thermal degradation products with $MW=m/z$ evolving from the sample in a specific temperature interval. The total weight loss was calculated for mass ranges of 100 Dalton and plotted in a cumulative way. Thus, the bottom line in the simulated TG curve represents the total relative weight loss of tar components with temperature. The bottom right hand figures (3d-5d) show the integrated Py-FI mass spectra of the low temperature pyrolysis products. The integrated temperature interval is hatched in the upper left hand figures (3a-5a).

There are two distinct maxima in the TII profiles. The early peak is most dominant in low volatile bituminous (lvb) Pocahontas #3 coal (Figure 5a) whereas high volatile bituminous (hvb) Pittsburgh #8 coal shows a least pronounced peak in the same temperature interval (Figure 4a). The absolute weight loss of the Pittsburgh coal in the low temperature region, however, may be higher since the TII recorded represents only the tar components in the mass range m/z 50-900 excluding the gas components $m/z < 50$. Three spectra around the maximum of the early peaks were summed and shown in Figures 3d-5d.

In Beulah-Zap coal (Figure 3d), there is little if any contribution of naphthalenes as may be expected in lignite coals. Instead, it shows a distinct homologous series of FI signals at m/z 368, 396, 424, 452, 480 which may be due to n-fatty acids or monomeric esters (C_{24} - C_{32}) and an abundant FI signal at m/z 544, which could indicate the presence of an aromatic diester. The described signals are known from Py-FIMS analyses of soil organic matter in temperature ranges below 300 C and may be due to stable degradation products of plant lipids or aliphatic biopolymers such as cutin or suberin [12].

The lignite (Beulah Zap) releases most of its thermal degradation products at higher temperatures around 440 C (Figure 3a). These products are known to be mainly derived from fossil lignin-like components [13] and, hence, the most prominent FI signals in integrated Py-FI mass spectrum over the whole temperature range (Figure 3b) can be seen at m/z 94, 110, 124, 138 and 152 indicating phenol and alkyl-substituted dihydroxy-benzenes, respectively. Besides the high MW aliphatic compounds released mainly in the lower temperature range, the Py-FI mass spectrum in Figure 3b also shows FI signals of short-chain alkenes at m/z 56, 70 and 84. Obviously, no condensed high-molecular weight pyrolysis products $MW > 400$ are formed during the high temperature pyrolysis of the lignite sample.

The Pittsburgh coal behaves in a similar manner by releasing most of its thermal degradation products detected in the higher temperature range (Figure 4a). Hence, the integrated Py-FI mass spectrum (Figure 4b) is very different from the corresponding low-temperature spectrum (Figure 4d) showing primarily FI signals of pyrolysis products which have been evolved at temperatures above 400 C. The most prominent signals in Figure 4b at m/z 94, 108, 122, 136 and 150 are due to alkyl-substituted phenols. Furthermore, the signal at m/z 64 (SO_2^+) indicates the presence of oxidized sulfur forms.

In the low temperature region Pittsburgh #8 coal releases noticeable amounts of alkyl-substituted naphthalenes which form molecular FI ion signals at m/z 142, 156, 170, 184, 198 and 212 (Figure 4d). The most abundant species are the C_2 - and C_3 -alkyl substituted naphthalenes at m/z 156 and 170. A homologous series of alkyl-substituted FI signals of acenaphthene species can be seen at m/z 168, 182, 196, 210, 224 and 238 with the C_3 - and C_4 -alkyl substituted species being most abundant. Recent high resolution Py-FIMS analyses of Polish coals showed that the homologous series of FI signals at m/z 204, 218, 232, 246, 260 and 274 may be primarily due to alkyl-substituted cyclopentaphenanthrenes [13]. According to the Py-FI mass spectrum, the C_4 - and C_5 -alkyl substituted species would be dominant in the low temperature release step of Pittsburgh #8 coal. At present detailed interpretation of higher mass signals is not possible, however it should be noted that two $(CH_2)_2$ -homologous series of FI signals at m/z 308, 336, 364, 392, 420 and at m/z 296, 324, 352, 380, 408, 436 dominate the mass range $m/z > 300$.

As most of the thermal degradation products are already released from Pocahontas coal in the low-temperature range 300-400 C (Figure 5a), the corresponding spectrum (Figure 5d) looks very similar to the integrated spectrum in (Figure 5b). Major differences are due to high temperature pyrolysis products in the mass range $m/z > 500$ and in the mass range $m/z < 200$. The latter products account for alkyl-substituted benzenes at m/z 78, 92, 106, 120, naphthalenes at m/z 142, 156, 170 and phenanthrenes at m/z 178, 192, 206, 220.

Pocahontas #3 coal shows insignificant contributions of naphthalenes in the early devolatilization step (Figure 5d). Thus, in contrast to the Pittsburgh coal, the most abundant Py-FI mass signals have been recorded in the mass range $m/z > 210$. The mass range $m/z < 325$ is dominated by pyrene species as the homologous series of alkyl-substituted pyrenes at m/z 216, 230, 244, 258, 272, 286 and the homologous series of alkyl-substituted benzopyrenes at m/z 252, 266, 280, 294, 308, 322 show. For both components the most abundant species are the C_3 -alkyl species at m/z 244 and at m/z 294. Again it is difficult to interpret the higher mass signals, but other CH_2 -homologous series at m/z 316, 330, 344, 358, 373, 386, 400 and m/z 326, 340, 354, 368, 382, 396, 410, 424 dominate the mass range $m/z > 300$ of the Pocahontas coal when compared with the Pittsburgh coal.

CONCLUSIONS

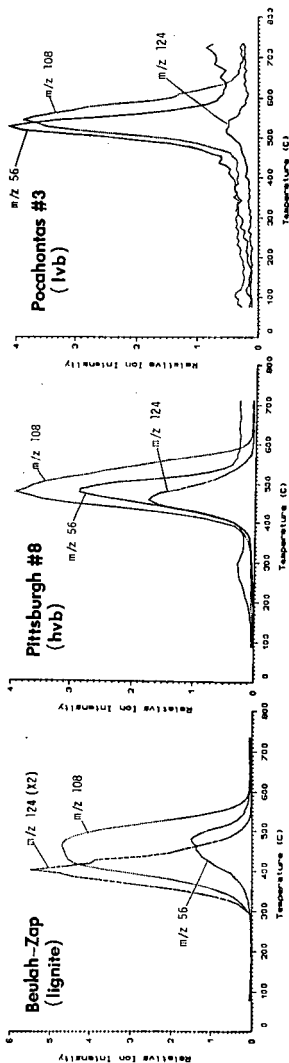
There are dramatic effects of rank (and probably depositional environment) on the devolatilization behavior of each coal. Although the main focus of coal pyrolysis modeling is on bituminous coals due to their higher yield in coal conversion processes, preferably the chemical pyrolysis model should have the ability to predict tar MW distributions as a function of temperature as well as to predict the chemical nature of tar molecules produced by different rank coals. Time-resolved soft ionization mass spectrometric techniques provide detailed information on the thermal evolution of distinct pyrolysis products. In particular FIMS is suited to obtain molecular weight distributions of tar components. Using single mass profiles, it is feasible to estimate kinetic parameters for pyrolysis products. The estimated kinetic parameters of thermal degradation products reflect the coal rank, the polarity of the pyrolysis products and the fitting technique employed. First order Arrhenius parameters enable a satisfactory fit to the temperature resolved mass profiles at $T < T_{max}$ whereas for $T > T_{max}$ higher reaction orders ($1 < n < 2$) markedly improve the goodness of fit. By contrast, the use of distributed activation energies, although improving the overall fit, tends to lead to unexpectedly high values for mean activation energies and pre-exponential factors.

ACKNOWLEDGEMENTS

This work was sponsored by the Advanced Combustion Engineering Research Center. Funds for this center are received from the National Science Foundation, the State of Utah, and 23 industrial participants. FIMS work was supported in part by the Deutsche Forschungsgemeinschaft, Bonn-Bad Godesberg (F.R.G.). The authors wish to thank R. Muller, Taunusstein for technical assistance.

REFERENCES

1. Gavalas, G.R., Coal Pyrolysis, Elsevier, Amsterdam, 1982.
2. Chakravarty, T., Meuzelaar, H.L.C., Khan, R.H., "Modeling and Prediction of Pyrolysis Liquid Composition Based on Pyrolysis Mass Spectra of the Parent Fuels using Canonical Correlation Technique", submitted to Ind. Eng. Res., 1989.
3. Grant, D.M, Pugmire, R.J., ACS Preprints (Div. of Fuel Chem.), 33(2), 1988, 322-332.
4. Suuberg, E.M., Peters, W.A., Howard, J.B., I&EC Process Des. Dev., 17(1), 1978, 37-46.
5. Yun, Y., Meuzelaar, H.L.C., ACS Preprints (Div. of Fuel Chem.), 33(3), 1988, 75-84.
6. Schulten, H.-R., Simmleit, N., Muller, R., Anal. Chem., 59 (1987) 2903-2908.
7. Vorres, K.S., Janikowski, S.K., ACS Preprints (Div. of Fuel Chem.), 32(1), 1987, 492-499.6.
8. Schulten, H.-R., J. Anal. Appl. Pyrol. 12 (1987), 149-186.
9. Marquardt, D.W., J. Soc. Ind. Appl. Math., 11(2), 1963, 431-441.
10. Howard, J.B., Chemistry of Coal Utilization, Chap. 12, Elliott, M.A., ed., Wiley, New York, 1981.
11. Nip, M., de Leeuw, J.W., Schenck, P.A., Meuzelaar, H.L.C., Stout, S.A., Given, P.H., Boon J.J., J. Anal. Appl. Pyrol. 8 (1985), 221-239.
12. Hempfling, R., Zech, W., Schulten, H.-R., Soil Science, 146 (1988), 262-276.
13. Schulten, H.-R., Marzec, A., Simmleit, N., Dylan, P., Muller, R., Energy & Fuels (1989) in press.



m/z	coal		Beulah-Zap		Pittsburgh #8		Pocahontas #3	
	E_0	n	1st order	nth order	1st order	nth order	1st order	nth order
m/z 56	E_0		25.6	25.6	47.5	47.5	51.0	51.0
	ΔE		0	0	0	0	0	0
m/z 108	E_0		3.9×10^5	3.9×10^5	7.8×10^{11}	7.8×10^{11}	1.1×10^{12}	1.1×10^{12}
	ΔE		1.0	1.05	1.0	1.60	1.0	1.45
m/z 124	E_0		27.9	27.9	40.0	40.0	51.2	51.2
	ΔE		0	0	0	0	0	0
m/z 124	E_0		2.4×10^6	2.4×10^6	5.9×10^9	5.9×10^9	7.2×10^{11}	7.2×10^{11}
	ΔE		1.0	1.40	1.0	1.70	1.0	1.80
m/z 124	E_0		35.8	35.8	39.1	39.1	37.9	37.9
	ΔE		0	0	0	0	0	0
m/z 124	E_0		4.9×10^9	4.9×10^9	1.2×10^{10}	1.2×10^{10}	2.4×10^8	2.4×10^8
	ΔE		1.0	1.70	1.0	1.75	1.0	1.30
			DAE	DAE	DAE	DAE	DAE	DAE
			26.0	26.0	40.0	40.0	57.0	57.0
			0.01	0.01	7.4×10^{11}	7.4×10^{11}	3.1	3.1
			2.3×10^7	2.3×10^7	7.4×10^{11}	7.4×10^{11}	4.3×10^{16}	4.3×10^{16}
			1.0	1.0	1.0	1.0	1.0	1.0
			40.4	40.4	40.0	40.0	57.0	57.0
			2.7	2.7	0	0	0	0
			7.4×10^{11}	7.4×10^{11}	5.9×10^9	5.9×10^9	4.3×10^{16}	4.3×10^{16}
			1.0	1.0	1.0	1.0	1.0	1.0
			37.2	37.2	39.1	39.1	44.1	44.1
			1.0	1.0	0	0	0	0
			7.4×10^{11}	7.4×10^{11}	1.2×10^{10}	1.2×10^{10}	7.3×10^{14}	7.3×10^{14}
			1.0	1.0	1.0	1.0	1.0	1.0
			58.1	58.1	58.1	58.1	58.1	58.1
			1.8	1.8	1.8	1.8	1.8	1.8
			1.3×10^{15}					
			1.0	1.0	1.0	1.0	1.0	1.0

($E_0, \Delta E$ in Kcal/mol, A is s^{-1})

Figure 1. Kinetic parameters estimated for selected nominal mass signal profiles recorded during TG/EIMS analysis of three coals. Parameters have been calculated by fitting the normalized raw data to 1st order, nth order and distributed activation energy (DAE) models.

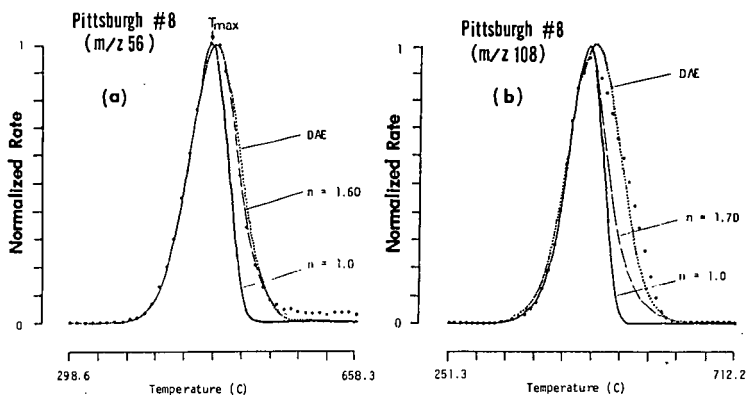


Figure 2. Selected examples of recorded temperature/EI mass signal profiles (*) and simulated mass signal profiles using kinetic parameters estimated by 1st and nth order model and DAE model. Principally, it was aimed to fit the rising part and the baseline of the profile. (a) shows a good fit of the whole profile, whereas (b) shows a bad fit of the declining part of the profile.

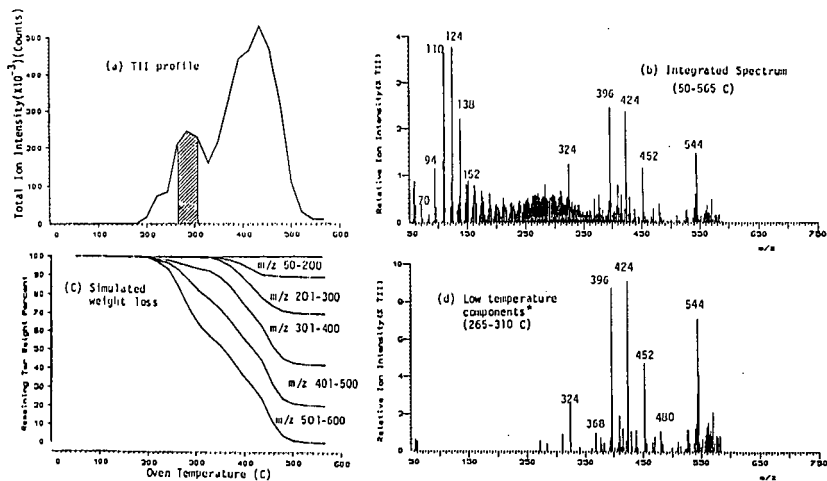


Figure 3. Py-FIMS results from Beulah Zap (lignite) coal. Simulated weight loss curves are cumulative for each mass range, thus the lowest curve shows the total weight loss of tar components. *Integrated spectrum of hatched area in (a).

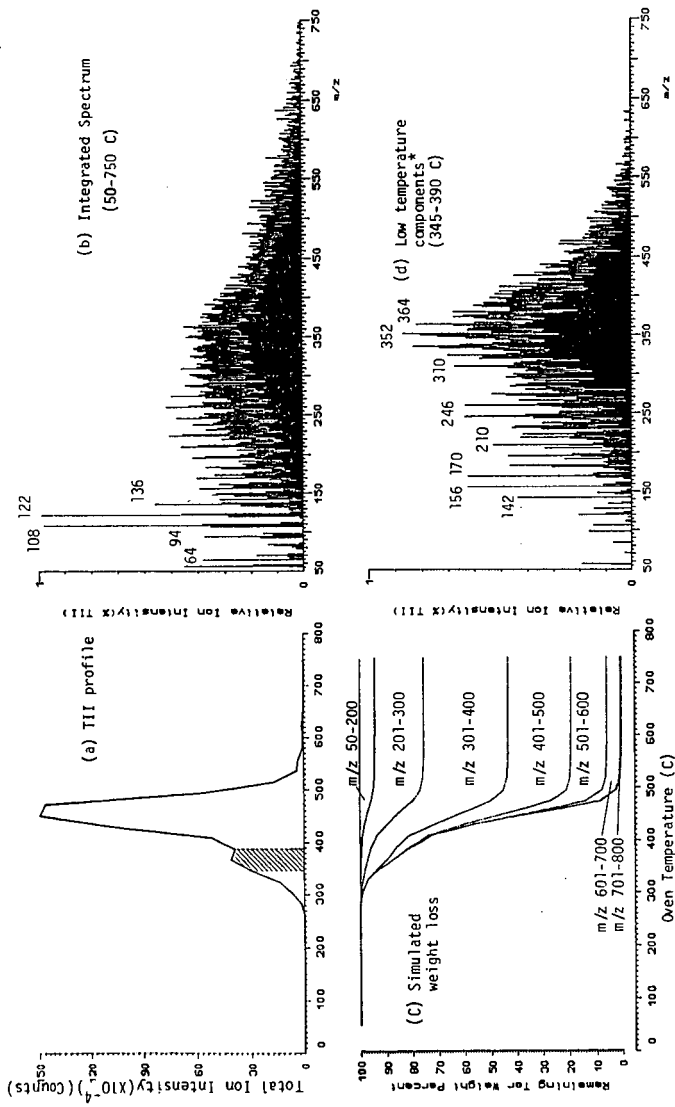


Figure 4. Py-FIMS results from Pittsburgh #8 (hvb) coal. Simulated weight loss curves are cumulative for each mass range, thus the lowest curve shows the total weight loss of tar components. *Integrated spectrum of hatched area in (a).

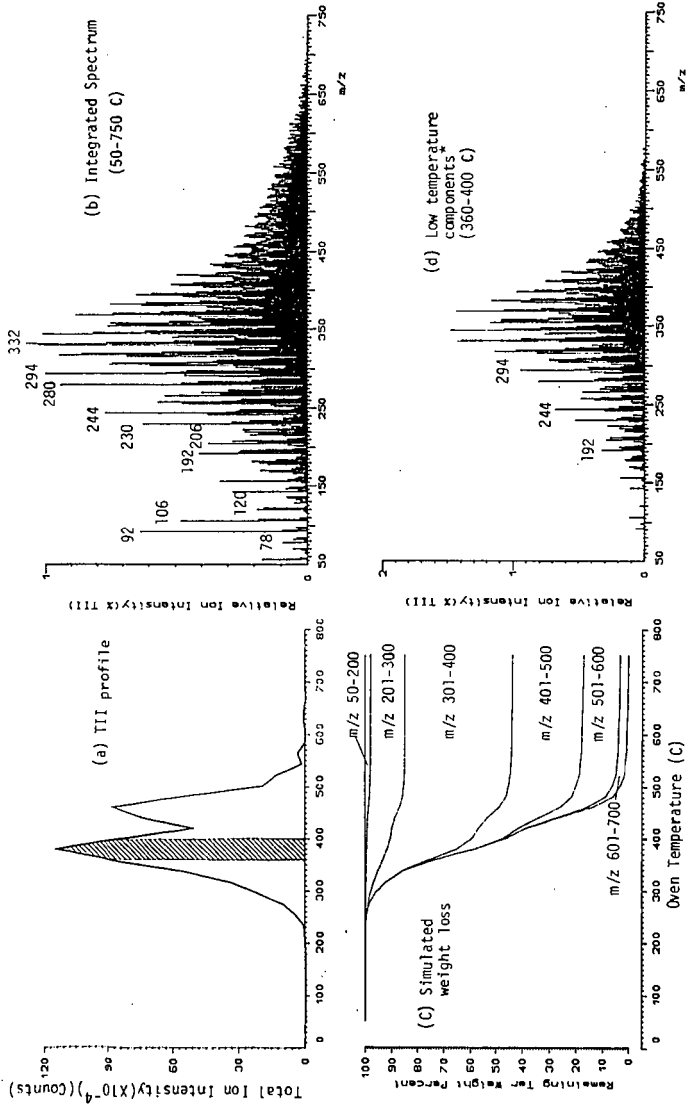


Figure 5. Py-FIMS results from Pocahontas #3 (lvb) coal. Simulated weight loss curves are cumulative for each mass range, thus the lowest curve shows the total weight loss of tar components. *Integrated spectrum of hatched area in (a).

COAL THERMOLYSIS MODELING. THE EFFECTS OF
RESTRICTED DIFFUSION ON THERMAL REACTION PATHWAYS

A. C. Buchanan, III, P. F. Britt, and C. A. Biggs
Chemistry Division
Oak Ridge National Laboratory
P. O. Box 2008
Oak Ridge, Tennessee 37831-6197

INTRODUCTION

The technique of model compound immobilization by covalent surface attachment is being employed to investigate the potential impact of restricted diffusional mobility on the thermal reactivity of coal. This restricted mobility may be imposed in coal as a consequence of its cross-linked, macromolecular structure.¹ Thermolysis studies at 350-400 °C of model coal structures covalently attached to a silica surface have shown that significant perturbations in free-radical reaction mechanisms can occur, and result in altered reaction rates and product distributions compared with corresponding fluid phase behavior.²⁻⁴ A detailed study of the thermolysis of surface-immobilized bibenzyl ($\equiv\text{SiOPhCH}_2\text{CH}_2\text{Ph}$, represented as $\sim\text{PhCH}_2\text{CH}_2\text{Ph}$) showed that the rate of unimolecular C-C homolysis is similar to that in fluid phases.² However, restricted radical and substrate mobility led to the onset of complex free-radical chain pathways on the surface, which produced substantial isomerization, cyclization-dehydrogenation, and hydrodealkylation of bibenzyl moieties. Recent studies have focused on the thermally induced, free radical chain decomposition reactions for surface-immobilized 1,3-diphenylpropane ($\sim\text{Ph}(\text{CH}_2)_3\text{Ph}$, $\sim\text{DPP}$)³ and 1,4-diphenylbutane ($\sim\text{Ph}(\text{CH}_2)_4\text{Ph}$, $\sim\text{DPB}$).⁴ For $\sim\text{DPP}$, we find that both the reaction rate and product composition are strongly dependent on surface coverage and, hence, the proximity of $\sim\text{DPP}$ molecules and hydrogen abstracting radicals on the surface. The rates and selectivities of these key bimolecular reaction steps on the surface might also be affected by the structure of neighboring molecules. In the current study, we are beginning to probe this feature by examining the influence of the structure of co-attached aromatic molecules such as biphenyl ($\sim\text{PhPh}$) and diphenylmethane ($\sim\text{PhCH}_2\text{Ph}$) on the reaction rate and regioselectivity in the thermolysis of $\sim\text{DPP}$.

EXPERIMENTAL

Procedures for the synthesis of surface-attached 1,3-diphenylpropane ($\sim\text{DPP}$) by the condensation reaction of *p*-HOPh(CH₂)₃Ph (HODPP) with the surface hydroxyls of a high surface area, fumed silica have been fully described elsewhere.³ *p*-Phenylphenol (*p*-HOPhPh) was purified by multiple recrystallizations from benzene/hexanes to give a product with GC purity of >99.9%. *p*-Benzylphenol (*p*-HOPhCH₂Ph) was first eluted from a silica column with benzene, and then recrystallized two times from benzene/hexanes to give a product with GC purity of >99.9%.

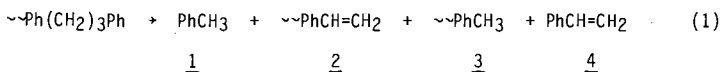
The two-component surfaces were prepared in a manner analogous to that used for preparation of $\sim\text{DPP}$ with both phenolic components adsorbed onto the surface in a single step prior to the surface attachment reaction. In one case for comparison, a batch of $\sim\text{DPP}/\sim\text{BP}$ was synthesized in two separate steps. A

saturation coverage batch of $\sim\sim$ BP was prepared and then reacted with HODPP in a second step to chemically exchange some $\sim\sim$ DPP molecules with $\sim\sim$ BP molecules. All surface coverages were analyzed by GC with internal standards following a base hydrolysis procedure that liberates the attached organics as phenols.³

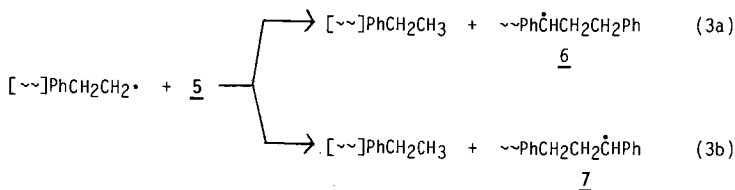
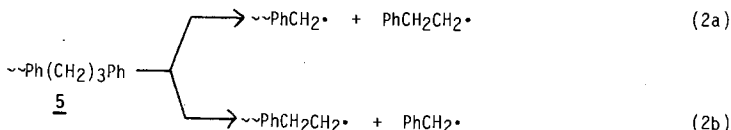
Thermolyses were conducted in sealed, evacuated (2×10^{-6} torr) T-shaped tubes as described previously.^{2,3} Volatile products were collected in a cold trap and analyzed by GC and GC-MS with the use of internal standards. Surface-bound products were removed from the silica by base hydrolysis, and the resulting phenols (or the corresponding trimethylsilyl ether derivatives) were analyzed as above.

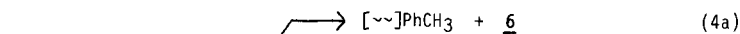
RESULTS AND DISCUSSION

Thermolysis of $\sim\sim$ DPP at 345-400 °C and low conversions produces the four major products shown in Eq. 1 analogous to the cracking reaction observed previously for fluid phase DPP.⁵⁻⁷ The formation of these products was explained by a



free-radical chain decomposition pathway shown in Eqs. 2-7 with the propagation steps being Eqs. 4-6.^{3a} The bracket notation used in Eqs. 3 and 4 indicates that two equations may be written in each case, one with a surface-immobilized species and one with a vapor-phase species.





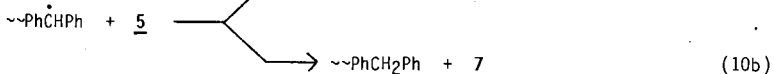
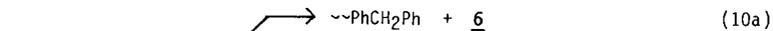
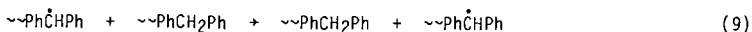
Regioselectivity in the reaction is determined by the relative rates of formation of radicals 6 and 7 by hydrogen abstraction, since the unimolecular β -scission steps (Eqs. 5 and 6) occur very efficiently. We found an increasing selectivity for formation of the product pair 3 and 4 (cycling through radical 7) with increasing $\sim\sim$ DPP conversion and decreasing initial surface coverage. The surface coverage effect is illustrated at low $\sim\sim$ DPP conversions in Table 1, which contains new data obtained at a coverage of 0.102 mmol/g. We again use the styrene/toluene yield ratio as the experimental measure of selectivity. Our interpretation is that, at lower coverages, geometrical constraints induced by restricted radical and substrate mobility increasingly favor hydrogen abstraction at the benzylic methylene site farthest from the surface (to favor formation of radical 7) as $\sim\sim$ DPP molecules become increasingly distant from hydrogen abstracting radicals on the surface. This concept is illustrated in Figure 1.

We also note that the rate of thermolysis of $\sim\sim$ DPP is more sensitive to changes in surface coverage than fluid phase DPP is to changes in concentration.^{5,6} A four-fold decrease in surface coverage resulted in a rate depression by a factor of 17-23.^{3a} This result again appears to reflect a substantial sensitivity of bimolecular reaction rates on the surface, such as in Eqs. 3 and 4, to the proximity of $\sim\sim$ DPP molecules and hydrogen abstracting radicals.

Initial results on the influence of co-attached aromatics on the thermolysis of $\sim\sim$ DPP are shown in Table 2. Surprisingly, the presence of co-attached biphenyl molecules does not have a major effect on the $\sim\sim$ DPP thermolysis rate or selectivity compared with corresponding coverages of $\sim\sim$ DPP alone. This does not appear to be the result of the sample preparation procedure since a $\sim\sim$ DPP (0.126 mmol/g)/ $\sim\sim$ BP (0.509 mmol/g) batch prepared by a two-step chemical exchange process (see experimental) gave results comparable to those from surfaces prepared by the conventional one-step procedure. The reason for the apparent 2-fold rate acceleration for the $\sim\sim$ DPP surface in the presence of $\sim\sim$ BP is under further investigation.

These preliminary data also show that the presence of diphenylmethane molecules has a dramatic effect on the thermolysis of $\sim\sim$ DPP. Independent control

experiments show that $\sim\text{DPM}$ alone is thermally stable under the reaction conditions employed (as is $\sim\text{BP}$).² In the presence of $\sim\text{DPM}$, the rate of $\sim\text{DPP}$ thermolysis is substantially accelerated (ca. 8-fold increase in conversion) compared with $\sim\text{DPP}$ alone at comparable coverages, while the product regioselectivity (which is normally >1.0 and increases with larger $\sim\text{DPP}$ conversions) is essentially eliminated. Our hypothesis at this stage is that bimolecular hydrogen transfer reactions on the surface involving $\sim\text{DPM}$ are providing a chemical means for "mobilizing" radical centers in an immobilized environment. This radical exchange concept is illustrated in Eqs. 8-10.



This hypothesis of rapid bimolecular hydrogen exchange reactions occurring on the surface is supported by our recent findings that surface-immobilized 1,4-diphenylbutane ($\sim\text{Ph}(\text{CH}_2)_4\text{Ph}$) at high coverages thermally cracks at 400 °C through both benzylic and nonbenzylic radical sites with little selectivity as a consequence of such hydrogen exchange reactions.⁴ In the present case, hydrogen transfer steps 8 and 9 could effectively decrease the distance between a radical center and a $\sim\text{DPP}$ molecule on the surface. This would remove the conformational restrictions leading to the regiospecificity in the reactions that favor formation of 7 over 6, which occur at equivalent $\sim\text{DPP}$ coverages without $\sim\text{DPM}$. By similar arguments, the enhanced $\sim\text{DPP}$ thermolysis rate could result from an enhanced rate of production of 6 and 7. Research is in progress to further elucidate this interesting reaction chemistry for mixed component surfaces.

SUMMARY

Two-component surfaces of surface-attached $\text{Ph}(\text{CH}_2)_3\text{Ph}$ ($\sim\text{DPP}$) with either PhPh ($\sim\text{BP}$) or PhCH_2Ph ($\sim\text{DPM}$) have been prepared, and their thermolysis behavior compared with that of $\sim\text{DPP}$ alone at comparable surface coverages. In the case of $\sim\text{DPP}/\sim\text{BP}$ surfaces, no major effects on the $\sim\text{DPP}$ thermolysis rate or product selectivity were observed. On the other hand, the presence of $\sim\text{DPM}$ molecules led to a significant acceleration (ca. 8-fold increase in conversion) in the $\sim\text{DPP}$ thermolysis rate while eliminating the regioselectivity in product formation that was observed previously for $\sim\text{DPP}$ alone. Our current hypothesis based on this preliminary data is that facile bimolecular hydrogen exchange reactions on the surface involving $\sim\text{DPM}$ are eliminating conformational restraints on hydrogen abstraction reactions from $\sim\text{DPP}$ by effectively placing

radicals more proximate to ~DPP molecules on the surface. These results have significant implications for the efficiency with which similar structural features will thermally decay in coal at low temperatures (350-400 °C) by radical chain processes under conditions of restricted diffusion.

ACKNOWLEDGMENT

Research was sponsored by the Division of Chemical Sciences, Office of Basic Energy Sciences, U.S. Department of Energy under contract DE-AC05-84OR21400 with Martin Marietta Energy Systems, Inc.

REFERENCES

1. (a) Green, T. K.; Kovac, J.; Brenner, D.; Larsen, J. W., In Coal Structure; Meyers, R. A., Ed.; Academic Press: New York, 1982; Chapter 6. (b) Larsen, J. W.; Green, T. K.; Kovac, J., J. Org. Chem. 1985, 50, 4729. (c) Brenner, D., Fuel 1985, 64, 167. (d) Lucht, L. M.; Peppas, N. A., Fuel 1987, 66, 803.
2. Buchanan, III, A. C.; Dunstan, T. D. J.; Douglas, E. C.; Poutsma, M. L., J. Am. Chem. Soc. 1986, 108, 7703.
3. (a) Buchanan, III, A. C.; Biggs, C. A., J. Org. Chem. 1989, 54, 517. (b) Buchanan, III, A. C.; Biggs, C. A., Prepr. Pap. - Am. Chem. Soc., Div. Fuel Chem. 1987, 32(3), 175.
4. Britt, P. F.; Buchanan, III, A. C.; Biggs, C. A., Prepr. Pap. - Am. Chem. Soc., Div. Fuel Chem., 1989, 34(2), 567.
5. Poutsma, M. L.; Dyer, C. W., J. Org. Chem. 1982, 47, 4903.
6. Gilbert, K. E.; Gajewski, J. J., J. Org. Chem. 1982, 47, 4899.
7. King, H.-H.; Stock, L. M., Fuel 1984, 63, 810.

Table 1. Effect of Surface Coverage on the Selectivity for Thermolysis of $\sim\text{Ph}(\text{CH}_2)_3\text{Ph}$ at 375 °C.

$\sim\text{DPP}$ Coverage (mmol/g)	$\sim\text{DPP}$ Conversion Range (%)	Selectivity ^a
0.566, 0.586 ^b	2.2 - 4.8	1.00 - 1.03
0.142 ^b	1.5 - 3.1	1.11 - 1.17
0.102	1.0 - 2.8	1.24 - 1.30

^aDefined as $\text{PhCH}=\text{CH}_2/\text{PhCH}_3$ yield ratio over the $\sim\text{DPP}$ conversion range given.

^bData from reference 3a.

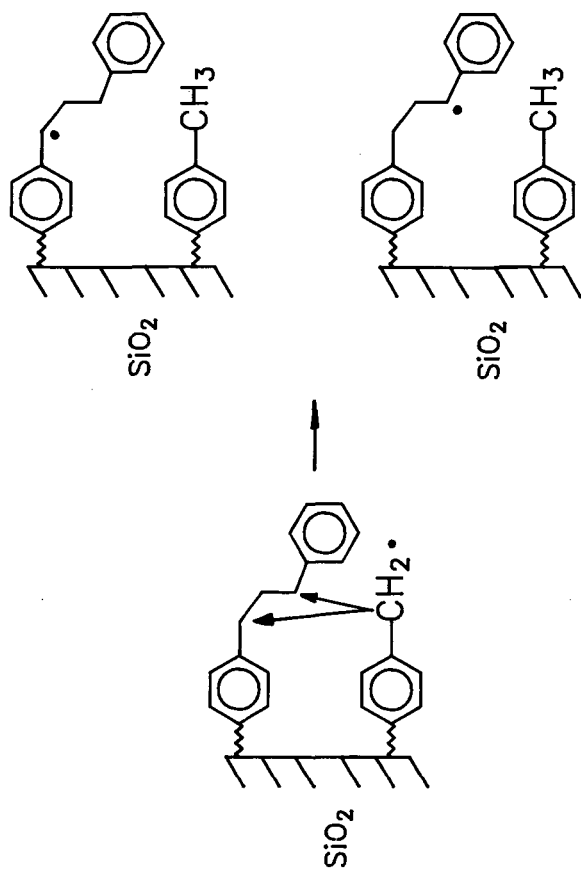
Table 2. Effect of Co-Attached Aromatics on the Thermolysis of $\sim\text{Ph}(\text{CH}_2)_3\text{Ph}$.^a

$\sim\text{DPP}$	Coverage (mmol/g)		$\sim\text{DPP}$ Conversion (%)	Selectivity ^c
	$\sim\text{BP}^b$	$\sim\text{DPM}^b$		
0.142 ^d	-	-	2.2	1.17
0.142 ^d	-	-	2.2	1.16
0.132 ^d	-	-	2.6	1.17
0.150	0.462	-	4.5	1.15
0.145	0.505	-	5.5	1.11
0.126 ^e	0.509	-	4.6	1.12
0.133	-	0.368	17	0.99
0.133	-	0.368	16	0.99
0.168	-	0.398	19	0.96

^aThermolyses were performed at 375 °C for 150 min. ^b $\sim\text{BP}$ and $\sim\text{DPM}$ are surface-attached biphenyl ($\sim\text{PhPh}$) and diphenylmethane ($\sim\text{PhCH}_2\text{Ph}$), respectively.

^cDefined as $\text{PhCH}=\text{CH}_2/\text{PhCH}_3$ yield ratio. ^dData from reference 3a. ^eMaterial prepared by a two-step exchange procedure; see text.

Figure 1 · Regiospecific Hydrogen Abstraction



THE EFFECT OF RANK ON COAL PYROLYSIS KINETICS

M.A. Serio, P.R. Solomon, Z.Z. Yu, R. Bassilakis,
J.R. Markham, and J.G. Klapheke

Advanced Fuel Research, Inc., 87 Church Street, East Hartford, CT 06108 USA

INTRODUCTION

The rank dependence of coal pyrolysis kinetics has been a subject of controversy for several years (1,2). Some have claimed that the rank variations are responsible for much of the several orders of magnitude variation in reported rates. Others have found that in experiments where the rank was the only experimental parameter, these differences were not very profound when compared to the large variations in reported rates. We subscribe to the latter view, but acknowledge that there are circumstances where relatively small rank variations may be important. One such case is the prediction of coal fluidity (3). The maximum fluidity observed experimentally depends strongly on rank and the time temperature history (heating rate, final temperature). When modeling fluidity, it was found that relatively small differences in the methane evolution rate (which is related in our model to moderate temperature crosslinking) and in the tar evolution rate (which is related to the bridge breaking rates) adversely affected the fluidity predictions (3).

This paper examines the variation in kinetic rate at both low and high heating rate. The rate for methane and for tar evolution from the Argonne premium coals were determined from a series of experiments which were done with these coals over a range of low heating rates. These will be compared with kinetic parameters determined by Burnham et al. (4) for the same coals. In addition, we report weight loss data obtained at high heating rates in a transparent wall reactor (TWR) on samples of Pittsburgh Seam and Zap Lignite coals, which provide further information on the rank variations of kinetic rates.

EXPERIMENTAL

Coal Properties - Elemental data are given for the Argonne coals in Ref. 5. The analyses of the Zap Lignite and Pittsburgh Seam bituminous coals used in the TWR experiments are given in Ref. 6.

Reactors - Pyrolysis experiments were done with the Argonne premium coals at heating rates 3, 30, 50, and 100°C/min up to 900°C in a TGA with FT-IR analysis of evolved products (TG-FTIR). The TG-FTIR is the TG/Plus from Bomem, Inc. The TG/Plus couples a Dupont 951 TGA with a Bomem Michelson 100 FT-IR spectrometer (7,8).

High heating rate measurements were made in a transparent wall reactor (TWR) which has been previously described (9). Nitrogen is passed through a heat exchanger and enters a reaction section at approximately 850°C. Coal entrained in cold nitrogen carrier gas is injected through a co-axial 7 mm diameter tube into the preheated stream. An octagonal glass enclosure shields the pyrolyzing stream from room air currents. This reactor allows particle temperature measurements to be made. One difficulty in making pyrolysis kinetic measurements at high temperatures is that the measurement of particle temperatures from the particle's emitted radiation is difficult if the pyrolysis reactor has hot walls. In this case, wall radiation scattered by the particles interferes with the emitted radiation. To overcome this problem, the reactor section has relatively cold walls. The glass enclosure has movable KBr windows to allow access to the flame for radiation measurements. Particle velocities were measured using a video camera under slightly oxidizing conditions which allowed a small

percentage of the particle to ignite.

Temperature Measurements - To measure the temperature of pyrolyzing coal particles, several other problems had to be overcome. Because pyrolysis in this reactor occurs at relatively low temperatures (600-800°C), the measurements are made in the mid-infrared where sufficient energy is emitted. In addition, coal is not a gray-body and its emissivity changes during pyrolysis. To overcome this problem, the temperature has been measured using the amplitude of the radiated energy in a frequency range where the emissivity is close to one and independent of the extent of pyrolysis. The transmission is used to determine the emitting surface area of the particles. Finally, soot radiation can make the particle temperature appear much higher than it really is. Measurements have been made with a gas temperature of 850°C so soot formation did not occur.

RESULTS AND DISCUSSION

Low Heating Rate Studies - A recent paper reported the development of a network model for coal fluidity based on the FG-DVC model and its application to predict fluidity data for a wide range of coals (3). In order to fit both the fluidity data and species evolution data, the bridge breaking and methane kinetic rates were adjusted from those used in the original model which were rank independent (5,6,10). An independent investigation was made of the rank dependence of the pyrolysis kinetics by doing experiments in a TG-FTIR reactor over a series of heating rates (3, 30, 50, 100°C/min) with three coals (Pocahontas, Pittsburgh, No. 8, and Zap lignite) which are at the extremes and midpoint of the rank range for the Argonne set. A comparison of the rank dependence of the rate constants for bridge breaking, tar evolution and CH₄ evolution at 450°C determined from analyzing the TG-FTIR data at several heating rates and from fitting the FG-DVC model to fluidity, weight loss and methane evolution data at a single heating rate (3°C/min) is shown in Fig. 1.

The rates for tar evolution are lower than those used in the FG-DVC model for bridge breaking. This makes sense since the latter does not include transport. The rates for tar evolution or bridge breaking vary by about a factor of 10 if the Pocahontas coal is excluded, which is consistent with previous results for coals from the same range of ranks. If the Pocahontas is included, the rank variation for the tar evolution or bridge breaking rates is about a factor of 50. The rates for tar evolution are consistent with those obtained by Burnham et al. for total hydrocarbon evolution from Rock Eval analysis of the same coals (6). This data is also shown in Fig. 1.

The kinetic parameters determined by either method for methane (loose) evolution are similar and show a much lower rank dependence. Finally, the rank independent parameters used in the original FG model are shown as horizontal dashed lines. These are in better agreement with results from the lower rank coals, which was expected since the set of coals used to obtain those parameters did not include the higher rank coals (5,6,10).

Experiments in the TWR - Particle temperatures were determined by matching the theoretical curves to the radiance at 1600 cm⁻¹, where the emissivity is approximately 1.0 (11,12). Measurements were obtained for both coals at positions between 5 and 40 cm. In addition, char samples were captured at a number of locations. The results for the Zap lignite are summarized in Fig. 2. Figure 2a shows the temperature measurements in the reactor made using a thermocouple and the FT-IR E/T technique to determine both particle and CO₂ temperatures (9,11-13). The CO₂ and particle temperatures agree to within 100°C. The thermocouple temperature measurements averaged across the estimated width of the particle stream are also in reasonable agreement except early in the reaction when the particle are heating and late when the gas is cooling. The particle's heating rate is about

5000°C/sec.

Figure 2b shows the weight loss determined by ash tracer analysis. These are compared to predictions of the FG-DVC model (10). The kinetic rates for bridge breaking used in the FG-DVC model is $k_b = 8.6 \times 10^{14} \exp(-228,500/RT) \text{ sec}^{-1}$. The predictions using 10 and 0.1 times this rate are also shown. The agreement for the Zap lignite is best with the highest of the three rates.

The results for the Pittsburgh Seam coal are presented in Fig. 3. These results also agree best for $k_b \times 10$. Consequently, the high heating rate data do not show much of a rank variation. However, these measurements are not as sensitive to factors of 10 difference in rate.

CONCLUSIONS

- The rank dependence of the chemical kinetic rates is important in the prediction of fluidity data. It can also be important in predicting tar evolution rates for very high rank coals (>90% carbon). It is less important in the case of methane.
- Both the low and high heating rate experiments support the previous conclusion that the rank variations for kinetic rates are usually less than a factor of 10, except for the case of tar evolution from very high rank coals.

ACKNOWLEDGMENTS

This work was supported under DOE Contract DE-AC21086MC23075. Richard Johnson is the Project Manager.

REFERENCES

1. Solomon, P.R. and Hamblen, D.G., Finding Order in Coal Pyrolysis Kinetics, Topical Report Submitted to the U.S. Department of Energy, under Contract No. DE-AC21-FE05122, (1983), also *Progress in Energy and Combustion Science*, **9**, 323, (1983).
2. Solomon, P.R. and Serio, M.A., "Evaluation of Coal Pyrolysis Kinetics", in Fundamentals of the Physical-Chemistry of Pulverized Coal Combustion, (J. Lahaye and G. prado, Eds.), 126, Marinus Nijhoff Publishers, (1987).
3. Solomon, P.R., Best, P.E., Yu, Z.Z. and Deshpande, G.V., A Macromolecular Network Model for Coal Fluidity, to be presented at ACS Fuel Chem. Div. Meeting, Miami, FL, (9/89).
4. Burnham, A.K., Oh, M.S., Crawford, R.W. and Samoun, A.M., *Energy and Fuel*, **3**, 42, (1989).
5. Serio, M.A., Solomon, P.R., Yu, Z.Z., Deshpande, G.V. and Hamblen, D.G., *ACS Fuel Chem. Preprints*, **33**, (3), 91 (1988).
6. Serio, M.A., Hamblen, D.G., Markham, J.R., Solomon, P.R., *Energy and Fuel*, **1**, 138, (1987).
7. Carangelo, R.M., Solomon, P.R. and Gerson, D.J., *Fuel*, **66**, 960, (1987).
8. Whelan, J.K., Solomon, P.R., Deshpande, G.V., and Carangelo, R.M., *Energy and Fuel*, **2**, 65, (1988).
9. Solomon, P.R., Chien, P.L., Carangelo, R.M., Best, P.E., and Markham, J.R., "Application of FT-IR Emission/Transmission (E/T) Spectroscopy to Study Coal Combustion Phenomena", 22nd Symp. (Int) on Combustion, The Combustion Institute, Pittsburgh, PA (in press).

10. Solomon, P.R., Hamblen, D.G., Carangelo, R.M., Serio, M.A. and Deshpande, G.V., *Energy and Fuel*, **2**, 405, (1988).
11. Best, P.E., Carangelo, R.M., Markham, J.R., and Solomon, P.R., *Combustion & Flame*, **66**, 47, (1986).
12. Solomon, P.R., Carangelo, R.M., Best, P.E., Markham, J.R., and Hamblen, D.G., 21st Symp. (Int) on Combustion, The Combustion Institute, Pittsburgh, PA p. 437, (1986).
13. Solomon, P.R., Carangelo, R.M., Best, P.E., Markham, J.R., and Hamblen, D.G., *Fuel*, **66**, 897, (1987).

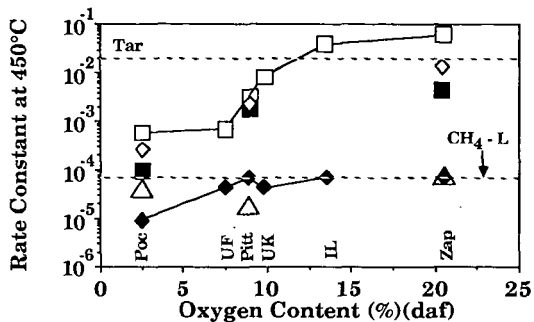


Figure 1. Comparison of Kinetic Rates at 450°C for Bridge Breaking (BB), Tar Formation, and Methane-Loose (CH₄-L) Formation. (■) BB, (△) CH₄-L from FG-DVC Model Fits; (□) Tar, (●) CH₄-L from TG-FTIR Data; (◇) Tar from Burnham et al. (4). Dashed Lines are Rank Independent Parameters.

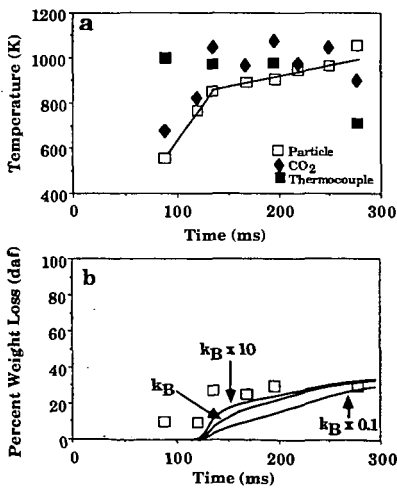


Figure 2. Pyrolysis Results for Zap North Dakota Lignite.

a) Temperatures and b) Weight Loss.

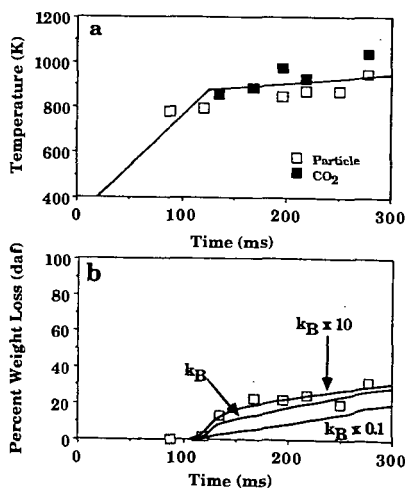


Figure 3. Pyrolysis Results for Pittsburgh Seam Bituminous.

a) Temperatures and b) Weight Loss.

Development of Char Structure During Pyrolysis of a hvB Bituminous Coal

Guangwei Huang and Alan W. Scaroni
The Combustion Laboratory
The Pennsylvania State University
404 Academic Activities Bldg
University Park, PA 16802

Introduction

When coal particles are heated rapidly they undergo radical changes in chemical and physical properties. The sequence of events in the pyrolysis of caking coals includes heatup of the coal particles, plasticity development in part of, or the whole coal particle, swelling, and resolidification. The occurrence and the nature of these events depend on the rank of the coal and its thermal history. The rate of evolution of gaseous products of pyrolysis is affected by mass transfer inside the pores. There has been much work published on the thermoplastic behavior of coals and the development of char structure during pyrolysis of pulverized coal (1-7). However, very little work has been published recently on the behavior of millimeter-sized coal particles, even though this size is widely used in fluidized-bed combustors. The objective of this work was to study the morphological and compositional changes in the chars produced during pyrolysis of single particles of a hvB bituminous coal using scanning electron microscopy (SEM) and elemental analysis (CHN). The mechanism for the transport of volatiles out of the pyrolyzing coal particle is also discussed.

Experimental

Pyrolysis experiments on single coal particles 1.0 to 1.5 mm in diameter were performed in an electrically heated reactor, details of which have been provided elsewhere (8,9). A hvB bituminous coal (volatile matter 48.3%, fixed carbon 47.1%, ash 4.6%) was used in this study. For each run, a coal particle was injected into the preheated reactor which was maintained at a temperature of 973 K under an atmosphere of nitrogen. The temperature gradients in the gas surrounding the particle were measured using a thermocouple array and the particle surface temperature history was obtained by extrapolation of the measured gas temperature gradients (10). Before particle injection, the gas flow was stopped so that the experiments were carried out essentially in a stagnant system.

Char particles were collected and weighed after the required residence time by quickly withdrawing them from the reaction zone into an extension of the quartz reactor and cooling them to ambient temperature using a high flow rate of nitrogen. A calculation considering the heat lost by convection and radiation from the particles estimated that cooling to below 400 °C occurred in about 0.5 s.

Results and Discussion

The elemental analyses of the coal and the chars were performed using a Leco CHN-600 Determinator and are given in Table 1. Weight Loss was calculated by averaging the weight of the chars from 10 runs conducted at the same residence time. The weight loss (ΔW) and the average rate of weight loss ($\Delta W/\Delta t$) between successive

residence times are also listed in Table 1. The rate of weight loss reached its maximum between 3.0 to 4.5 s, representing a 21% loss in weight in 1.5 s (weight loss from 15 to 36 %), and then decreased sharply. Little weight loss was observed after 6 s. The overall H/C ratio for the volatiles evolved was 1.48. The atomic H/C ratio for the volatiles released between successive residence times (H/C (VM)) was determined from a mass balance using the weight loss and ultimate analysis data. The H/C ratio for the volatiles released before 763 K was slightly greater than one, probably due to the carbon oxides released during decarboxylation. The H/C ratio for the volatiles released during the maximum rate of weight loss was one, which is almost the same as the value for the starting coal (0.94). These numbers indicate that a) the relatively weakly held volatiles such as those physically adsorbed in micropores or weakly bonded to the coal matrix are released early and possess intermediate H/C values (1 to 2); b) the major fraction of the volatiles escaping the coal particles by evaporation or diffusion during the peak devolatilization rate has the lowest H/C value, (~1); and c) the volatiles released last, produced by cracking or repolymerization reactions, have the highest H/C value (~4).

A scanning electron microscope was used to examine the changes in morphology of the coal particles at different extents of reaction. Figure 1 shows the surface of a raw coal particle. At 1000 \times magnification the surface appears smooth with some scattered mineral clusters. An obvious morphological change (Figure 2) is observed for the char after 1.5 s corresponding to about 10 % weight loss. The coal particle appears to have become partially molten and some open holes and bubbles have appeared. Further pyrolysis (Figure 3) yields a char having a molten surface with fewer bubbles than observed at shorter residence time. The fact that some bubbles adjacent to open holes have deflated instead of bursting suggests the development of internal pores which allowed the decomposed gaseous products trapped in the bubbles to escape through new tunnels into neighboring open holes. The char morphology shown in Figure 4 clearly indicates a surface structure resulting from resolidification of the fluid phase. A lower magnification of 500 \times was used for Figure 4 to show a larger region of the char surface. It is noteworthy to see a strong viscous fluid pattern for a hvB bituminous coal classified as a poor coking coal. The viscous coal melt has flown over the particle surface and sealed some open holes. The exiting gases have had to escape from a very viscous melt to create vortex-like structures (as seen in the concentric patterns in Figure 4). A similar behavior for a lignite was reported by Solomon et al (11), suggesting that the melting, bubbling, and swelling phenomena may be due to the high heating rate, which mitigates the crosslinking reactions responsible for decreasing fluidity.

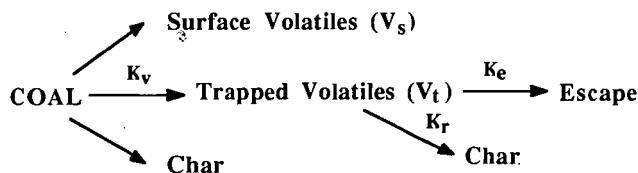
The open holes mentioned above are defined as those found on the particle surface throughout the pyrolysis (from beginning to end). An open hole is distinguished from a blowhole by its smooth rim and larger size (5~30 μm in diameter). The cause of early open holes on the coal surface may be the expansion of existing micropores or the localized acceleration of devolatilization due to catalytic pyrolysis by the dispersed mineral clusters.

In order to examine internal structural changes, a char particle collected at a residence time of 5 s at about 40% weight loss was cut in half and the electronmicrograph of its cross section is shown in Figure 5. The very porous internal structure shown in Figure 5 consists of interconnected pores formed by coalescence of bubbles of various size, with a few large pores (up to 400 μm) in the center and many smaller ones near the surface. The surface, however, is a relatively dense crust with a thickness of about 30 μm . Figure 6 shows the pore structure beneath the dense crust, revealed by peeling off the surface layer of the char, indicating a more developed structure consisting of many macro-

and meso-pores. The internal surface area provided by these pores, nevertheless, would generally be inaccessible for char gasification and/or combustion unless the reactants could pass through the dense crust.

A major morphological change in the chars during the maximum rate of evolution of volatiles can be seen from Figure 3 (residence time of 3 s and 15% weight loss) and Figure 4 (residence time of 5 s and 40% weight loss). Before the peak rate of volatiles evolution (Figures 2 and 3), the coal particle undergoes melting, bubbling, and release of volatiles through the open pores and from the external surface. Blowholes generated from bursting of bubbles were not observed before 15% weight loss. Most bubbles caused by the buildup of pressure of the gaseous products in the coal melt either flattened (Figure 3), or later burst (Figure 4) during the period of the maximum rate of volatiles evolution.

Suuberg et al (12) suggested a competitive kinetic scheme for metaplast evaporation and repolymerization. In order to explain the increased rate of evolution of volatiles with higher heating rate Niksa et al (13) classified the products of primary devolatilization into two categories, namely the light, stable volatiles from the elimination of peripheral groups and the reactive intermediates from bridge cleavage. A similar scheme with more emphasis on volatiles transfer out of coal particles is proposed below:



Here, surface volatiles (V_s) represent the easily released volatiles, generated by decomposition reactions on the external surface or on the internal surface of the open holes, leaving the particle as soon as they are formed. The resistance to volatiles liberation from the coal particle is negligible. Trapped volatiles (V_t) are those produced within the tortuous micropores or trapped in the bubbles, and are not registered as weight loss even though they are decomposed from the coal matrix. Trapped volatiles can either: (1) leave the particle by bursting the bubbles or penetrating to the particle surface or neighboring open holes, or (2) redeposit onto the solid residue (R) by repolymerization. The total yield of volatiles is given by the sum of V_s and V_t . The K_v , K_r , and K_e , represent the rate constants for the formation and repolymerization of the trapped volatiles, and the overall mass transfer coefficient for the liberation of trapped volatiles, respectively. Both the trapped volatiles formation and the repolymerization processes have been modeled as first order reactions (14). It is suggested that K_e should be proportional to an ordinary bulk diffusion coefficient, which in turn varies inversely with pressure. Therefore, the total yield of volatiles should also be pressure sensitive.

Unlike the cenospheres found with smaller particles, large caking coal particles were observed to form porous, but not hollow, char structures with dense external crusts under the experimental conditions of this study. The volatiles were formed mainly in the internal micropores (due to the larger surface area) as trapped volatiles rather than on the external surface or in open holes as surface volatiles. This implies a dependence of the total yield of volatiles on pressure and heating rate. High pressure is detrimental to high yields

because the coal melt is more viscous and less penetrable. On the other hand, a high heating rate is beneficial due to an increased internal pressure and increased fluid range of the coal melt.

Conclusions

Two kinds of holes were found on the surface of the chars produced from the hvB bituminous coal particles under the experimental conditions studied. The open holes played the predominant role during volatiles release, whereas the blowholes made a contribution to the weight loss only near the maximum rate of devolatilization. The average H/C ratio of the released volatiles was about 1.5. The volatiles released at higher conversion had H/C ratios as high as 4. Micrographs of the cross sections of the char particles indicated a well developed internal pore structure covered by a dense crust at the particle surface.

References

- 1 Solomon, P. R., Ch 4 in 'Chemistry of Coal Conversion' (Ed. R.H. Schlosberg), Plenum Press, New York, 1985
- 2 Tsai, C. Y. and Scaroni, A. W., Fuel 1987, 66, 220
- 3 Khan, M. R., Lee, C. W., and Jenkins, R. G., Fuel Processing Technol., 17, 1987, 63-71
- 4 Lowenthal, G., Wanzl, W., and Heek, K. H. V., Fuel, 1986, 65, 346
- 5 Shibaoka, M., J. Inst. Fuel 1969, 59, 42
- 6 Khan, M. R., and Jenkins, R. G., Fuel 1986, 65, 725
- 7 Gray, V. R., Fuel 1988, 67, 1298
- 8 Huang, G., Vastola, F. J., and Scaroni, A. W., Prepr. Am. Chem. Soc., Div. Fuel Chem., 1987, 32 (3), 1
- 9 Huang, G., Vastola, F. J., and Scaroni, A. W., Energy & Fuels, 1988, 2, 385
- 10 Huang, G., Vastola, F. J., and Scaroni, A.W., Prepr. Am. Chem. Soc., Div. Fuel Chem., 1988, 33 (1), 283
- 11 Solomon, P. R., Serio, M. A., Carangelo, R. M., and Markham, J. R., Fuel, 1986, 65, 182
- 12 Suuberg, E. M., Peters, W. A., and Howard, D. B., 17th Symp. (International) on Combustion, The Combustion Institute, Pittsburgh, 1979, 117
- 13 Niksa, S., Heyd, L. E., Russel, W. B., and Saville, D. A., 20th Symp. (International) on Combustion, The Combustion Institute, Pittsburgh, 1984, 1445
- 14 Anthony D. A., Howard, J. B., Hottel, H. C., and Meissner, H. P., 15th Symp. (International) on Combustion, The Combustion Institute, Pittsburgh, 1974, 1303

Table 1. Characterization of the Coal, Chars, and Volatiles

Time (s)	0	1.5	3.0	4.5	6.0	9.0
Weight Loss* (g/coal×100)	0	9.1	14.8	35.8	41.0	43.2
ΔW (g/coal×100)		9.1	5.7	21.0	5.2	2.2
$\Delta W/\Delta t$ (g/coal/s×100)		6.1	3.8	14.0	3.4	0.7
Ultimate Analysis**						
C	75.9	77.7	77.3	77.6	78.7	80.9
H	5.9	5.7	5.3	4.7	3.3	3.2
N	1.5	1.4	1.5	1.5	1.6	1.6
S+O	13.1	11.3	11.7	10.7	10.4	8.1
Ash	3.6	3.9	4.2	5.5	6.0	6.2
H/C (char)	0.94	0.88	0.82	0.73	0.51	0.48
H/C (VM)***	1.13	2.27	1.01	3.77	3.82	

* Weight loss is the average for 10 runs

** Dry basis

*** Overall H/C for released volatiles is 1.48

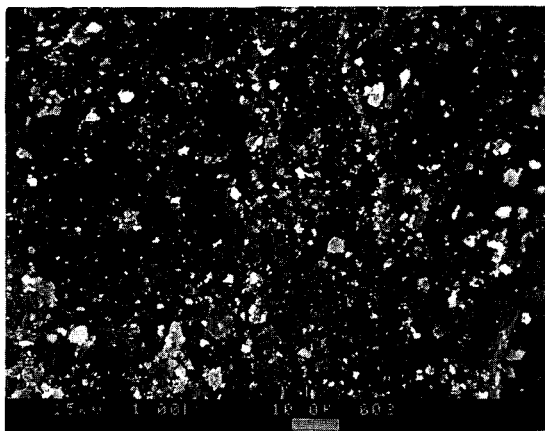


Figure 1 SEM micrograph of a PSOC 435 coal particle

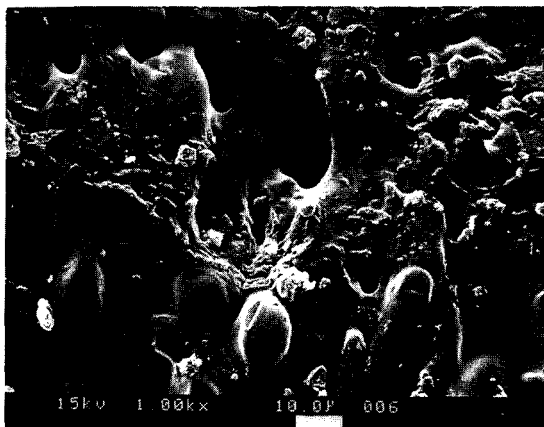


Figure 2 SEM micrograph of a char particle from pyrolysis of PSOC 435 at 973 K, 1.5 s

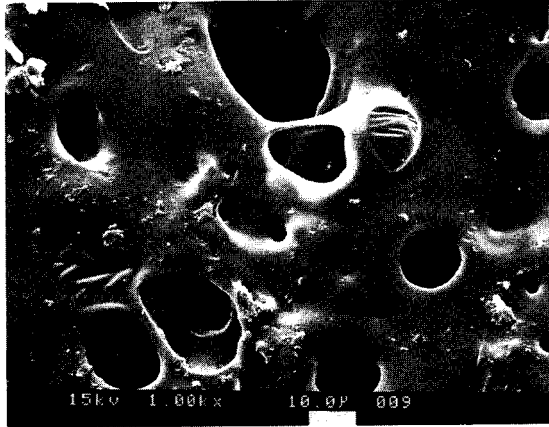


Figure 3 SEM micrograph of a char particle from pyrolysis of PSOC 435 at 973 K, 3.0 s

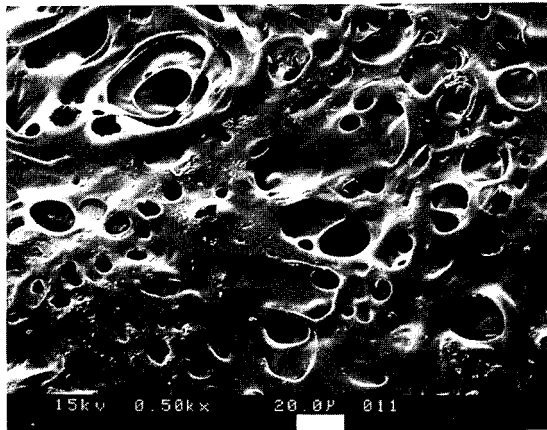


Figure 4 SEM micrograph of a char particle from pyrolysis of PSOC 435 at 973 K, 5.0 s

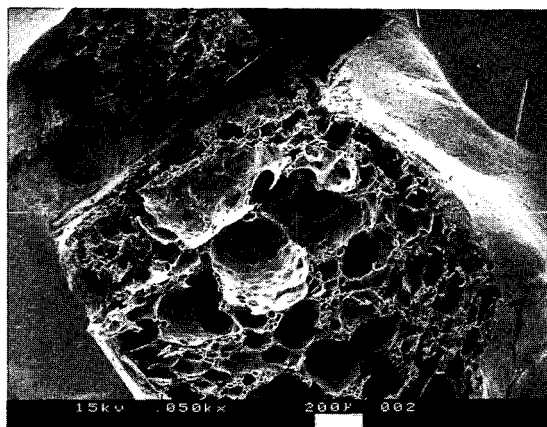


Figure 5 SEM micrograph of the cross section of a char particle from pyrolysis of PSOC 435 at 973 K, 5.0 s

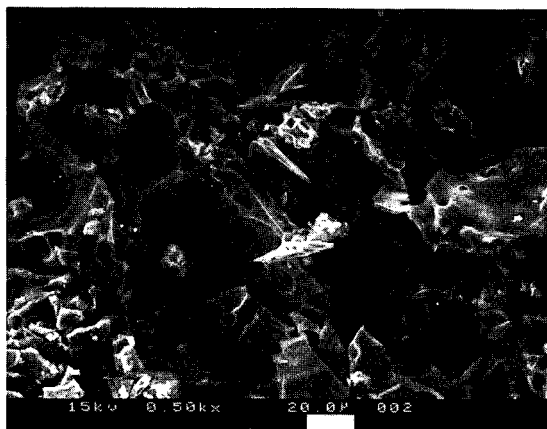


Figure 6 SEM micrograph of the pore structure beneath the particle surface of a char particle from pyrolysis of PSOC 435 at 973 K, 5.0 s

Solid State ^{13}C NMR Studies of Coal Char Structure Evolution

M.S. Solum, R.J. Pugmire, D.M. Grant, T.H. Fletcher, and P. Solomon

University of Utah
Salt Lake City, Utah 84112

Combustion Research Facility
Sandia Livermore National Laboratory
Livermore, California 94550

and
Advanced Fuel Research
Hartford, Connecticut 06108

ABSTRACT

Solid state ^{13}C NMR techniques have been used to study the evolution of char structure during pyrolysis processes. The effects of residence time, heating rate, and final char temperature are observed. The NMR data demonstrates that extensive loss of aromatic ring bridge material precedes significant change in aromatic cluster size.

I. Introduction

All coal conversion processes are controlled by thermal decomposition in which the coal is transformed into volatiles and char. To study this process, investigators have focused on how various parameters change with the extent of decomposition (such as weight loss, volatile evolution, functional group composition, reactivity, solvent swelling ratio, tar molecular weight distribution, extract yields, etc.) In this study a series of chars for which weight loss and volatile evolution data has been previously obtained has been subjected to a variety of measurements to characterize the coal to char transformation. This report focuses on ^{13}C solid state NMR spectroscopy to obtain functional group composition and other structure data. A subsequent paper will present characteristics of the same chars obtained by ^{13}C NMR, FT-IR, solvent swelling, and oxygen reactivity¹. The identification of the chemistry of the coal to char transformation is particularly important to the development of network models for coal thermal decomposition (1,2).

In the past decade ^{13}C solid state NMR spectroscopy, because of its nondestructive nature and unique capabilities, has been used in the structural analysis of solid fossil fuel samples.^{3,4} Using cross-polarization⁵⁻⁹ (CP), magic angle spinning^{7,10-12} (MAS), and dipolar decoupling techniques^{12,13} a direct measurement of the relative number of aromatic and non-aromatic carbons is possible.¹⁴ The aromaticity, f_a' , has been reported for whole coals, macerals, soil and other fossil fuel related materials.¹⁴⁻¹⁹ Other researchers have also used dipolar dephasing (DD) techniques²⁰⁻²² along with normal CP/MAS integrations over selected chemical shift ranges to subdivide f_a' values into the amount of protonated and nonprotonated carbon²³⁻²⁷. These techniques have recently been used to estimate the average aromatic cluster size of the eight coals in the Argonne Premium Coal Sample Bank (APCSB).²⁸ In more sophisticated experiments, the analysis of chemical shielding tensor

components has been used to estimate the cluster size of anthracite coals and a fusinite coal maceral.²⁹

We have recently turned our attention to the study of coal chars in order to assess the changes in the carbon skeletal structure of the char as compared to the parent coal. The char cluster size has been of particular interest as part of our long range goal of understanding the relationship between char structure and reactivity. We have recently begun a study of a series of chars produced from different coals at different heating rates and final temperatures.

II. Experimental

A. NMR Experiments

The data on coals and chars were obtained according to the method described by Solum.²⁸ Relaxation parameters were determined on the parent coal and each char as well as the carbon structural distribution.

B. Char Preparation

Chars for this study were prepared at AFR (Zap and Pitt. #8 coals) by pyrolysis in an inert atmosphere in one of three reactors as discussed in Reference 30. The chars from the Illinois No. 6 coal were prepared in an entrained flow reactor at the Combustion Research Facility at Sandia National Laboratories as described in Reference 31.

III. Results and Discussion

A. Cluster Size Determination

The carbon skeletal structure of the parent coals and related chars are presented in Tables 1-4. The definition of these carbon structural distribution parameters is given by Solum, et. al.²⁸ As pointed out in the analysis of the APCSB coals, the amount of bridgehead carbon f_a^B present is an important structural parameter. The mole fraction of aromatic bridgehead carbons, χ_b is defined as $\chi_b = f_a^B / f_a'$ where f_a' is the fraction of aromatic carbons present in the sample. This parameter is important as it can be used to estimate the aromatic cluster size (see reference 28).

B. Char Structure Analysis

The data in Tables 1-4 represent a variety of experimental conditions on different coals. The data on the Zap coals were obtained by both rapid and slow heating techniques on two different coal samples. For the slow heating case, the chars were produced by heating an APCSB Zap coal at 0.5 deg/sec with a 3 minute hold at the final temperature. The rapid heating Zap, Illinois #6, and Pittsburgh #8 data were taken at heating rates of $\sim 10^4$ deg/sec at various temperatures and residence times. The Illinois #6 data was obtained from a set of char samples produced from a 106-125 μ coal. The reactor residence times were 50 ms and 105 ms with sample temperatures measured at 850 and 1100°K, respectively for the two samples.

At this stage of the work, it appears that four structural parameters are informative. In Figure 1, the relationship between aromaticity and cluster size is apparent for the Pitt. #8 coal and related chars. Only char data from Table 3 for similar residence times are included in the plot. It is apparent from the remainder of the data on Pitt. #8 (and the Illinois #6 data) that

residence time at a given temperature is an important consideration. However, sufficient data is not available at the present time to permit a detailed assessment of this effect although the general trend is obvious from the data. While the aromaticity changes with temperature, it is clear that the cluster size has not changed at 973°K. At 1073°K, one observes the onset of cluster growth (but not at the shorter residence time, i.e., 1073°K/12" in Table 1) by a factor of 25% while at 1373°K the cluster size has doubled. In Figure 2 the percent of aliphatic carbon is compared to the aromatic attachment sites/100 carbons. As the pyrolysis temperature increases a significant reduction is noted in the aliphatic carbon content. However, the number of attachment sites (alkyl and alkoxy functional groups) on aromatic carbons exhibits essentially no change. Similar effects are noted in Figures 3 and 4 for the rapid and slow heating conditions for Zap lignite.

The data on PSOC-1493 represents only two samples from the pyrolysis series. While the aromaticity has started to increase at 1100°K (105 ms residence time) the aromatic cluster size has not changed (Figure 5). However, the decrease in aliphatic carbon content together with little or no change in the number of aromatic attachment sites per 100 carbon atoms is similar to the other char data.

The four sets of char data demonstrate a consistent pattern. As the temperature and/or residence time for pyrolysis increases, one observes an increase in aromaticity of the char (relative to the parent coal) and a concomitant decrease in the amount of aliphatic carbon remaining in the char. The average aromatic cluster size does not change in the 850-1100°K temperature range for the two high volatile bituminous coals studied and only increases significantly above ~ 1100°K. In the case of the Zap coals, the slow heating data displays a monotonic relationship between cluster size and final temperature. In the rapid heating case, the effects of residence time on cluster size is clearly evident. Whether this effect is due to the fact that the temperatures are in excess of 1000°K (1073 and 1873) or to the nature of the coal is not clear from this limited data set.

The other significant phenomena are the decrease in aliphatic carbon content with essentially no variation in the number of aromatic bridge and side chain attachment sites. These data are consistent with models^{1,2} for coal devolatilization wherein tar production is accompanied by expulsion of bridge material and stabilization of dangling free radicals by hydrogen transfer reactions or expulsion as light gases. Hence, the data suggest that the evolution of char structure is a function of heating rate, final temperature, and residence time. During pyrolysis, aliphatic rich material is preferentially expelled as tar and light gases. In the initial stages of pyrolysis, it appears that there is no onset of aromatic cluster size growth until the temperature approaches 1100°K in the fast heating regime, i.e., ~ 10⁴/sec. The loss of aliphatic carbon appears to be through expulsion of bridge material which leaves a host of short side chains and bridges still intact. The details of this mechanism are being evaluated and we will supplement these preliminary char studies with a more extensive set of data³⁰ and a set of carefully prepared char/tar pairs.

Acknowledgements

This work was supported by the National Science Foundation under Cooperative Agreement No. CDR 8522618. Also participating in the funding of this effort in alphabetical order, were a consortium of organizations that include: Advanced Fuel Research Inc.; Allison Division (General Motors Corp.); Babcock and Wilcox; Chevron Research Co.; Combustion Engineering, Inc.; Conoco, Inc.; Convex Computer Corp.; Corning Glass Works; Dow Chemical USA; Electric Power Research Institute; Empire State Electric Energy Research Corp.; Foster Wheeler Development Corp.; Gas Research Institute; General Electric Co.; Los Alamos National Laboratory; Morgantown Energy Technology Center (U.S. Dept. of

Energy); Pittsburgh Energy Technology Center (U.S. Dept. of Energy); Pyropower Corp.; Questar Development Corp.; Shell Development Co.; Southern California Edison; the State of Utah; Tennessee Valley Authority; and Utah Power and Light Co. Brigham Young University and the University of Utah financial support is also acknowledged. Additional support (for Advanced Fuels Research) was provided by the DOE through the Morgantown Energy Technology Center (for AFR, Contract DEAC21-86MC23075) and the Pittsburgh Energy Technology Center (for CRF and through the Consortium for Fossil Fuel Liquefaction Science for the University of Utah).

References

1. Solomon, P.R.; Hamblen, D.G.; Carongelo, R.M.; Serio, M.A.; and Desphande, G.V. *Energy & Fuels*, 1988 2, 405.
2. Grant, D.M.; Pugmire, R.J.; Fletcher, T.H.; and Kerstein, A.R. *Energy & Fuels*, 1989, 8, (in press).
3. Axelson, D.E. *Solid State Nuclear Magnetic Resonance of Fossil Fuels*; Multi Science: Canada, 1985.
4. Davidson, R.M. *Nuclear Magnetic Resonance Studies of Coal*; IEA Coal Research: London, 1986.
5. Hartmann, S.R.; Hahn, E.L. *Phys. Rev.*, 1962, 128, 2042.
6. Pines, A.; Gibby, M.G.; Waugh, J.S. *J. Chem. Phys.*, 1972, 56, 1776.
7. Mehring, M. In *High Resolution NMR Spectroscopy in Solids*; Diehl, P.; Fluck, E.; Kosfeld, R., Eds.; NMR-Basic Principles and Progress; Springer Verlag: New York 1976; Vol 11.
8. Alemany, L.B.; Grant, D.M.; Pugmire, R.J.; Alger, T.D.; Zilm, K.W. *J. Am. Chem. Soc.*, 1983, 105, 2133.
9. Alemany, L.B.; Grant, D.M.; Pugmire, R.J.; Alger, T.D.; Zilm, K.W. *J. Am. Chem. Soc.*, 1983, 105, 2142.
10. Andrew, E.R.; Bradbury, A.; Eades, R.G. *Nature*, 1959, 183, 1802.
11. Lowe, I.J. *Phys. Rev. Lett.*, 1959, 2, 285.
12. Schaefer, J.; Stejskal, E.O.; Buchdahl, R. *Macromolecules*, 1975, 8, 291.
13. Pines, A.; Gibby, M.G.; Waugh, J.S. *J. Chem. Phys.*, 1973, 59, 569.
14. VanderHart, D.L.; Retcofsky, H.L. *Fuel*, 1976, 55, 202.
15. Botto, R.E.; Wilson, R.; Winans, R.E. *Energy & Fuel*, 1987, 1, 173.
16. Sullivan, J.J.; Maciel, G.E. *Anal. Chem.*, 1982, 54, 1615.
17. Vassallo, A.M.; Wilson, M.A.; Collin, P.; Oades, J.M.; Waters, A.G.; Malcolm, R.L. *anal. Chem.*, 1987, 59, 558.

18. Hagaman, E.W.; Chambers, R.R.; Woody, M.C. *Anal. Chem.*, 1986, 58, 387.
19. Vassallo, A.M.; Wilson, M.A.; Edwards, J.H. *Fuel*, 1987, 66, 622.
20. Alla, M.; Lippmaa, E. *Chem. Phys. Lett.*, 1976, 37, 260.
21. Opella, S.J.; Frey, M.H. *J. Am. Chem. Soc.*, 1979, 101, 5854.
22. Alemany, L.B.; Grant, D.M.; Alger, T.D.; Pugmire, R.J. *J. Am. Chem. Soc.*, 1983, 105, 6697.
23. Alemany, L.B.; Grant, D.M.; Pugmire, R.J.; Stock, L.M. *Fuel*, 1984, 63, 513.
24. Wilson, M.A.; Collin, P.J.; Pugmire, R.J.; Grant, D.M. *Fuel*, 1982, 61, 959.
25. Wilson, M.A.; Pugmire, R.J.; Karas, J.; alemany, L.B.; Woolfenden, W.R.; Grant, D.M.; Given, P.H. *Anal. Chem.*, 1984, 56, 933.
26. Soderquist, A.; Burton, D.J.; Pugmire, R.J.; Beeler, A.J.; Grant, D.M.; Durand, B.; Huk, A.Y. *Energy & Fuels*, 1987, 1, 50.
27. Derenne, S.; Largeau, C.; Casadervall, E.; Laupretre, F. *Fuel*, 1987, 66, 1086.
28. Solum, M.S.; Pugmire, R.J.; and Grant, D.M. *Energy & Fuels*, 1989, 3, in press.
29. Sethi, N.K.; Pugmire, R.J.; and Grant, D.M. *Anal. Chem.*, 1988, 60, 1574.
30. Solum, M.S.; Pugmire, R.J.; Grant, D.M.; Fletcher, T.H.; and Solomon, P.R. solid State ¹³C NMR Studies of Coal Char Structure Evolution: I. Submitted.
31. Fletcher, T.H. Time-Resolved Temperature Measurements of Individual Coal Particles During Devolatilization Sandia Report , SAND88-8635, September, 1988.

TABLE 1. Carbon Structural Parameters for Chars Produced from A Zap Coal Under Rapid Heating (10^4 deg/sec) Conditions

MATERIAL	f_a	$f_{a'}$	f_a^C	f_a^H	f_a^N	f_a^P	f_a^S	f_a^B	f_{a1}	f_{a1}^H	f_{a1}^*	f_{a1}^O
AFR ZAP	.74	.61	.13	.23	.38	.10	.19	.09	.26	.15	.11	.07
CHAR 800°C (0.5 m)	.75	.63	.12	.21	.42	.10	.17	.15	.25	.12	.13	.07
CHAR 800°C (2.4 m)	.87	.83	.04	.35	.48	.06	.19	.23	.13	---	---	.07
CHAR 1600°C (60 ms)	.83	.77	.06	.38	.39	.06	.18	.15	.17	---	---	.10
CHAR 1600°C (160 ms)	.88	.84	.04	.26	.58	.06	.22	.30	.12	---	---	.07

MATERIAL	X_b	CARBONS PER CLUSTER
AFR ZAP	0.148	8.5
CHAR 800°C 0.5 m	0.238	11.4
CHAR 800°C 2.4 m	0.277	13.3
CHAR 1600°C 0"	0.195	9.8
CHAR 1600°C 4"	0.357	17.8

TABLE 2. Carbon Structural Parameters for Chars Produced from Argonne PCSB Zap Coal. Hold Time at Final Temperature was 3 Minutes.

MATERIAL	f_a	$f_{a'}$	f_a^C	f_a^H	f_a^N	f_a^P	f_a^S	f_a^B	f_{a1}	f_{a1}^H	f_{a1}^*	f_{a1}^O
ZAP COAL	.61	.54	.07	.26	.28	.06	.13	.09	.39	.25	.14	.12
CHAR 200°C (3 min)	.72	.62	.10	.24	.38	.08	.17	.13	.28	.21	.07	.08
CHAR 300°C (3 min)	.77	.69	.08	.28	.41	.08	.18	.15	.23	---	---	.06
CHAR 400°C (3 min)	.79	.72	.07	.27	.45	.08	.19	.18	.21	---	---	.07
CHAR 500°C (3 min)	.86	.79	.07	.29	.50	.10	.17	.23	.14	---	---	.06

MATERIAL	X_b	CARBONS PER CLUSTER
ZAP COAL	0.167	9.0
CHAR 200°C (3 min)	0.210	10.4
CHAR 300°C (3 min)	0.217	10.6
CHAR 400°C (3 min)	0.250	12.0
CHAR 500°C (3 min)	0.291	14.1

TABLE 3. Carbon Structural Parameters for Pittsburgh #8 Coal and Char Produced at Different Temperatures and Residence Times

MATERIAL	f_a	f_a'	f_a^C	f_a^H	f_a^N	f_a^P	f_a^S	f_a^B	f_{a1}	f_{a1}^H	f_{a1}^*	f_{a1}^O
PITTSBURGH #8	.71	.67	.04	.28	.39	.09	.16	.14	.29	.17	.12	.07
CHAR 700°C 24"	.80	.75	.05	.34	.41	.08	.19	.14	.20	.10	.10	.08
CHAR 800°C 12"	.76	.71	.05	.29	.42	.08	.20	.14	.24	.12	.12	.08
CHAR 800°C 24"	.80	.77	.03	.35	.42	.06	.16	.20	.20	.10	.10	.08
CHAR 1100°C 20"	.88	.85	.03	.33	.52	.04	.16	.32	.12	---	---	.06
CHAR 1100°C 24"	.89	.85	.04	.27	.58	.04	.21	.33	.11	---	---	.06

MATERIAL	x_b	CARBONS PER CLUSTER
PITTSBURGH #8	0.209	10.3
CHAR 700°C 24"	0.187	9.6
CHAR 800°C 12"	0.197	9.9
CHAR 800°C 24"	0.260	12.5
CHAR 1100°C 20"	0.376	18.6
CHAR 1100°C 24"	0.388	19.2

TABLE 4. Carbon Structural Parameters for Char Produced from an Illinois No. 6 Coal

MATERIAL	f_a	f_a'	f_a^C	f_a^H	f_a^N	f_a^P	f_a^S	f_a^B	f_{a1}	f_{a1}^H	f_{a1}^*	f_{a1}^O
PSOC-1493 COAL	.71	.67	.04	.27	.40	.08	.17	.15	.29	.15	.14	.07
CHAR 1250 K 40 mm	.72	.67	.05	.29	.38	.09	.19	.10	.28	.18	.10	.07
CHAR 1250 K 100 mm	.79	.74	.05	.34	.40	.07	.19	.14	.21	---	---	.08

MATERIAL	x_b	C	$\sigma + 1$
PSOC-1493	0.224	10.8	4.0
CHAR 1250 K 40 mm	0.149	9.6	4.0
CHAR 1250 K 100 mm	0.189	9.7	3.4

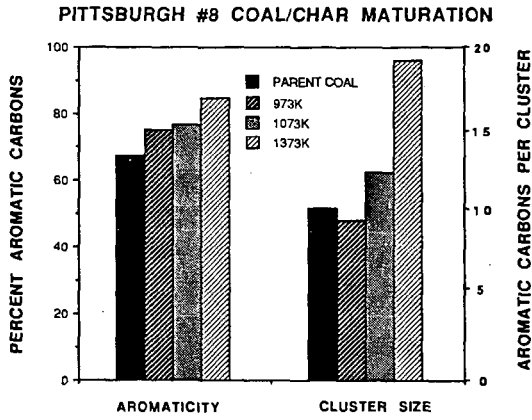


Figure 1. Relationship between aromaticity and cluster size for a Pitt. #8 coal and related chars.

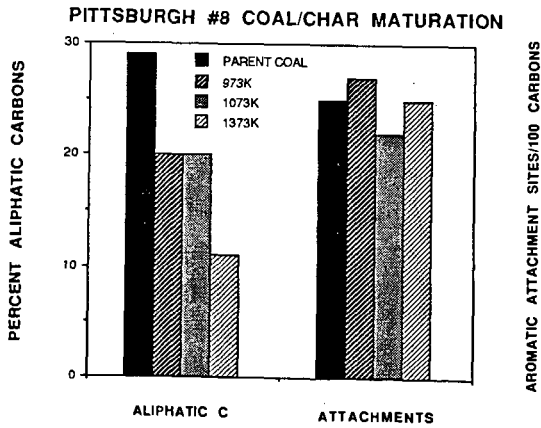


Figure 2. Relationship between aliphatic carbon content and number of aromatic attachment sites 1100 carbons for a Pitt. #8 coal and related chars.

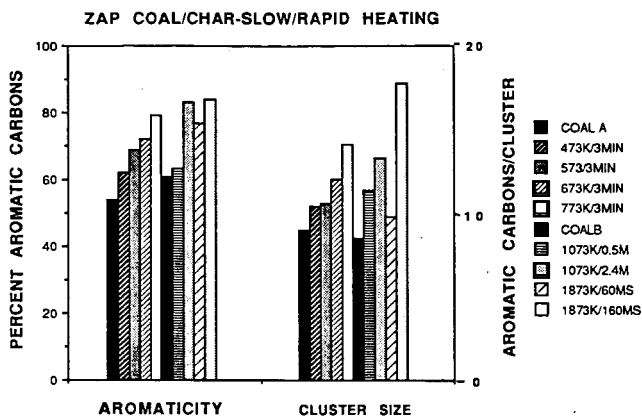


Figure 3. Relationship between aromaticity and cluster size for Zap coals and related chars heated under rapid heating conditions and APCSB Zap coal heated at 0.5 deg/sec with a hold time of 3 minutes.

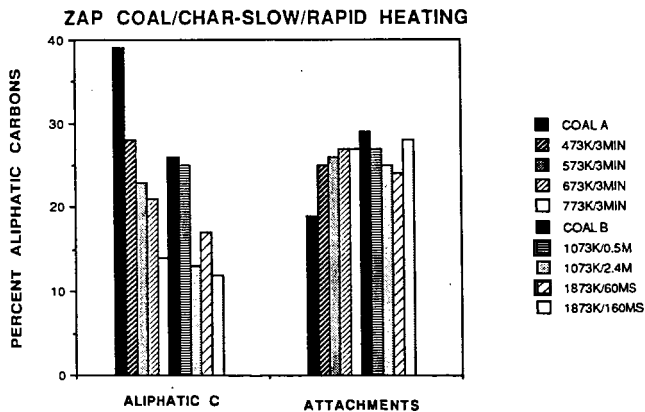


Figure 4. Relationship between aliphatic carbon content and number of aromatic attachment sites/100 carbons for the coals described in Figure 5.

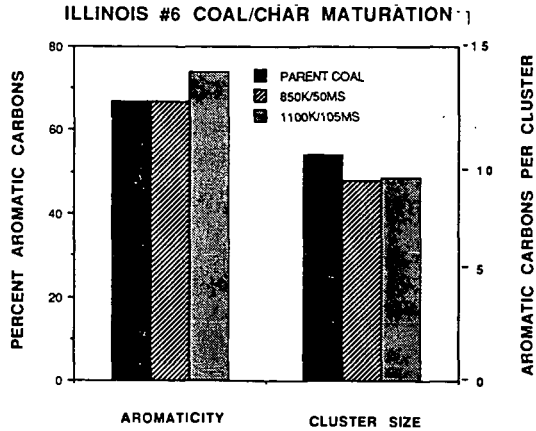


Figure 5. Relationship between the aromaticity and cluster size for an Illinois #6 coal (PSOC-1493) and related chars.

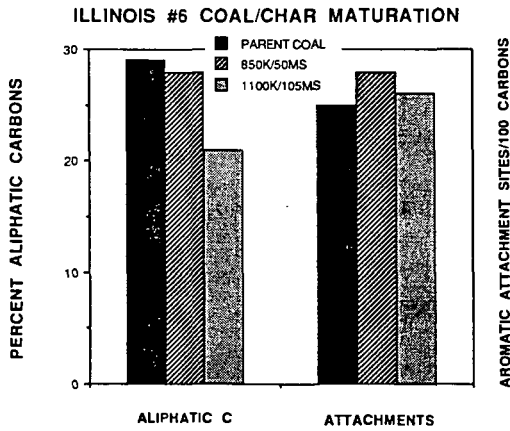


Figure 6. Relationship between aliphatic carbon content and number of aromatic attachment sites/100 carbons for the Illinois #6 coal and associated chars.

RAPID COAL DEVOLATILIZATION IN A RADIANT COAL FLOW REACTOR

John Chen, Y. Cleo Chang, and Stephen Niksa
High Temperature Gasdynamics Laboratory
Mechanical Engineering Department
Stanford University
Stanford, CA 94305

INTRODUCTION

Determinations of the product distributions from coal devolatilization under simulated pulverized fuel (p.f.) firing will enable better descriptions of the heat release, pollutant formation, sooting, and the evolution of polycyclic aromatic compounds (PAC). While these connections are widely recognized, only a handful of product distributions from very rapid coal devolatilization have been reported. Moreover, most of the available data was taken in entrained flow reactors, in which the time-temperature histories are obscured by mixing between preheated gases and the cold coal suspension at the injector as, for example, in Nenniger's study.¹ Also, since entrained process streams are very hot, the product distributions from primary devolatilization are significantly altered by secondary homogeneous chemistry.²

In this study, we introduce a novel radiant coal flow reactor which eliminates mixing and minimizes the extent of secondary chemistry. This system relies upon radiant heating of a thin coal suspension entrained into a stable, one-dimensional flow field. This furnace configuration is supported by rapid quenching to resolve reaction times on a scale of several milliseconds, aerodynamic segregation of particulate, aerosol, and gaseous products, and a battery of chemical analyses. Transient weight loss, tar yields, elemental compositions of the condensed products, and tar molecular weight distributions (MWDs) are reported for an Illinois #6, HVA bituminous coal. These results depict the devolatilization behavior at atmospheric pressure for particle residence times to 130 msec., furnace temperatures from 1000 to 1850K, heating rates exceeding 10^4 K/s, and suspension loadings to 2400 particles/cm³.

EXPERIMENTAL

Overview and Performance Characteristics

A schematic of the radiant coal flow devolatilization experiment appears in Fig. 1. At the top of the system, a feeder delivers fuel particles into an argon entrainment stream, forming an optically-thin suspension which flows downward into a radiant furnace section. The radiant section consists of a quartz tube situated on the axis of an inductively-heated graphite cylinder. Near-blackbody thermal emission from the graphite rapidly heats the particles as they traverse the furnace. Note that since the suspension is optically thin, the radiant heat flux is uniform, and that no mixing with a preheated gas stream is involved. Also, since the argon is transparent to the radiation, the gas remains relatively cool, thereby minimizing secondary reactions among the volatiles. Even though suspension loadings up to several thousand particles per cubic centimeter are maintained, the behavior in this system can be interpreted in terms of single-particle phenomena because the interparticle separation is at least ten particle diameters.

A schematic of the induction furnace section appears in Fig. 2. It consists of a 10 cm I. D., 5 cm long graphite cylinder encased in zirconium-oxide insulation which is wrapped by four turns of a water-cooled, copper induction coil. This assembly is mounted within water-cooled copper plates and a quartz housing. The overall height of the furnace is 9.5 cm. The graphite is heated inductively by a 10 kW, 450 kHz power supply. Wall temperatures are monitored with a disappearing filament pyrometer sighted onto the graphite through a small hole in the insulation to an uncertainty of 20K. In characterization studies with two-color pyrometry, axial temperature profiles within the graphite enclosure are uniform to within 98% of the mean temperature, except for the outermost 5 mm at both ends, over which the temperature falls to about 75% of the mean value.

The coal suspension enters the 22 mm O. D. quartz tube located on the axis of the furnace from a 10 mm tube, and is stabilized by a co-flowing, argon sheath flow. The relative flowrates of

the entrainment and sheath flows are set to minimize the extent of particle dispersion over the length of the furnace. They are not matched; rather, the conditions which yielded a uniform, pencil-like flow of coal over the furnace length at each gas velocity in cold-flow visualization studies are implemented in the experiments. Also, the suspension loadings reported here are based on the cross section of the entrainment stream only, the calculated slip velocity of the particles, and the calibrated coal feedrate.

Time resolution is achieved by varying the gas transit time from the furnace inlet to an argon quench nozzle mounted near the outlet of the radiant section. The reported residence times are based on direct measurements under experimental conditions. Residence times are assigned as the time interval between the interruption of two HeNe laser beams by the leading edge of a long pulse of fuel suspension. The two beams are separated by 11 cm, and placed as close to the inlet and outlet of the furnace as possible; nevertheless, this configuration does not necessarily contain the entire length of the active radiant zone.

The pyrolysis products are segregated into char particles, tar aerosol, and noncondensable gases using virtual impaction in an aerodynamic classifier, which is sketched in Fig. 3. All of the condensed phase products (char and tar) are recovered, and the coal feedrate is stable and reproducible, so that their respective yields can be assigned gravimetrically. At the inlet, the cooled process stream contains char particles, tar aerosol, and noncondensable gases at low levels in an argon stream. Following Nenninger's⁴ design guidelines, the inlet jet is turbulent ($Re_j = 7000$), and the jet diameters and spacings are set at prescribed ratios. Most of the inlet gas stream is diverted radially outward into the annulus while a small portion passes through the central nozzle. This split is maintained by valves downstream of the impactor. Particles with sufficient inertia, viz. char particles, pass through this virtual impaction surface and into a wire mesh basket. Nominal sizes for the tar aerosol are only a few microns, while the char particles are at least 50 microns, so the separation efficiency is very high. For 50 micron coal particles, the separation efficiency into the mesh basket exceeded 97% in characterization studies, so that carry-over of char into the annulus is negligible.

A small portion of the inlet gas stream, typically 5%, passes through the lower nozzle, while the remainder of the flow convects the aerosol products into the annulus, where they deposit onto a four-stage assembly of glass fiber filters. Even though no tars could penetrate a single filter element, multiple stages are needed to manage the increasing pressure drop as the tars accumulate. The top three stages are punctured to decrease their flow resistance; nevertheless, most of the tar deposits onto these stages. The final stage scavenges the stream at the size threshold of the filters at 0.3 microns. Small amounts of aerosol also deposit onto the impactor wall, so this surface is isolated with a polypropylene liner, and such deposits are included in the reported aerosol yields.

Pure tar samples for subsequent chemical analyses are prepared by extraction with tetrahydrofuran (THF) in an ultrasonic bath, and filtration through a 0.5 micron Teflon membrane; any residue is weighed and denoted as the soot yield. The tar solution is concentrated before the remaining solvent is evaporated, following a procedure developed by Lafleur et al.⁵

Elemental compositions of the char and tar are measured with a Control Equipment 240X analyzer. Tar MWDs are based on gel-permeation chromatography in a Hewlett-Packard HP-1090 HPLC using three μ Styragel columns (500Å and two 100Å) in series and broadband diode-array detection (212 to 400 nm). We adapted the calibration introduced by Rogers et al.⁶ to diode-array detection using model compounds with molecular weights from 128 to 950; H/C ratios from 0.5 to 1.09; and proton aromaticities from 0.25 to 1. The calibration equation is:

$$\ln(MW \cdot (H/C)^{-0.0189}) = 10.7339 - 0.7611 \cdot \ln H_a + (-0.2202 - 0.0726 \cdot (\ln H/C)) \cdot V$$

where

MW = Molecular weight

H/C = Hydrogen to carbon atomic ratio

H_a = Proton aromaticity, aromatic/(aromatic+aliphatic protons)

V = Retention volume, retention time*flow rate

Proton distributions are determined by ¹H NMR with a Varian XL-400 spectrometer operating at 400 MHz and are interpreted with tabulated chemical shifts.⁷

Coal Characteristics

The coal in these experiments is an Illinois #6, HVA bituminous coal (PSOC 1493D) obtained from the Pittsburgh Energy Technology Center (PETC). The ultimate and proximate analyses as reported by PETC are listed in Table I. The measured weight loss is converted to the dry, ash-free (daf) basis using the high-temperature ash value provided by PETC. These samples are aerodynamically classified, and two nominal size fractions are examined: 45-63 and 75-106 microns. All coal samples are dried at 60°C under vacuum for at least 12 hours and stored under argon.

RESULTS

Transient Devolatilization Behavior

The results in this section depict the influences of residence time and furnace wall temperature on the devolatilization behavior of the 75-106 micron sample. All of the results which follow are recorded at a reactor pressure a few inches of water above atmospheric, and a suspension loading of 400 particles/cm³. The volatiles yields as a function of the reactor wall temperature at average inlet gas velocities of 0.25, 0.67, and 2.0 m/s appear in Fig. 4. For a fixed inlet gas velocity, residence times at different wall temperatures will vary because the acceleration due to the changing gas density is significant.

As expected, the onset of devolatilization shifts to higher wall temperatures as the gas velocity is increased, going from 1450K at 0.25 m/s to 1800K at 2.0 m/s. For velocities greater than 0.67 m/s, the available residence times are insufficient to achieve complete devolatilization at even the highest wall temperature, indicating that the particle temperature at the furnace outlet is substantially lower than the wall temperature. But at 0.25 m/s, the ultimate yield of 56 wt% is observed at a wall temperature of 1840K. This value is significantly greater than the proximate volatile matter, as expected for these conditions of rapid heating. Also at 0.25 m/s, devolatilization commences at a wall temperature of 1500K and the product evolution rates increase rapidly for higher wall temperatures. Note that replicate runs in the study are generally reproducible to within 2 wt%.

The aerosol yields at a gas velocity of 0.25 m/s is shown with the corresponding total weight loss in Fig. 5. The aerosol yield becomes significant at 1600K and increases monotonically with temperature up to the maximum yield at 1840K, which constitutes 42% of the total volatiles yield. While the ultimate proportion of tar is consistent with expectations for atmospheric pyrolysis of HVA bituminous coals, the relatively small amount of tar at lower temperatures is surprising. For HVA Pittsburgh seam bituminous coals, the initial proportions of tar to noncondensable gases are typically 10:1 (but in studies at lower heating rates^{6,7}), while these proportions are inverted for this Illinois #6 coal. The tar samples from these conditions were analyzed for soot, but negligible amounts were observed in all cases. This observation strongly corroborates the absence of secondary homogeneous chemistry in this system, since pyrolysis tars rapidly convert to soot at temperatures above 1450K.²

The next study examines variations in residence time, which are measured at selected wall temperatures to characterize the kinetics of mass loss and tar evolution; results appear in Fig. 6 for wall temperatures of 1570, 1680, and 1840K. Although the wall temperatures are fixed in these studies, particle temperatures are increasing exponentially with increasing residence times, and probably never achieve the wall temperature in the available furnace length.

The onset of devolatilization shifts to shorter residence times as the wall temperature is increased, as expected. The complete transient evolution is evident only at 1840K, and shows two distinct stages of product evolution which are delineated by a distinct surge in the evolution rate between 72 and 77 msec. As seen above in Fig. 5, the proportions of tar to noncondensibles are surprisingly low during the initial stages of product formation. The transient data at 1840K also show that tar evolution ceases long before the ultimate yield is achieved, as seen in the behavior of HVA bituminous coals at slower heating rates. The fraction of soot in the aerosols is again found to be negligible for all conditions. Although they do not cover the entire approach to ultimate yields, the transient yields at 1680 and 1570K reliably convey the onset of devolatilization, and the relatively small amount of tar formed during the initial stages.

The proportions of carbon, hydrogen, and nitrogen (CHN) in the char and tar for various residence times at 1840K appear in Fig. 7. Note that all values are normalized by the distributions in the parent coal as reported by PETC, and that the error bars represent the range of measured values for replicate cases. Carbon and nitrogen contents of the chars (Fig. 7a) remain the same throughout devolatilization, but the hydrogen content falls monotonically during product evolution. The corresponding elemental distributions for the tar aerosols in Fig. 7b are markedly insensitive to residence time and, hence, the extent of devolatilization. The carbon content of the aerosols closely resembles the parent coal's, but the tars are deficient in nitrogen, especially for tar collected during the earliest stages of devolatilization. As expected from the decreasing hydrogen content of the chars, the tars are uniformly enriched in hydrogen by about 40%.

Molecular weight distributions of tar generated at 66 msec. and 1840K (Fig. 6) are shown in Fig. 8. These distributions are partially integrated to depict the mass or mole fractions within 100 g/g-mole of the values on the abscissa. All tar samples have similar shapes with respect to the shoulders in the distributions. They do differ with extent of devolatilization, however, in both average molecular weights and proton aromaticity as shown in Table II for the tars generated at 1840K. With increasing residence time, hence, extent of devolatilization, the average molecular weight and proton aromaticities increase monotonically.

The Influence of Particle Size

In the next study, the nominal particle size was reduced to 50 microns, while the suspension loading was increased by a factor of six to 2400 particles/cm³. The temperature dependence of weight loss and tar yields at constant inlet gas velocity (1.0 and 0.25 m/s) appear in Fig. 9. Note the similarities to the features in Figs. 4 and 5 for the larger sizes at lower loading, especially at a gas velocity of 0.25 m/s. The data are virtually identical for these two cases, for both weight loss and aerosol yields. This agreement may seem counterintuitive in that these studies involve stages of transient heating and the heating rates, being inversely proportional to size, should be higher for the smaller sizes. So higher yields at lower temperatures could have been expected for the smaller sizes, but are not observed.

In conventional entrained flow systems, increasing the suspension loading decreases the aggregate convective heat flux because of poorer mixing and the higher thermal capacitance of the suspension, so thermal transients extend over longer times; i. e., heating rates are lower for denser suspensions, all else the same. But the radiant furnace behaves differently. Since the suspensions remain optically thin at even the highest loadings of interest, the radiant flux is independent of loading. But the convective losses from the suspension increase with increasing surface area, and, consequently, with increasing loadings. Consequently, higher loadings increase the heating rate of the gases, so that the gas temperature more closely tracks the increasing temperature of the suspension. In summary, in this experiment the heating rates of the suspension and of the entrainment gas increase as the loading is increased.

This argument explains the agreement among the data in Figs. 5 and 9, in so far as the higher loading would tend to increase the gas temperature, while the smaller size would tend to decrease the suspension temperature. Apparently, these two factors are compensating, although temperature measurements are needed to demonstrate this. Note that arguments which invoke interparticle interactions seem implausible because the minimum interparticle spacing is at least 12 diameters for the cases in Fig. 9.

Discussion

In the radiant coal flow experiment, the thermal history of the fuel particles is not complicated by mixing between hot gases and cold suspensions, which will enable more reliable determinations of the fuel's time-temperature history. Since secondary chemistry among the volatiles is minimized in this system, detailed characterizations of the product distributions from pyrolysis at very rapid heating rates are also feasible.

Weight loss and tar aerosol yields from an Illinois #6 HVA bituminous coal were recorded for furnace temperatures to 1850K and residence times to 130 msec. for two different size-cuts of coal. Qualitatively, the transient data and elemental compositions of the condensed products exhibit

several interesting features, particularly (1) a distinct surge in the devolatilization rate midway through the process; (2) surprisingly low proportions of tar (for an HVA bituminous coal) during the first stage of product evolution; and (3) a shift to higher average molecular weight and proton aromaticity with increasing weight loss.

While these data reliably convey the experimental uncertainties and operating domain of this experiment, they are not yet suitable for rate determinations or model validation studies. The fuel's thermal histories are particularly uncertain, and both models and diagnostics are now being developed to assign the particle and gas temperatures. Also, the impact on the devolatilization behavior of the short unheated length of flow tube from the furnace outlet to the quench point and the effectiveness of the argon quench have not been assessed.

Acknowledgement

We are happy to acknowledge funding for this work from the Exploratory Research Program of the Electric Power Research Institute and, for John Chen, a fellowship from the Link Foundation for partial financial support.

References

1. Nenniger, R.D., Howard, J.B., and Sarofim, A.F.: Proceedings from the 1983 International Conference on Coal Science, IEA, Pittsburgh, 1983, pp.521-524.
2. Wornat, M.J.: *Pyrolysis-Induced Changes in the Composition of Polycyclic Aromatic Compounds from a Bituminous Coal*, Sc.D. thesis, Department of Chemical Engineering, MIT, 1988.
3. Ballantyne, A., Chou, H., Neoh, K., Orozco, N., and Stickler, D.: Final Report prepared for the U. S. DOE, Pittsburgh Energy Technology Center, Contract No. DE-AC22-84PC30291, October 1983.
4. Nenniger, R.D.: *Aerosols Produced from Coal Pyrolysis*, Sc.D. thesis, Department of Chemical Engineering, MIT, 1986.
5. Lafleur, A.L., Monchamp, P.A., Plummer, and E.F., Kruzel, E.L.: *Analytical Letters* 19 (21 & 22), 2103 (1986).
6. Oh, M.S.: *Softening Coal Pyrolysis*, Sc.D. thesis, Department of Chemical Engineering, MIT, 1985.
7. Bautista, J.R., Russel, W.B., and Saville, D.A.: *Ind. Engr. Chem. Fundam.* 25, 536, 1986.
8. Rogers, P.A., Creagh, A.L., Prange, M.M., and Prausnitz, J.M.: *Ind. Engr. Chem. Res.* 26, 2312-2318, 1987.
9. Collin, P.J., Tyler, R.J., and Wilson, M.A.: *Fuel* 59, 479-486, 1980.

Size (Microns)	Volatile Matter	Moisture Free Weight Percent					
		Ash	C	H	N	O	S
75 - 106	37.5	13.5	68.3	4.6	1.3	7.4	4.9
45 - 63	38.9	14.6	66.0	4.6	1.3	7.6	6.0

Table I: Proximate and Ultimate Analyses for Illinois #6, PSOC 1493D

Residence Time (ms)	Wt. Avg. M_w	No. Avg. M_n	Aromaticity H_a
66	706	501	0.28
72	807	557	0.28
77	813	556	0.29
87	834	568	0.33

Table II: Molecular Weight and Aromaticity of Tars Produced at 1840K

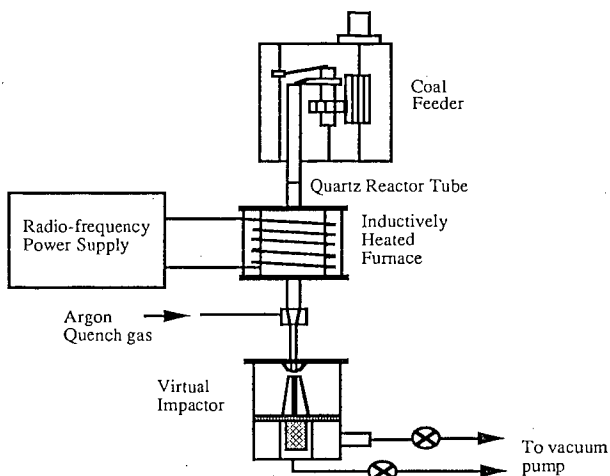


Fig. 1: The Radiant Coal Flow Reactor

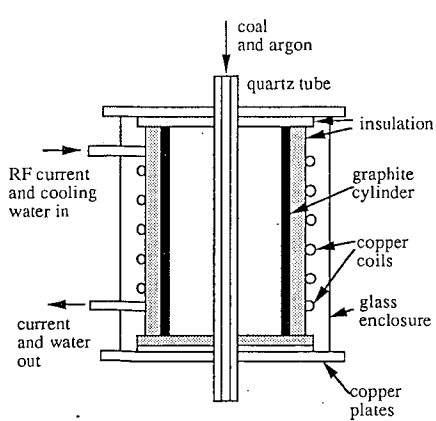


Fig. 2: The Inductively-Heated Furnace

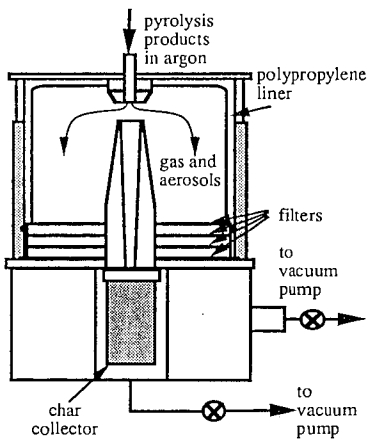


Figure 3: Schematic of the Virtual Impactor.

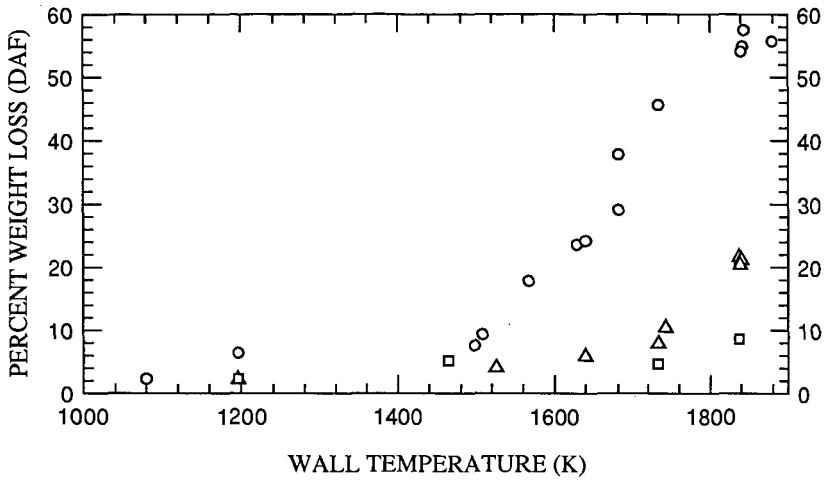


Fig. 4: Dry, ash-free weight loss for Illinois #6 coal, 75-106 μm , \circ 0.25 m/s, \triangle 0.67 m/s, \square 2.0 m/s inlet gas velocity, 400 particles/cc.

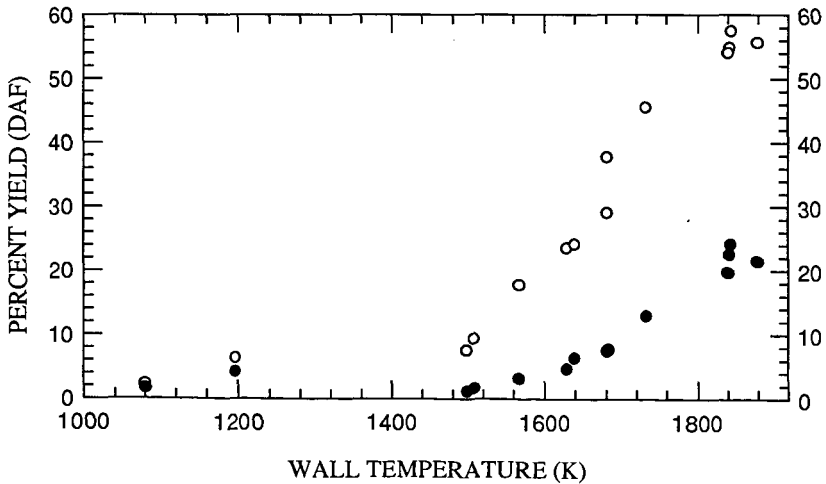


Fig. 5: Weight loss (OPEN symbols) and aerosol yield (FILLED symbols) for Illinois #6 coal, 75-106 μm particles, 0.25 m/s inlet gas velocity, 400 particles/cc.

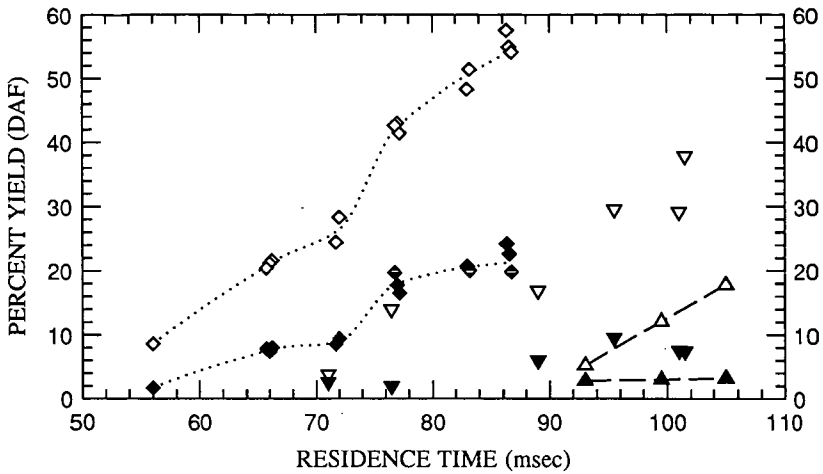


Fig. 6: Total (OPEN symbols) and aerosol yield (FILLED symbols) for Illinois #6 coal, 75-106 μm , ◇ 1840, ▽ 1680, △ 1570 K wall temperature, 400 particles/cc.

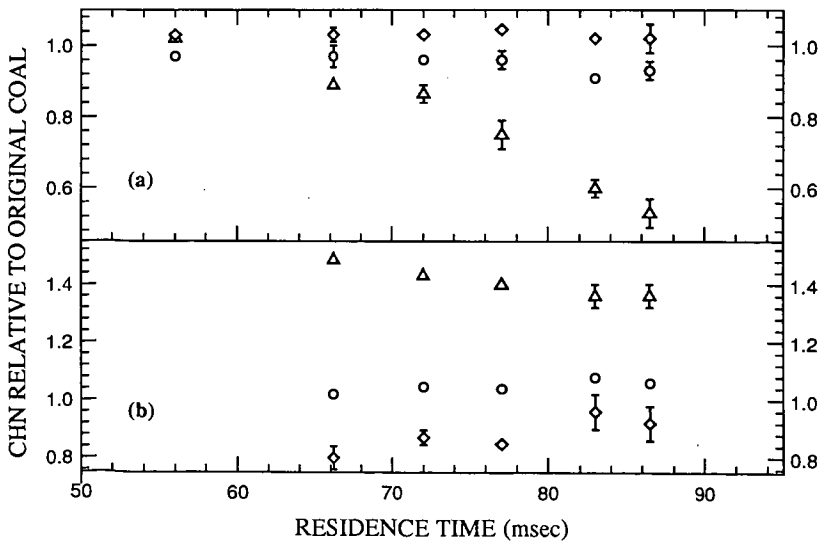


Fig. 7: Elemental composition of chars(a) and tars(b) for Illinois #6 coal, 75-106 μm , ○ carbon, △ hydrogen, ◇ nitrogen, $T_w=1840$ K, 400 particles/cc.

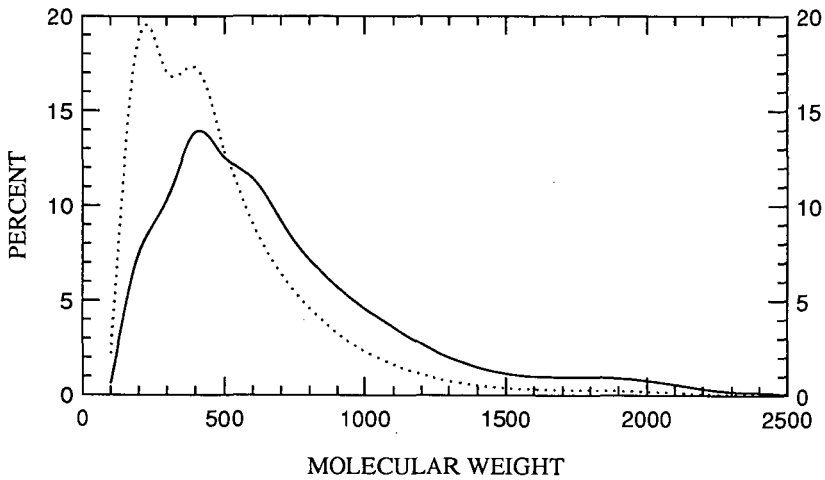


Figure 8: Molecular weight distributions of tar from Fig. 6 at 66 msec. and 1840K.
 — weight-average distribution, number-average distribution.

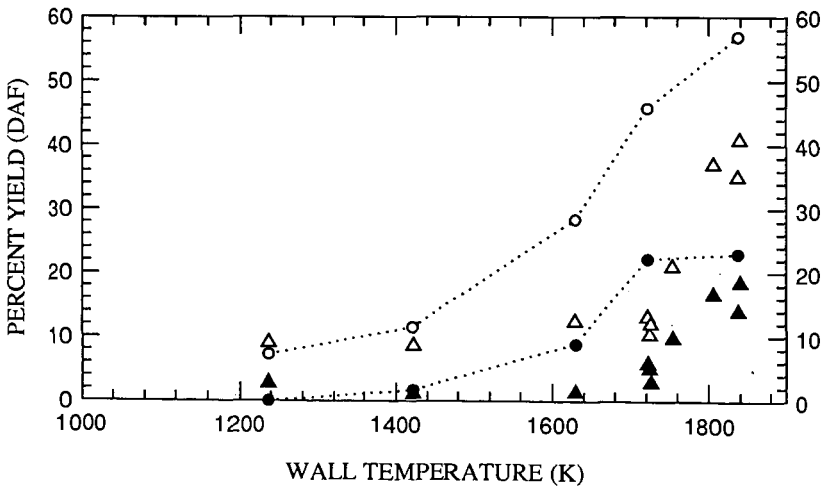


Fig. 9: Total (OPEN symbols) and aerosol yield (FILLED symbols) for 45-63 μm particles \circ 0.25 m/s, Δ 1.0 m/s inlet gas velocity, 2400 particles/cc.

MODELING OF A COAL CARBONIZER

Amir Rehmat and Anil Goyal
Institute of Gas Technology
3424 S. State Street
Chicago, IL 60616

James Van Hook and Archie Robertson
Foster Wheeler Development Corporation
12 Peach Tree Hill Road
Livingston, NJ 07039

ABSTRACT

A computer model has been developed, using data currently available in the literature, to simulate air-blown pyrolysis of coal in a carbonizer. A sorbent (limestone or dolomite) can also be added to the carbonizer to capture in-situ sulfur released into the gas. The sorbent, besides reacting with sulfur, also influences the product yields by cracking some tar to gases and soot, and hence like temperature and pressure, forms an independent parameter of the system. The char, soot, tar, spent sorbent, sulfur capture, air feed, and product gas flow rates and their compositions are determined by the computer model. This model has been used to predict carbonizer performance for Pittsburgh No. 8 bituminous coal at different operating conditions.

INTRODUCTION

A team of companies, led by Foster Wheeler Development Corporation and consisting of Gilbert/Commonwealth, Institute of Gas Technology (IGT), Combustion Turbine Operations Division of Westinghouse Electric Corporation, and Research and Development Division of Westinghouse Electric Corporation, has embarked upon a three-phase 5-year program with the Department of Energy (DOE) to develop an advanced second-generation Pressurized Fluidized Bed (PFB) Combustion system. The targeted goals of this second-generation PFB combustion plant are a 45% efficiency and a cost of electricity that is at least 20% lower than conventional pulverized-coal-fired plants with stack gas scrubbers. In addition, the plant emissions should be within New Source Performance Standards and it should have high availability, be able to process different ranks of coal, and incorporate modular construction technologies. These goals are achieved by shifting power generation to the more efficient gas turbine cycle and away from the steam cycle while maintaining sulfur capture by the sorbent, and by providing significantly higher gas turbine inlet temperatures without increasing the bed temperature through the incorporation of a topping combustor in the system. In this arrangement, a carbonizer generates a coal-derived low-Btu fuel gas at approximately 1500°F which is mixed with flue gases from a PFB combustor operating at 1500° to 1600°F and is burned in a topping combustor to increase the gas turbine inlet temperature to approximately 2100° to 2200°F. The combustion air to the topping combustor is provided by high excess air present in the flue gas from the PFB combustor. The carbonizer thus, is an essential element of this system. The coal is primarily fed to the carbonizer. The coal char residue from the carbonizer is burned in the PFB combustor along with the balance of the plant coal, if there is any left. Calcium-based sorbent is injected into the carbonizer and PFB combustor to minimize carbonizer tar yield and

desulfurize the gases from both units. The targeted efficiency is dependent upon the performance of the carbonizer.

The coal carbonizer, depending upon the coal properties, can be designed as a bubbling or a fast fluidized-bed reactor, each having its own characteristics with respect to the coal and air injection and product recovery. These constraints associated with the carbonizer design were recognized and therefore a highly generalized model was developed to accommodate various coal carbonizer configurations. The model can simulate a bubbling or a fast fluidized-bed reactor with or without fines recycle in which the coal and sorbent can be introduced into the fluidized-bed region and/or into the freeboard region of the carbonizer. Later, the model was tailored specifically for the three most practical configurations of the carbonizer.

LITERATURE SEARCH AND DATA CORRELATIONS

An extensive literature search was conducted and correlations were developed for yields of various species as a function of coal properties and carbonizer operating parameters. Out of numerous data available on the subject of pyrolysis, only a handful of data were applicable for the type of coal processing used here. Much of the data for coal pyrolysis were obtained in a heated grid reactor where the coal is subjected to the desired temperature from a fraction of a second to about 2 seconds yielding only a fraction of the pyrolysis product. On the other hand, in a fluidized-bed reactor, coal is subjected to a sufficiently long residence time (a gas residence time of over 5 seconds and a solids residence time of several minutes) so that the maximum yield is typically obtained. The data available in this category were used to develop the correlations for the coal carbonization product yields and their compositions. These correlations have been developed for bituminous coals as well as for lignites to cover a wide range of feedstock properties.

The details of the literature findings and correlations development are beyond the scope of this paper. However, as an example, the effects of various parameters on the tar yield from bituminous coals are given below.

In Figure 1, the tar yield at 1 atm of inert pressure expressed as a fraction of feed carbon is plotted against temperature. The tar yield increases up to about 1250°F after which it decreases because of the increased activity of the secondary reactions of tar cracking. With respect to the effect of pressure, Suuberg *et al.* (1978) and Arendt and van Heek (1981) conducted experiments with bituminous coals and reported a considerable reduction in the carbon conversion to tar with an increase in pressure from 1 atm to 100 atm, as shown in Figure 2. The data indicate that the tar yield decreases logarithmically with pressure. A similar effect on the tar yield has been shown by Eklund and Wanzl (1981) with a subbituminous coal at 1472°F. Regarding the effect of limestone or dolomite addition, Yeboah *et al.* (1980) and Longwell *et al.* (1985) have reported an appreciable decrease in the tar yield when limestone or dolomite was added during the pyrolysis of coal (Figure 3). Simultaneously, an increase in the hydrocarbon gases, along with some soot formation on the surface of the limestone, was noticed. The effect of CaO on the char yield and other gases was very little. These observations led to a conclusion that the addition of limestone or dolomite during coal pyrolysis causes some of the evolved tar to crack into hydrocarbon gases and

soot. The effect of oxygen feed on tar yield is shown in Figure 4. The oxygen reacts with tar as well as char [Howard and Essenhig (1967), Boley and Fegley (1977), and Saito *et al.* (1987)] yielding primarily CO and CO₂. However, the yields of methane, ethylene, and ethane are also higher in the presence of oxygen than those in the absence of oxygen. The increased yields are attributed to tar cracking. It should be recognized that the amount of tar and char reacting with the oxygen will depend on the amount of oxygen fed to the carbonizer, which is dictated by the reactor energy balance.

MODEL DESCRIPTION

The primary function of the model developed in this program is to make an estimate, for a given coal, of the product yields from a coal carbonizer operating at a specified temperature and pressure. In addition, sorbent (limestone or dolomite) may be added to capture *in-situ* sulfur released into the gas. The sorbent, besides reacting with sulfur, also influences the product yields from the coal carbonization and hence like temperature and pressure, forms distinctly an independent parameter of the system. The coal carbonizer, depending upon the coal properties, can take many forms from a bubbling fluidized bed to an entrained-flow reactor, each having its own peculiarities associated with the coal and air introduction and product recovery. These constraints were recognized and as a result a highly generalized model has been developed to accommodate different features that may be found in a coal carbonizer. Later, the model was tailored specifically to consider three practical configurations of the carbonizer.

General Description

For modeling purposes, and to accommodate various carbonizer configurations, the reactor has been divided into two sections, namely, the upper zone and the lower zone. The various streams leaving and entering these zones are shown in Figure 5.

The coal (stream S1) and sorbent (stream S2) are fed into the upper zone along with the transport gas (stream G4). The transport gas could be an inert gas, recycled gas, and/or air. Two additional gas streams (secondary gas streams G2 and G3) can also enter this zone, if needed. The product gas stream from the lower zone (stream G9) also enters this upper zone. Basically, the coal devolatilization takes place in the upper zone. If the air is fed to this zone (stream G1 or G4), then the oxygen present in the air will also react in this zone. The combustion in the upper zone and the sensible heat of the solids/gas from the lower zone provide the heat required for the coal devolatilization. The sulfur in the gas is captured by the sorbent present in this zone. The solids elutriated from this zone (stream S8) are captured by a cyclone and returned to the solids splitter (stream S7). The gas leaving this zone (stream G8) is the gas yield from the carbonizer. The carbonizer product gas also contains some char/sorbent fines (stream S4) and evolved tars (stream T1). The coal devolatilization temperature could be specified differently from the exit product gas temperature. Furthermore, the tar cracking occurs when sorbent is added to the system, producing soot and hydrocarbon gases. The soot formed in the carbonizer leaves the upper zone (stream S13) and enters the cyclone. The soot produced in the carbonizer may deposit on the char and the sorbent particles and thus leave the gasification system along with various solids

discharge streams (such as streams S4, S5, S6, and S12). However, for modeling purposes, this stream is assumed to be withdrawn from the cyclone (stream S14) along with the cyclone fines. The composition and flow rate of streams S13 and S14 are identical; however, they may differ in temperature.

The combustion air (stream G5) enters the lower zone along with the recycled char and reacted sorbent (stream S9) from the upper zone. The primary reaction in the lower zone is the char combustion reaction. If the temperature of this zone is high enough, then some slow rate gasification reactions will also take place. However, at present no such gasification reactions have been considered in the model. The solids stream containing char and spent sorbent (stream S5) can leave the carbonizer system from this zone. Alternatively, a part of the solids stream captured by the cyclone which contains char and spent sorbent (stream S7), may be removed from the system (stream S6). The sorbent (stream S3) can also be fed into this lower zone along with the transport gas (stream G7). For modeling purposes, it is assumed that the sorbent fed to the lower zone is calcined, if thermodynamically permitted, in this zone and transferred into the upper zone (stream S11). An additional gas stream (secondary gas stream G6) may also enter this zone, if needed. The gas produced in this lower zone enters the upper zone (stream G9).

The sorbent can be fed into the upper zone or the lower zone or into both the zones simultaneously. This will depend upon its sulfur capture capability and the system energy balance requirements for each zone. Furthermore, the temperature in each zone is assumed to be uniform, but not necessarily the same as the gas leaving the zone.

As shown in Figure 5, there are:

- Fourteen solids streams, 10 of which are unknown. Each solids stream can contain up to 15 species (C, H, O, N, S, Cl, Ash, Moisture, CaCO_3 , MgCO_3 , CaO, MgO, CaS, CaSO_4 , Inert).
- Nine gas streams, four of which are unknown. Each gas stream can contain up to 22 species (CO , CO_2 , H_2 , H_2O , CH_4 , C_2H_6 , O_2 , N_2 , H_2S , COS, NH_3 , HCN, HCl, C_2H_4 , C_2H_2 , C_3H_8 , C_3H_6 , C_4H_{10} , C_6H_6 , C_7H_8 , C_{10}H_8 , $\text{C}_6\text{H}_5\text{OH}$).
- One tar stream which is unknown (this stream is actually part of the product gas; however, for modeling purposes, it has been represented separately).

The above two zone model is an appropriate description of a fluidized-bed reactor or a fast fluidized-bed reactor in which the coal is fed into the reactor above the bed, that is, in the freeboard region. The model would also accommodate a carbonizer in which coal, sorbent, and air are fed in a single zone.

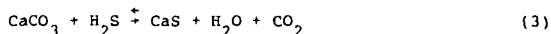
Yield Determination

The method employed for the determination of the product yields in the carbonizer is illustrated in Figure 6. Basically, complete information is available for the coal pyrolysis as a function of temperature at 1-atm pressure in inert atmosphere. The individual effects of pressure, sorbent

(limestone or dolomite), and oxygen on these product yields are also available. However, the literature lacks information about the combined effects of these factors on the product yields. The model has been constructed by superimposing effects of these factors (Figure 6) to yield information about the products of coal pyrolysis as a function of temperature, pressure, sorbent, and oxygen.

As illustrated in Figure 6, the product yields are determined in four steps. In the first step, a complete product slate is determined for coal carbonization at 1-atm pressure in an inert atmosphere and at specified carbonizer temperature. In the second step, the yields are adjusted for pressure. In the third step, using the information derived for the effect of oxygen on pyrolysis yield at 1-atm pressure, and assuming the same effect to hold at pressure, the yields obtained in the second step are adjusted for the effect of oxygen feed. Finally in the fourth step, the effect of sorbent is integrated into the above third step. When doing so, it is again assumed that the relationships derived at 1-atm pressure between products of pyrolysis with and without the addition of sorbent in the inert atmosphere are also valid at elevated pressure in the presence of oxygen. The yields and compositions obtained in the fourth step are thus considered to have accounted for all the process parameters namely, temperature, pressure, sorbent, and oxygen.

Depending upon the partial pressure of CO_2 in the carbonizer, the CaCO_3 in the sorbent will either exist as CaCO_3 or get calcined to CaO . This will also determine whether the H_2S will react with CaCO_3 or CaO . The extent of the sulfur capture by sorbent will be determined by its approach to the appropriate reaction equilibrium. The following reactions show the calcination of CaCO_3 , the reaction of H_2S with CaO , and the reaction of H_2S with CaCO_3 , respectively.



Determining equilibrium decomposition pressures of calcite (Equation 1) has proved a durable problem, and dubious values have appeared in the literature. The following correlation (Squires, 1967) has been used here:

$$\log_{10} (P_{\text{CO}_2}) = -8799.7/\text{TK} + 7.521 \quad (4)$$

where --

P_{CO_2} = equilibrium decomposition partial pressure of CO_2 in gas, atm

TK = temperature, °K

The equilibrium for the above reactions 2 and 3 are given by the following equations (Squires *et al.*, 1971):

$$\log_{10} \{(\text{H}_2\text{O})/(\text{H}_2\text{S})\} = 3519.2/\text{TK} - 0.268 \quad (5)$$

$$\log_{10} [(H_2O)(CO_2)(P)/(H_2S)] = 7.253 - 5280.5/TK \quad (6)$$

where --

- P = total system pressure, atm
- (H₂O) = mole fraction of H₂O in gas
- (CO₂) = mole fraction of CO₂ in gas
- (H₂S) = mole fraction of H₂S in gas
- TK = temperature, °K

The product gas is also considered to be at water-gas shift equilibrium at the carbonizer exit temperature.

MODEL PREDICTIONS

Carbonizer Configuration

The computer model has been kept as general as possible to accommodate various possible carbonizer configurations. However, for the current study the simple configuration for the carbonizer shown in Figure 7 is considered. Here, coal and dolomite (sor bent) are fed into the fluidized bed, and the fines captured by the cyclone are not recycled to the reactor, instead they are directed to the combustor. The bed is fluidized primarily using air. A model representation for this case is also given in this figure. The carbonizer is essentially represented by a single stage (upper zone) configuration. The solids stream S7 is equal to the solids stream S6, while the solids streams S3, S5, S9, S10, and S11 are zero. Furthermore, the gas stream G9 is also equal to zero.

Model Predicted Carbonizer Performance at 14-atm Pressure

The model predicted carbonizer performance at 14-atm pressure for several cases is given here. Besides the base case at 14-atm pressure and 1500°F temperature for the Pittsburgh No. 8 bituminous coal containing 2.5% moisture, the other cases have accounted for the effect of using as-received coal without drying (6% moisture), operating the carbonizer at 1600°F, and using coal/water slurry instead of dried feed. The operating conditions and the results of the model predictions are summarized in Table 1. This table is based on a 1000 pounds of moisture-free coal feed to the carbonizer. The results on the moisture-free coal feed basis provide a better comparison of yields at different operating conditions. A detailed material balance for the base case at 14-atm pressure and 1500°F temperature is given in Figure 8.

The char, soot, spent dolomite, tar, air feed, and product gas flow rates and their compositions are determined by the computer model. The air feed requirement is based on the energy balance around the carbonizer. The heat losses from the carbonizer are assumed to be negligible. The relative humidity of the air is 50% at 70°F, which is equivalent to 1.235 mole percent moisture in the air. The H₂S in the product gas is based on 92% approach to the equilibrium concentration, that is, the ratio of calculated equilibrium H₂S

content in the product gas (using Equation 5 or 6) to the actual H_2S content in the product gas is 0.92. The dolomite feed rate to the carbonizer is based on feed Ca/S molar ratio of 1.75. It is also assumed that $CaSO_4$ formation does not take place in the carbonizer. The product gas is in water-gas shift at the carbonizer exit gas temperature. The fines leaving the carbonizer have been included in the discharged solids stream. The computer model allows the formation of acetylene (C_2H_2), naphthalene ($C_{10}H_8$), and hydrogen cyanide (HCN). However, due to the lack of literature information, amounts of these species have been assumed to be zero in all the balances.

Model Predicted Carbonizer Performance at 10-atm Pressure

To determine the effect of pressure on the carbonizer performance, four balances were prepared under conditions similar to those of 14-atm pressure cases given above, except the pressure was reduced to 10 atm. These balances include carbonizer operation at 1500°F with the Pittsburgh No. 8 bituminous coal containing 2.5% moisture, and the effect of using as-received coal without drying (6% moisture), operating the carbonizer at 1600°F, and using coal/water slurry instead of dry feed. The operating conditions and the results of the model predictions are summarized in Table 2. The basis of these balances are the same as used for 14-atm cases.

CONCLUSIONS

The mathematical model has been used to predict carbonizer performance for Pittsburgh No. 8 bituminous coal at different operating conditions. The following conclusions are derived from this study.

- An increase in pressure results in a decrease in the amount of tar and soot, but somewhat reduced sulfur capture at a specified temperature.
- An increase in temperature results in a reduction in the amount of tar and soot as well as an improvement in the sulfur capture at a specified pressure.
- An increase in feedstock moisture or the use of slurry requires additional air, which in turn results in reduced amounts of tar and soot and lower quality product gas. Also, the sulfur capture is reduced due to higher steam partial pressure in the product gas.

ACKNOWLEDGMENT

The authors thank the Department of Energy, Morgantown Energy Technology Center, for their support of this work under Contract No. DE-AC21-86MC21023.

REFERENCES

- Arendt, P. and van Heek, K. H., "Comparative Investigations of Coal Pyrolysis Under Inert Gas and H_2 at Low and High Heating Rates and Pressures Up to 10 MPa," Fuel **60**, 779 (1981).
- Boley, C. C. and Fegley, M. M., "Design and Operation of Two Refractory-Lined, Internally Heated, Entrained-Bed Carbonizers," Grand Forks Energy Research Center Report, Grand Forks, North Dakota, GFERC/R1/77/1 (1977).

Eklund, H. and Wanzl, W., "Pyrolysis and Hydropyrolysis of Solid Fuels at High Heating Rates (10^4 K/s) Using Curie-Point Technique," Proceedings of the International Conference on Coal Science, Dusseldorf, Germany, D18, 701 (1981).

Floess, J. K., Plawsky, J., Longwell, J. P. and Peters, W. A., "Effects of Calcined Dolomite on the Fluidized-Bed Pyrolysis of a Colorado Oil Shale and a Texas Lignite," Ind. Eng. Chem. Process Des. Dev. 24, No. 3, 730 (1985).

Freihaut, J. D. and Seery, D. J., "An Investigation of Yields and Characteristics of Tars Released During the Thermal Decomposition of Coal," Preprints ACS Div. Fuel Chem. Prep. 26, No. 2, 133 (1981) March 29-April 3.

Graff, R. A., Zhou, P. and Brandes, S. D., "Conditioning Techniques for Mild Gasification to Produce Coproducts," Proceedings of Sixth Annual Gasification Contractors Meeting, 144 (1986) June.

Howard, J. B. and Essenhigh, R. H., "Pyrolysis of Coal Particles in Pulverized Fuel Flames," Ind. Eng. Chem. Process Des. Dev. 6, No. 1, 74 (1967).

Landers, W. S., Wagner, E. O., Gomez, M., Boley, C. C. and Goodman, J. B., "Entrained-Bed Carbonization of Bituminous Coal," U.S. Bureau of Mines, RI6608 (1965).

Longwell, J. P., Chang, C. S. and Peters, W.A., "Coal Gasification and Tar Conversion Reactions Over Calcium Oxide," Final Technical Report for the Period August 7, 1981-August 6, 1984, DOE/MC/16026-1839 (DE85011734), MIT, Cambridge, MA, May (1985).

Saito, M., Sadakata, M., Sato, M. and Sakai, T., "Devolatilization Characteristics of Single Coal Particles for Combustion in Air and Pyrolysis in Nitrogen," Fuel 66, 717 (1987).

Squires, A. M., "Cyclic Use of Calcined Dolomite to Desulfurize Fuels Undergoing Gasification," Advances in Chemistry Series: Fuel Gasification 69. Washington, D.C.: American Chemical Society, 1967.

Squires, A. M., Graff, R. A. and Pell, M., "Desulfurization of Fuels With Calcined Dolomite. Part 1. Introduction and First Kinetic Results," Chemical Engineering Progress Symposium Series: Important Chemical Reactions in Air Pollution Control 67, No. 115, 23. New York: American Institute of Chemical Engineers, 1971.

Suuberg, E. M., Peters, W. A. and Howard, J. B., "Product Composition and Formation Kinetics in Rapid Pyrolysis of Pulverized Coal -- Implication for Combustion," Proceedings of 17th Symposium (International) on Combustion, Leeds, England, 117 August 20-25 (1978).

Tyler, R. J., "Flash Pyrolysis of Coals. Devolatilization of Bituminous Coals in a Small Fluidized-Bed Reactor," Fuel 59, 218 (1980).

Xu, W. and Tomita, A., "Effect of Coal Type on the Flash Pyrolysis of Various Coals," Fuel 66, 629 (1987).

Yeboah, Y. D., "The Fluidized-Bed Pyrolysis of Coal in Both the Presence and the Absence of Dolomite Compounds," DSC Thesis, MIT (1979).

Yeboah, Y. D., Longwell, J. P., Howard, J. B., and Peters, W. A., "Effect of Calcined Dolomite on the Fluidized-Bed Pyrolysis of Coal," Ind. Eng. Chem. Process Des. Dev. 19, No. 4, 646 (1980).

Yeboah, Y. D., Longwell, J. P., Howard, J. B. and Peters, W. A., "Pyrolytic Desulfurization of Coal in Fluidized-Beds of Calcined Dolomite," Ind. Eng. Chem. Process Des. Dev. 21, No. 2, 324 (1982).

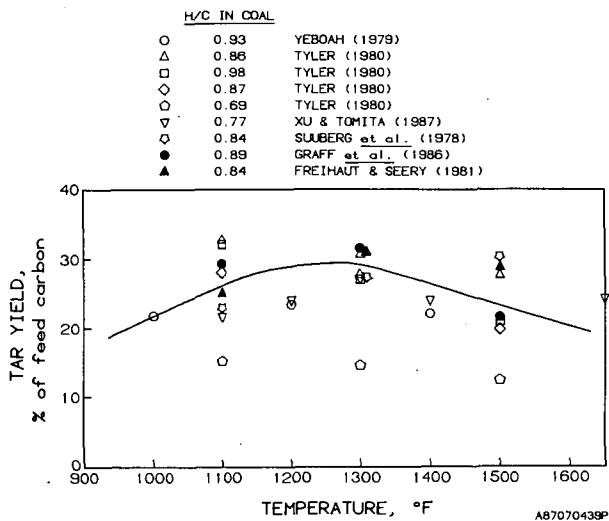


Figure 1. TAR YIELD AS A FUNCTION OF TEMPERATURE FOR BITUMINOUS COALS (Inert Atmosphere, 1 atm Pressure)

32WP/PAP/agpaper

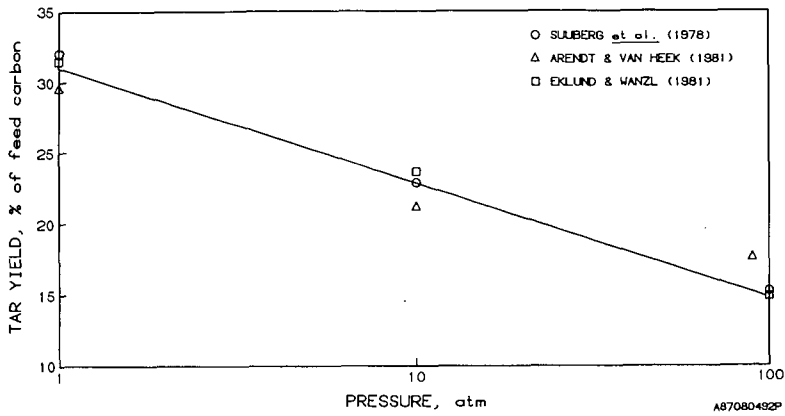


Figure 2. EFFECT OF PRESSURE ON TAR YIELD DURING PYROLYSIS OF BITUMINOUS COALS (Inert Atmosphere)

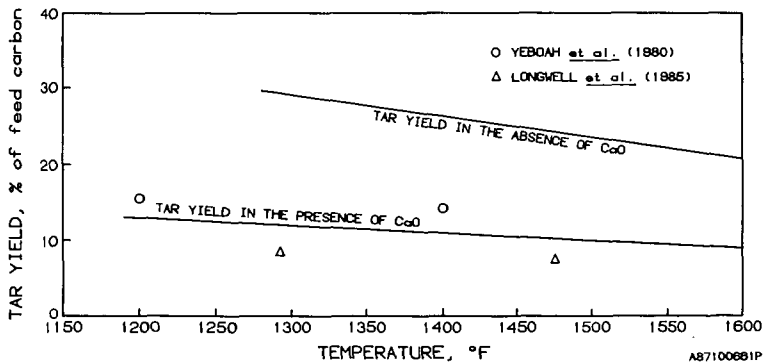


Figure 3. EFFECT OF LIME ADDITION ON TAR YIELD FOR BITUMINOUS COALS (Inert Atmosphere, 1 atm Pressure)

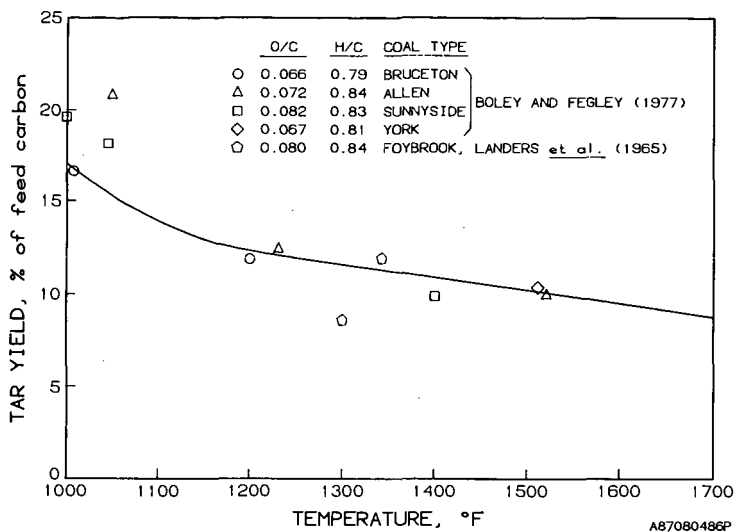


Figure 4. TAR YIELD BITUMINOUS COALS PYROLYSIS IN THE PRESENCE OF OXYGEN (1 atm Pressure)

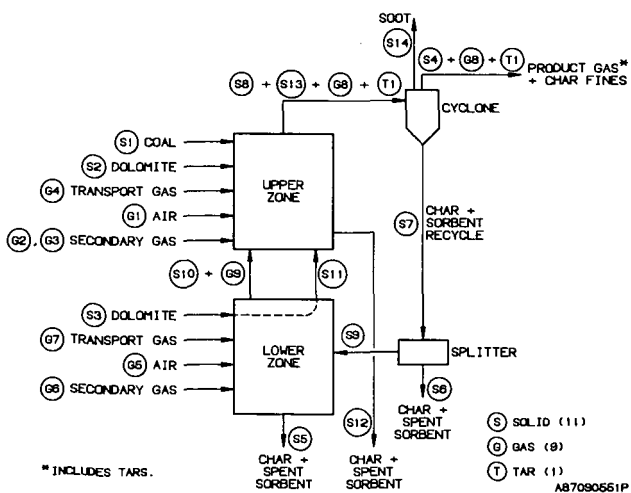


Figure 5. SCHEMATIC OF CARBONIZER MODEL

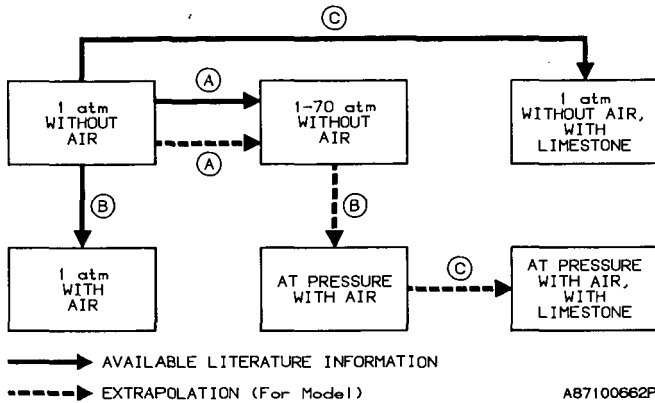


Figure 6. METHODOLOGY FOR CARBONIZER PRODUCT YIELD DETERMINATION

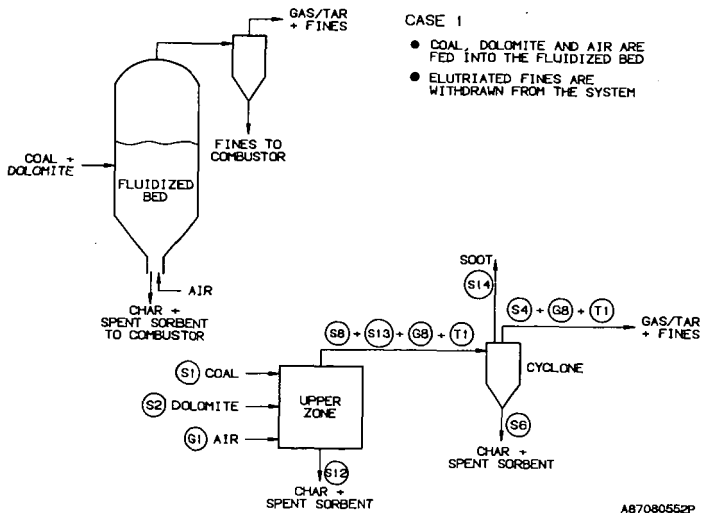


Figure 7. CARBONIZER CONFIGURATION FOR MODEL PREDICTIONS

Fuel Gas Flow (lb/h) 1489.42
 HHV (Btu/lb) 3139
 LHV (Btu/lb) 2917
 LHV (Btu/SCF) 207.2 (Gas Only)

	Char-Sorbent (Flow = 846.9 lb/h)			
	Char	Soot	Spent Dolomite	
Carbon	462.89	10.58	63.73	MgO
Hydrogen	7.67	0.04	129.73	CaCO ₃
Sulfur	16.77	0.07	27.45	CaS**
Nitrogen	8.34	0.03	5.23	Inerts
Oxygen	8.25	0.01	--	
Moisture	--	--	--	
Ash	105.70	--	--	
Total	609.62	10.73	226.14	
HHV (Btu/lb)	11830	14568		
LHV (Btu/lb)	11711	14536		

Tar
 (Flow Rate = 28.71 lb/h)

Gas*
 (Flow Rate = 1460.71 lb/h,
 54.54 mol/h)

MW = 13.0449

Atomic Composition:

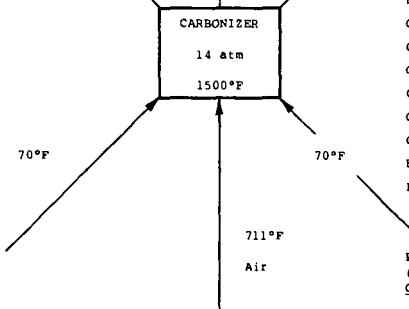
CH_{0.462}O_{0.018}N_{0.0076}S_{0.0053}

HHV (Btu/lb) 15485

LHV (Btu/lb) 15147

wt % mol %

CO	11.26	10.77
CO ₂	20.47	12.46
H ₂ O	5.80	8.63
H ₂	0.54	7.20
CH ₄	3.60	6.00
C ₂ H ₆	0.957	0.852
C ₂ H ₄	2.975	2.840
NH ₃	0.204	0.321
H ₂ S	0.082	0.065
N ₂	52.36	50.06
COS	0.020	0.009
C ₃ 's	0.787	0.495
C ₄ 's	0.134	0.062
C ₆ H ₆	0.192	0.066
C ₇ H ₈	0.374	0.109
C ₆ H ₅ OH	0.244	0.069
HHV (Btu/lb)	2896	
LHV (Btu/lb)	2677	



Plum Run Dolomite
 (Flow Rate = 307.9 lb/h;
 Ca/S = 1.75)

Pittsburgh Coal
 (Flow Rate = 1025.64 lb/h)

Carbon	737.90
Hydrogen	48.10
Sulfur	30.70
Nitrogen	12.90
Oxygen	64.70
Moisture†	25.64
Ash	105.70
HHV (Btu/lb)	12913
LHV (Btu/lb)	12469

(Flow Rate = 1002.37 lb/h)

(Relative Humidity: 50% at 70°F)

O ₂	231.65 lb/h
N ₂	762.95
Moisture	7.77
	1002.37

wt % lb/h

CaCO ₃	54.5	167.81
MgCO ₃	43.3	133.32
Moisture	0.5	1.54
Inerts	1.7	5.23
Total	100.0	307.90

*Excludes Tar.

**92% Approach to H₂S/Sorbent Reaction Equilibrium.

†After Drying.

Figure 8. CARBONIZER BALANCE FOR PITTSBURGH COAL AT 14 atm, 1500°F, and 2.5% MOISTURE (Base Case)

Table 1. SUMMARY OF CARBONIZER MATERIAL BALANCES AT 14-atm PRESSURE
(Basis: 1000 lb Moisture-Free Coal Feed)

Case Description	Base Case	6% Moisture	1600°F	30% Slurry
Carbonizer Temperature, °F	1500	1500	1600	1500
Coal Feed (moisture-free), lb	1000	1000	1000	1000
Moisture in Coal Feed, %	2.5	6.0	2.5	30.73*
Coal Feed (as-fed), lb	1025.6	1063.8	1025.6	1443.6
Sorbent (Dolomite) Feed, lb	307.9	307.9	307.9	307.9
Air Feed, lb	1002.4	1069.5	1102.0	1765.8
Char in Solids Discharged From Carbonizer, lb	609.6	605.1	598.5	558.4
Spent Sorbent in Solids Discharged From Carbonizer, lb	226.1	226.4	225.0	228.9
Soot Leaving Carbonizer System, lb	10.7	10.0	0.0	2.8
Product Gas (tar-free) Leaving Carbonizer, lb	1460.7	1572.8	1592.7	2719.6
Tars Leaving Carbonizer, lb	28.7	26.9	19.3	7.6
Product Gas (tar-free) HHV, Btu/lb	2896	2709	2917	1685
Tars HHV, Btu/lb	15485	15485	15462	15485
Feedstock HHV, Btu/lb (MF)	13244	13244	13244	13244
Total (product gas + tars) HHV/Feedstock HHV, %	35.3	35.3	37.3	35.5
Total (product gas + tars) LHV/Feedstock LHV, %	34.0	33.9	35.9	33.6
Product Gas (tar-free) HHV, Btu/SCF	224.2	212.8	227.5	146.7
Feedstock Carbon Conversion to Gas, %	32.25	33.14	35.93	42.31
Feedstock Carbon Conversion to Gas + Tars, %	35.84	36.49	38.33	43.26
MAF Coal Conversion to Gas, %	39.24	40.03	42.74	48.21
MAF Coal Conversion to Gas + Tars, %	42.45	43.03	44.89	49.06
Ca/S Feed Molar Ratio	1.75	1.75	1.75	1.75
Approach to H ₂ S/Sorbent Reaction Equilibrium, %	92.0	92.0	92.0	92.0
Sulfur Captured by Sorbent, % of Coal Sulfur	39.73	38.85	43.82	29.51
Sulfur Appearing in Product Gas + Tars, % of Coal Sulfur	5.40	6.79	3.42	21.34

* Includes slurry water.

Table 2. SUMMARY OF CARBONIZER MATERIAL BALANCES AT 10-atm PRESSURE
(Basis: 1000 lb Moisture-Free Coal Feed)

Case Description	2.5% Moisture	6% Moisture	1600°F	30% Slurry
Carbonizer Temperature, °F	1500	1500	1600	1500
Coal Feed (moisture-free), lb	1000	1000	1000	1000
Moisture in Coal Feed, %	2.5	6.0	2.5	30.73*
Coal Feed (as-fed), lb	1025.6	1063.8	1025.6	1443.6
Sorbent (Dolomite) Feed, lb	307.9	307.9	307.9	307.9
Air Feed, lb	1000.8	1068.2	1100.3	1767.9
Char in Solids Discharged From Carbonizer, lb	606.4	602.1	596.5	557.4
Spent Sorbent in Solids Discharged From Carbonizer, lb	225.9	226.0	224.9	227.4
Soot Leaving Carbonizer System, lb	11.3	10.5	0.0	2.9
Product Gas (tar-free) Leaving Carbonizer, lb	1460.7	1573.2	1592.2	2724.2
Tars Leaving Carbonizer, lb	30.1	28.2	20.2	7.7
Product Gas (tar-free) HHV, Btu/lb	2907	2718	2927	1682
Tars HHV, Btu/lb	15485	15485	15462	15485
Feedstock HHV, Btu/lb (MF)	13244	13244	13244	13244
Total (product gas + tars) HHV/Feedstock HHV, %	35.6	35.6	37.6	35.5
Total (product gas + tars) LHV/Feedstock LHV, %	34.3	34.2	36.2	33.6
Product Gas (tar-free) HHV, Btu/SCF	225.4	213.8	228.6	146.6
Feedstock Carbon Conversion to Gas, %	32.42	33.30	36.08	42.44
Feedstock Carbon Conversion to Gas + Tars, %	36.18	36.81	38.59	43.40
MAF Coal Conversion to Gas, %	39.38	40.17	42.86	48.32
MAF Coal Conversion to Gas + Tars, %	42.76	43.32	45.12	49.17
Ca/S Feed Molar Ratio	1.75	1.75	1.75	1.75
Approach to H ₂ S/Sorbent Reaction Equilibrium, %	92.0	92.0	92.0	92.0
Sulfur Captured by Sorbent, % of Coal Sulfur	40.70	40.22	44.31	35.07
Sulfur Appearing in Product Gas + Tars, % of Coal Sulfur	4.42	5.39	2.84	15.58

* Includes slurry water.